# METHODS FOR HIGH DIMENSIONAL UNCERTAINTY QUANTIFICATION: REGULARIZATION, SENSITIVITY ANALYSIS, AND DERIVATIVE ENHANCEMENT

A DISSERTATION
SUBMITTED TO THE DEPARTMENT OF AERONAUTICS AND ASTRONAUTICS
AND THE COMMITTEE ON GRADUATE STUDIES
OF STANFORD UNIVERSITY
IN PARTIAL FULFILLMENT OF THE REQUIREMENTS
FOR THE DEGREE OF
DOCTOR OF PHILOSOPHY

Gary Tang
June 2013

I certify that I have read this dissertation and that, in my opinion, it is fully adequate in scope and quality as a dissertation for the degree of Doctor of Philosophy.

**Gianluca Iaccarino, Primary Adviser**

I certify that I have read this dissertation and that, in my opinion, it is fully adequate in scope and quality as a dissertation for the degree of Doctor of Philosophy.

**Juan Alonso**

I certify that I have read this dissertation and that, in my opinion, it is fully adequate in scope and quality as a dissertation for the degree of Doctor of Philosophy.

**Marco Pavone**

I certify that I have read this dissertation and that, in my opinion, it is fully adequate in scope and quality as a dissertation for the degree of Doctor of Philosophy.

**Michael Eldred**

Approved for the Stanford University Committee on Graduate Studies.

**Patricia J. Gumport, Vice Provost Graduate Education**

*This signature page was generated electronically upon submission of this dissertation in electronic format. An original signed hard copy of the signature page is on file in University Archives.*

# Abstract

Surrogates are used to mitigate the aggregate cost of simulation needed to perform a comprehensive uncertainty quantification (UQ) analysis. A realistic uncertainty analysis of any engineering system involves a large number of uncertainties, and as a result, the surrogates take inputs in a high dimensional space. We investigate surrogates that take the form of a truncated Legendre polynomial series, from which the coefficients associated to each polynomial basis function must be estimated. High dimensional estimation is a known instance of the *curse of dimensionality*, and for sufficiently "complex" functions, an unsolved problem. In order to break the curse, we assume the function to be approximated is sparse in the Legendre polynomials and employ the machinery of $\ell_1-$regularized regression. We make three contributions under this theme. Firstly, we present a novel approach to choosing sample (design) points and show that it yields lower estimation error over a broad range of functions compared to existing sampling approaches. Secondly, we give a novel sparse estimator that effectively uses (partial) derivative information for estimation and show empirically that estimation using derivatives can be *more* efficient than function values if the derivatives are sparser than the function. Thirdly, we show that by exploiting the *best k-term approximation* property of $\ell_1$-methods, we can quickly identify the most signfiicant uncertainties and reduce the dimensionality of the input space accordingly. We conclude by demonstrating the efficacy of these methods in a UQ analysis of a notional vertical axis wind turbine design.

# Acknowledgements

Firstly, I would like to thank my advisor, Gianluca Iaccarino. Above all, I thank him for his unwavering support and infinite patience as I sought my own path. He always made himself available to my (sometimes clumsy) ruminations and probed my ideas with the proper dose of criticism and encouragement. He pushed me to be a disciplined thinker, for which I will be forever grateful.

I would also like to thank my reading and oral committee members: Juan J. Alonso, Karthik Duraisamy, Michael S. Eldred, Marco Pavone, and Michael Saunders. I had the great pleasure of taking Advanced Aerodynamics and Sustainable Aviation from Professor Alonso and am always in awe of the breadth and depth of his knowledge and ideas. In addition to chairing my oral defense, Professor Saunders directly contributed to this work by developing the solver PDCO, from which many of my results were generated. I thank Dr. Eldred and his colleague Dr. Laura P. Swiler for graciously hosting me at Sandia National Labs. They were indispensable as mentors and collaborators as I started my journey with uncertainty quantification.

I am lucky to be blessed with great friends and family, without whom none of this would be possible. The members of the UQ lab have been like a second family. I thank Per, Paul, David, Riccardo. In particular, I thank my officemates and brothers-from-another-mother John and Mike. Finally, I thank my father and mother who risked everything in hopes of better lives for their children. I dedicate this thesis to them.

# Contents

# List of Tables

# List of Figures

# Chapter 1

# Introduction

One of the many goals of computational science is the ability to predict physical phenomena using numerical simulations, to which the field of uncertainty quantification (UQ) plays a critical role. UQ assesses the impact of uncertainty on *a priori* chosen quantities of interest computed through numerical simulation. These uncertainties may arise from uncertain operating environments, imprecise geometry, or the choice of physical model. In real engineering systems, the uncertainties are innumerable, and any comprehensive UQ analysis will be nominally *high dimensional*. The prevailing constraint to such analyses is the aggregate cost of simulations needed to study the effect of the uncertainties. Today, the cost of "high fidelity" simulations are at least on the order of thousands of CPU-hours.

One approach to mitigate aggregate simulation cost is to build an accurate, cheap-to-evaluate surrogate model that can be interrogated in place of expensive simulations. This work focuses on the efficient construction of surrogates where the number of uncertainties is large ($\geq 10$). The surrogates under consideration take the form of truncated Legendre series polynomials, and we utilize the machinery of $\ell_1-$regularized regression to estimate the coefficients. Here, the *curse of dimensionality* degrades the efficacy of classical estimators and algorithms. Using the machinery of $\ell_1$-methods, we propose several methods that allow us to estimate build surrogates that take inputs nearing one hundred and possibly higher with parallelizable algorithms.

The contents of this thesis are partitioned into five major chapters. Chapter 2

provides the background material needed to make the thesis self contained. Chapter 3 describes our contribution to sample (design) point selection in the context of estimating Legendre polynomial chaos. We introduce a new sparse estimator utilizing derivative information in Chapter 4 and give empirical evidence to the notion of *super efficiency* of derivatives. Chapter 5 introduces variance-based global sensitivity analysis and the functional ANOVA decomposition. In addition to closed form estimates for the sensitivity indicies, we show how the *best $k$-term approximation* property of $\ell_1$-penalized regression can identify important variables using very few function evaluations, even in the presence of numerical noise. Finally, we employ some of the $\ell_1$-methodologies described in previous chapters to perform a high dimensional UQ analysis of vertical axis wind turbines.

# Chapter 2

# Background

## 2.1 Nomenclature

This work is motivated from branches of applied mathematics and engineering and thus nomenclature varies. We attempt to be consistent but may use some terms interchangeably for clarity and ease of understanding. In general, we follow the standard convention of viewing *functions* $f(x)$ as *maps* that take arguments in $x \in \mathcal{D}$ and maps them into the reals $f : \mathcal{D} \to \mathbb{R}$. Occasionally, we view it as a element in some vector space (e.g. $f \in L^2$) and drop the explicit dependence on $x$. We also adopt the aliases *response* or *quantity of interest* when appropriate. In practice, functions take both deterministic and random inputs. For the purposes of this work, it is safe to assume all *inputs* i.e. *variables* represent *uncertainties* and behave like random variables. The choice of weight function implies the density from which the variables are independently and identically generated; typically, this is the uniform density. Finally, we use the term *data*, used to estimate the coefficients $\{\alpha_{\boldsymbol{j}}\}_{\boldsymbol{j}\in\mathbb{N}^p}$, to describe the ensemble of pairs of *sample points* $\boldsymbol{x}_i \in \mathcal{D}$ and *function values* $f(\boldsymbol{x}_i)$ $i = 1, \ldots, m$. It is assumed that the function values are obtained by performing a numerical simulation at the prescribed sample points.

## 2.2 Polynomial approximation

### 2.2.1 $L^2[-1,1]^p$ and orthogonal polynomials

This work deals exclusively with functions that belong to the weighted Lebesgue space $L^2_w[-1,1]^p$. In Chapter 4, we will also consider the Sobolev space of functions $H^m[-1,1]^p$ which is a restriction of $L^2$ functions that also have order-$m$ derivatives in $L^2$. This section reviews some basic definitions and properties of this space. More detailed expositions can be found in [16, 58, 95].

The weighted Lebesgue space $L^2_w[-1,1]$ is an infinite-dimensional Hilbert space endowed with the inner product

$$\langle u, v\rangle_{L^2_w[-1,1]} = \int_{[-1,1]} u(x)v(x)w(x)dx, \quad u, w \in L^2_w[-1,1] \tag{2.1}$$

where we consider the constant weight function $w(x) = 1/2$ and induces the norm

$$\|u\|_{L^2_w[-1,1]} = \left(\int_{[-1,1]} |u(x)|^2 w(x)dx\right)^{1/2} \tag{2.2}$$

Then, for a Lebesgue measurable function $f : [-1,1] \to \mathbb{R}$, $f$ is a element of $L^2_w[-1,1]$ if $\|f\|_{L^2_w[-1,1]} < \infty$. In the sequel, we will drop the subscript $w$ from $L^2_w[-1,1]$ and the subscripts from the norm (2.2) and inner product (2.1) for ease of notation.

Denote $\mathbb{P}_M$ to be the space of polynomials of degree $\leq M$. Assume that $\{\phi_j\}_{j=0}^{\infty}$ to be a system of algebraic polynomials of degree $j$ that are mutually orthonormal with respect to the inner product (2.1)

$$\langle \phi_j, \phi_\ell \rangle = \delta_{j\ell} \tag{2.3}$$

where $\delta_{j\ell}$ is the Kroneker delta. The Weierstrass Approximation Theorem [74] implies that such a system completes the space $L^2[-1,1]$ and are known as the orthonormal Legendre polynomials. Completeness of the space implies that any function $f \in$

$L^2[-1,1]$ admits a series expansion of the form

$$f \overset{L^2}{=} Sf = \sum_{j=0}^{\infty} \alpha_j \phi_j \tag{2.4}$$

where $\overset{L^2}{=}$ impiles $\|f - Sf\| = 0$. The expansion coefficients $\alpha_j$ are defined as

$$\alpha_j = \int_{[-1,1]} f(x)\phi_j(x)w(x)dx \tag{2.5}$$

Equation (2.4) represents the Legendre transform of $f$. It follows that

$$\sum_{k=0}^{\infty} \alpha_k^2 < \infty \tag{2.6}$$

For any integer $M > 0$, the truncated series of $f$ of order $M$ is the polynomial

$$\mathcal{P}_M f = \sum_{k=0}^{M} \alpha_k \phi_k \tag{2.7}$$

From orthogonality, $\mathcal{P}_M$ is the orthonormal projection onto the space $\mathbb{P}_M$ and completeness of $\{\phi_j\}_{j=0}^{\infty}$ implies that

$$\|f - \mathcal{P}_M f\| \to 0 \quad \text{as } M \to \infty \tag{2.8}$$

The previous definitions can be extended in a straightforward way to multiple dimensions $p > 1$. Namely, we have the analogous definitions

$$\langle u, v \rangle_{L_w^2[-1,1]^p} = \int_{[-1,1]^p} u(\boldsymbol{x})v(\boldsymbol{x})w(\boldsymbol{x})d\boldsymbol{x}, \quad u, w \in L_w^2[-1,1]^p \tag{2.9}$$

where $w(\boldsymbol{x}) = 2^{-p}$ and induces the norm

$$\|u\|_{L_w^2[-1,1]^p} = \left( \int_{[-1,1]^p} |u(\boldsymbol{x})|^2 w(\boldsymbol{x})d\boldsymbol{x} \right)^{1/2} \tag{2.10}$$

Similarly, functions $f \in L^2_w[-1,1]^p$ admit a series representation in the the tensor product Legendre polynomials $\{\phi_{\boldsymbol{j}}\}_{\boldsymbol{j}\in\mathbb{N}^p}$

$$f \overset{L^2}{=} Sf = \sum_{\boldsymbol{j}\in\mathbb{N}^p} \alpha_{\boldsymbol{j}}\phi_{\boldsymbol{j}} \tag{2.11}$$

where the tensor product Legendre polynomials are given by

$$\phi_{\boldsymbol{j}}(\boldsymbol{x}) = \prod_{k=1}^{p} \phi_{j_k}(x_k), \quad \boldsymbol{j} = (j_1, j_2, \ldots, j_p) \in \mathbb{N}^p \tag{2.12}$$

and the coefficients $\alpha_{\boldsymbol{j}}$ are represented by the inner product between the function $f$ and $\phi_{\boldsymbol{j}}$

$$\alpha_{\boldsymbol{j}} = 2^{-p} \int_{[-1,1]^p} f(\boldsymbol{x})\phi_{\boldsymbol{j}}(\boldsymbol{x})d\boldsymbol{x}, \quad \boldsymbol{j} \in \mathbb{N}^p \tag{2.13}$$

The stochastic analogue to the Legendre polynomial series expansion is the Legendre polynomial chaos. The polynomial chaos arrives at the expansion from a slightly different thread. Namely, it seeks a series representations of finite variance functions from a polynomial sequence that is orthogonal with respect to a probability measure on the pre-image space. It was shown by Ernst [39] that there exists a complete orthogonal sequence if and only if the probability measure is uniquely determined by its moments. The construction of the generalized polynomial chaos is discussed in Chapter 3.1.

### 2.2.2 Subspaces of $L^2[-1,1]^p$

Denote the finite set of $p$-variate, maximal degree $P$ tensor-product Legendre polynomials to be $\Lambda_p^P$.

$$\Lambda_p^P = \{\phi_{\boldsymbol{j}}\}_{\boldsymbol{j}\in\mathcal{A}_p^P} \tag{2.14}$$

where

$$\mathcal{A}_p^P = \{\boldsymbol{j} \in \mathbb{N}^p \ : \ \sum_{k=1}^{p} j_k \leq P\} \tag{2.15}$$

The subspace spanned by these polynomials can be constructed in two ways. Denote this space to be $W_p^P$. Firstly, we can consider the atomistic construction

$$W_p^P \triangleq \text{span}(\Lambda_p^P) \tag{2.16}$$

Secondly, as more traditional, consider the tensor product of one dimensional subspaces. Denote $\{\phi_j\}_{j=0}^P$ as the set of Legendre polynomials of maximal degree $P$. Then, its spanning space is

$$W^P \triangleq \left\{v : L^2[-1,1] \ : \ v \in \text{span}(\{\phi_j\}_{j=0}^P)\right\} \tag{2.17}$$

The corresponding $p$-dimensional tensor product subspace is simply

$$W_p^P \triangleq \bigotimes_{|\boldsymbol{j}| \leq P}^{p} W^{j_k} \tag{2.18}$$

where the tensor product is over all combinations of $\boldsymbol{j} \in \mathbb{N}^p$ that sum to less than $P$. The dimensionality of this space, described by the number of basis functions in 2.18, is

$$\dim\left(W_p^P\right) = \binom{P+p}{p} \tag{2.19}$$

### 2.2.3 Truncated Legendre series

The thrust of this work is to construct an accurate approximation to $f$ using a truncated form of the infinite series in Equation (2.11). For an *a priori* chosen set of basis

functions $\Lambda$, the $M+1 = |\Lambda|$ term approximation is given by

$$Sf \approx f_M(\boldsymbol{x}) = \sum_{j=0}^{M} \alpha_j \phi_j(\boldsymbol{x}), \quad \phi_j \in \Lambda \tag{2.20}$$

where we assume some bijective ordering that switches from the multi-index $\boldsymbol{j}$ to the single index $j$. For our purposes, $\Lambda$ generally corresponds to the set of $p$-variate polynomials of maximal degree $P$, $\Lambda_p^P$. In other words, we seek an approximation to $f$ by finding the "closest" function in $W_p^P$. It is easy to see this function is the orthogonal projection $\mathcal{P}_{\mathcal{A}_p^P} f$, and it remains to estimate the coefficients $\{\alpha_{\boldsymbol{j}}\}_{\boldsymbol{j} \in \mathcal{A}_p^P}$.

In general, the series truncation (2.20) incurs an error $\epsilon_M$

$$\epsilon_M = \|f - \mathcal{P}_{\mathcal{A}_p^P} f\|_{L^2} \tag{2.21}$$

$$= \left( \sum_{\boldsymbol{j} \notin \mathcal{A}_p^P} \alpha_{\boldsymbol{j}}^2 \right)^{1/2} \tag{2.22}$$

Clearly $\epsilon_M$ depends on the decay rate of the coefficients $\alpha_{\boldsymbol{j}}$. We will assume that the truncation is chosen judiciously such that the truncation error is always "small." When $\epsilon_M$ is nonzero, we can consider this unobservable quantity as the function approximation analogue to *noise* in the context of statistical estimation. Therefore, we will often use the terms noise and truncation error interchangeably.

## 2.3 Estimation of $\boldsymbol{\alpha}$

Although we have the coefficients $\{\alpha_{\boldsymbol{j}}\}_{\boldsymbol{j} \in \mathcal{A}_p^P}$ in closed form, its computation is not trivial as it involves integrating a function in high dimensional space. One could compute the integral using Monte Carlo integration [73] but we are deterred by its slow rate of convergence. One popular approach to integration is high-order numerical integration such as Gauss quadrature [81, 43]. Unfortunately, while effective in low dimensions, for a fixed error rate, the cost of tensor product quadrature grows exponentially with the dimension $p$; we note that numerical integration through the

use of *sparse grids* [44] offers a compelling means of estimating $\boldsymbol{\alpha}$ and is still a topic of great interest.

Let $\Phi$ be the $m \times (M+1)$ matrix whose columns are tensor product Legendre polynomials evaluated at the sample points $\Phi_{ij} = \phi_{j-1}(\boldsymbol{x}_i)$, $j = 1, \ldots, (M+1)$, $\phi_j \in \Lambda_p^P$, $\boldsymbol{\alpha}$ is the vector of coefficients ordered according to their respective polynomial, and $\boldsymbol{y}$ is the vector of function values corresponding to the sample points $\{\boldsymbol{x}_i\}_{i=1}^m$. We consider the penalized regression framework

$$\boldsymbol{\alpha}^* = \underset{\boldsymbol{\alpha}}{\operatorname{argmin}} \|\Phi\boldsymbol{\alpha} - \boldsymbol{y}\|_{\ell_2}^2 + \lambda G(\boldsymbol{\alpha}) \tag{2.23}$$

The first term is known as the *data fit* term and the function $G$ *regularizes* the solution $\boldsymbol{\alpha}^*$ by coercing a form that seeks a small data fit error while keeping $G(\cdot)$ small. When $G(\cdot) = 0$, this reduces to ordinary least squares (OLS). However, when $m < M+1$, the OLS is undefined and regularization plays a critical role in the structure of the solution. This work is primarily concerned with regularizers $G(\cdot)$ that utilize the $\ell_1$-norm. A short history of the $\ell_1$ penalty and its properties is given in the next section.

## 2.4 $\ell_1$-regularized regression

Since its introduction in the mid 1990s, there has been an explosion of research into $\ell_1$ penalized methods and we do not attempt to cover the many developments following. For an excellent and detailed overview of $\ell_1$ methods, see [6].

### 2.4.1 Definitions

Motivated [84] by Breiman's non-negative Garrote [5], Tibshirani [83] proposed the *LASSO* (least absolute shrinkage and selection operator) statistical estimator which

is a the solution to the $\ell_1$-constrained least squares problem

$$\begin{aligned} \underset{\boldsymbol{\alpha}}{\text{argmin}} \quad & \|\Phi\boldsymbol{\alpha} - \boldsymbol{y}\|_2^2 \\ \text{s.t.} \quad & \|\boldsymbol{\alpha}\|_1 \leq \tau \end{aligned} \tag{LASSO}$$

At the same time, Chen [19, 18] proposed *basis pursuit* and the noise-aware variant *basis purusuit denoising* which used an $\ell_1$ penalty in a signal processing context.

$$\begin{aligned} \underset{\boldsymbol{\alpha}}{\text{argmin}} \quad & \|\boldsymbol{\alpha}\|_1 \\ \text{s.t.} \quad & \|\Phi\boldsymbol{\alpha} - \boldsymbol{y}\|_2 \leq \eta. \end{aligned} \tag{BPDN}$$

The two methods are equivalent in the sense that for any $\tau$, there exists an $\eta$ that will yield the same solution. When referring to $\ell_1$-methods in general, we use the Lagrangian form

$$\boldsymbol{\alpha}^* = \underset{\boldsymbol{\alpha}}{\text{argmin}} \quad \|\Phi\boldsymbol{\alpha} - \boldsymbol{y}\|_2^2 + \lambda\|\boldsymbol{\alpha}\|_1 \tag{$P_1^\lambda$}$$

The defining feature of the $\ell_1$ penalty is that it tends to produce estimates $\boldsymbol{\alpha}^*$ that were *sparse*. That is, some of the coefficients $\alpha_j$ would be set exactly to zero. This is behavior can be see seen by the closed form solution of $P_1^\lambda$ when $\Phi^T\Phi = I$,

$$\alpha_j^* = sgn(\alpha_j^{LS})(|\alpha_j^{LS}| - \lambda)_+, \quad j = 1, \ldots, M+1, \tag{2.24}$$

where $\alpha_j^{LS}$ is the $j^{\text{th}}$ component of the least squares solution $\boldsymbol{\alpha}^{LS}$ and $(z)_+ = \max(z, 0)$ Unlike popular penalized estimators before it (e.g. ridge regression [52]), this property allowed the estimator to perform *variable selection*. While $\ell_q$ penalties, $0 < q < 1$ also induce sparsity in the solution [42], the $\ell_1$ penalty is convex (although not strictly) and can be solved efficiently. In particular, LASSO and $P_1^\lambda$ can be written as a linear program (LP) and BPDN can be written as a second order cone program (SOCP).

### 2.4.2 Consistency

The *consistency* of $P_1^\lambda$ describe its behavior in the presence of infinitely many data points and is a measure of an estimators utility. Consistency in estimation ensures that as the number of samples $m \to \infty$, we converge in probability to the coefficients in the $\ell_2$ norm. Consistency in model selection ensures that the support of the estimate converges in proability to the support of the true coefficients. While consistency is not guaranteed for an arbitrary set of basis functions [56, 98, 97, 60], consistency in estimation and model selection hold for the tensor product Legendre polynomials, when the inputs sampled from an orthogonalizing probability distribution and an appropriate growth rate on $\lambda = \lambda(m)$. Furthermore, while the solution to $P_1^\lambda$ may not always have a unique solution, again, the choice of basis functions ensure the solution is unique with probability one [86].

# Chapter 3

# Quadrature subsampling for sparse recovery

The generalized polynomial chaos (gPC) approximates a quantity of interest (QoI) by projecting it onto the space spanned by a set of multivariate basis functions. Generally, these basis functions are tensor-products of univariate polynomials that belong to a set of orthogonal polynomials. For many responses, we can efficiently project onto this space via high-order quadrature. For example, the classic result of numerical integration [26] tells us the amount of work required to achieve a prescribed accuracy decreases exponentially with the smoothness of a function. Quadrature allows us to perform this projection efficiently to machine precision for many responses of interest. Unfortunately, the work also *increases* exponentially with the number of uncertainties i.e. variables. As we explore more realistic UQ problems, the number of uncertainties inevitably grow. In this high dimensional setting, the challenge is to accurately estimate the gPC efficiently, necessitating as few computer simulations as possible.

The field of compressed sensing [11, 34, 15] offers promising insight. It suggests that the computational cost of estimation should only scale with the number of basis functions that have nonzero correlation with the response. That is, the cost should not grow with the dimensionality of the problem or the number of basis functions,

but the *sparsity* of the problem. Like smoothness, sparsity is a form of regularization imposed on a solution. And since most engineering problems are related to an underlying physical process, we expect a reasonable degree of regularity. Indeed, the work of [87, 35, 4] show that under weak assumptions, the solution exhibits sparsity in the properly chosen basis. Unfortunately, the conventional compressed sensing methodology gives up some favorable properties of quadrature based methods. For example, error estimates of are only given in the probabilistic sense. Also, the performance of compressed sensing is dependent on the sparsity of the solution, which makes its applicability questionable in low dimensions where quadrature is efficient. This makes it is unclear at which dimensionality one should switch to a compressed sensing methodology. As the two approaches are not compatible, this potentially wastes many simulations if the analysis must be restarted.

This work offers a new approach to the compressed sensing method for estimating gPC by structured sampling on quadrature points. It extends the idea of "subsampling" from discretized orthonormal systems such as the Discrete Fourier Transform [8, 9]. It bridges the quadrature and compressed sensing methodologies, and as a consequence, preserves many of the favorable properties lost by the current approaches. In the next section, we give an brief overview of generalized polynomial chaos and present some relevant results from the compressed sensing literature. Then, we provide a short review of Gaussian quadrature, introduce the Discrete Legendre Transform as a discretization of the Legendre polynomial system, and give the theorems for recovering Legendre PC when sampling from the discretized system. Finally, we compare our proposed sampling scheme against others presented in the literature via some numerical experiments.

## 3.1 Generalized polynomial chaos expansions

"Homogeneous chaos" was coined by Norbert Wiener [92] as the span of Hermite polynomial functionals in a sequence of independent Gaussian random variables. Cameron and Martin [7] showed that such expansions exist for any $L^2$ functional; that is, the span of Hermite polynomial functionals are dense in $L^2$. It's inception in UQ started

with Ghanem and Spanos [45] who used the polynomial chaos in the finite element method for solving stochastic partial differential equations. Later, Xiu and Karniadakis [93] generalized the notion by considering polynomial functionals belonging to the Askey scheme of polynomials and Ernst [39] established that such convergent expansions exist. Here, we review some basic concepts and assumptions and introduce notation useful for the remainder of the paper.

Given an abstract probability space $(\Omega, \mathcal{F}, P)$, let $Y$ be an arbitrary random variable in $L^2(\Omega, \mathcal{F}, P)$. The idea is to represent $Y$ by a countable number $p \in \mathbb{N}_0$ of independent random variables $\xi_1, \ldots, \xi_p$ where $\xi_k$ takes values on the probability space $(\mathbb{R}, \mathcal{B}(\mathbb{R}), F_{\xi_k}(dx_k))$. These are commonly called the "basic random variables" are denoted $\boldsymbol{\xi} \in \mathbb{R}^p$. For $k = 1, \ldots, p$, we assume the measures $F_{\xi_k}(dx_k)$ has bounded moments of all order and are continuous. It follows that each measure admits an associated sequence of orthonormal polynomials that form an orthonormal system in $L^2(\Omega, \sigma(\xi_k), P)$ where $\sigma(\xi_k)$ is the $\sigma-$algebra generated by $\xi_k$. Denoting $\{p_j^{(k)}(\xi_k)\}_{j\in\mathbb{N}_0}$ to be the polynomials orthonormal with respect to $F_{\xi_k}$, we define a set tensor-product polynomials given by

$$p_{\boldsymbol{\alpha}}(\boldsymbol{\xi}) = \prod_{k=1}^{p} p_{\alpha_k}^{(k)}(\xi_k), \quad \boldsymbol{\alpha} = (\alpha_1, \ldots, \alpha_p) \in \mathbb{N}_0^p \tag{3.1}$$

This sequence of polynomials form a complete orthonormal system for $L^2(\Omega, \sigma(\boldsymbol{\xi}), P)$. For any $Y$ measurable with respect to $\boldsymbol{\xi}$ i.e. $\mathcal{F} \subseteq \sigma(\boldsymbol{\xi})$, the Doob-Dynkin Lemma [68] ensures the existence of a measurable function $f : Y = f(\boldsymbol{\xi})$. Define the projection operator $\mathcal{P} : L^2(\Omega, \mathcal{F}, P) \to L^2(\Omega, \sigma(\boldsymbol{\xi}), P)$. Then the *generalized polynomial chaos (gPC) expansion* of $Y$ is given by

$$Y = \mathcal{P}Y = \sum_{\boldsymbol{\alpha}\in\mathbb{N}_{\mathbf{0}}^{\boldsymbol{p}}} a_{\boldsymbol{\alpha}} p_{\boldsymbol{\alpha}}(\boldsymbol{\xi}) \tag{3.2}$$

where the coefficients $a_{\boldsymbol{\alpha}}$ are given by the inner product

$$a_{\boldsymbol{\alpha}} = \langle Y, p_{\boldsymbol{\alpha}} \rangle = \int_{\mathbb{R}^p} f(\boldsymbol{x}) p_{\boldsymbol{\alpha}}(d\boldsymbol{x}) F_{\boldsymbol{\xi}}(d\boldsymbol{x}) \tag{3.3}$$

In this paper, we consider the basic random variables to be uniform random variables $\xi_k$ that take values in $([-1,1], \mathcal{B}([-1,1]), \nu)$ where $\nu$ is the normalized Lebesgue measure. This measure is associated to the orthonormal Legendre polynomials and in the sequence of independent uniform random variables it forms the *Legendre polynomial chaos*. In what follows, we will use Legendre polynomial chaos and gPC interchangeably unless noted or is made obvious from context.

For computational purposes, we truncate the expansion to a finite number of terms. This occurs in two ways. First, we make the customary *finite dimensional noise* assumption [2] which states that the stochasticity in $Y$ can be described by a finite number of random variables (i.e. $p < \infty$). Second, we truncate the infinite series to a finite number of terms. Usually, this is defined by the set of polynomials of maximal total degree $r$. That is, the set of polynomials $\{p_{\boldsymbol{\alpha}}\}_{\boldsymbol{\alpha}\in\mathcal{A}_r^p}$ where

$$\mathcal{A}_r^p = \{\boldsymbol{\alpha} \in \mathbb{N}_0^p : \sum_{k=1}^{p} \alpha_k \leq r\}, \quad M = |\mathcal{A}_r^p| = \binom{r+p}{p} \tag{3.4}$$

In general, define $\mathcal{P}_{\mathcal{A}}$ to be the projection onto the subspace spanned by $\{p_{\boldsymbol{\alpha}}\}_{\boldsymbol{\alpha}\in\mathcal{A}}$. Our task is to estimate the projected function

$$f_{\mathcal{A}}(\boldsymbol{\xi}) := \mathcal{P}_{\mathcal{A}} Y = \sum_{\boldsymbol{\alpha}\in\mathcal{A}} a_{\boldsymbol{\alpha}} p_{\boldsymbol{\alpha}}(\boldsymbol{\xi}) \tag{3.5}$$

## 3.2 Compressed sensing

Compressed sensing can be summarized as methods devoted to determining the minimal number $m$ of linear, non-adaptive measurements that can recover signals $\boldsymbol{a} \in \mathbb{R}^M$ with at most $s$ non-zero components. Formally, let $A$ be a $m \times M$ *measurement matrix* used to measure the signal and $\boldsymbol{y} \in \mathbb{R}^m$ be the resulting observations, corrupted with additive noise $\eta \in \mathbb{R}_+$. We wish to recover $\boldsymbol{a}$, $\|\boldsymbol{a}\|_0 = \#\{a_i : a_i \neq 0\} = s$, from the linear system $\boldsymbol{y} = A\boldsymbol{a} + \boldsymbol{\epsilon}$. For the case $m < M$, the system is under-determined and has infinitely many solutions. Having the knowledge that our solution is *sparse*,

we solve the basis pursuit de-noising problem [18, 29, 88, 83], which we denote $(P_1^\eta)$.

$$\hat{\boldsymbol{a}} = \underset{\boldsymbol{a}}{\operatorname{argmin}} \|\boldsymbol{a}\|_1 \text{ subject to } \|\boldsymbol{y} - A\boldsymbol{a}\|_2 \leq \eta \qquad (P_1^\eta)$$

For $\eta = 0$, this is simply the *basis pursuit* problem[19].

$$\hat{\boldsymbol{a}} = \underset{\boldsymbol{a}}{\operatorname{argmin}} \|\boldsymbol{a}\|_1 \text{ subject to } A\boldsymbol{a} = \boldsymbol{y} \qquad (P_1)$$

In our case, $A$ is the matrix whose columns are the multivariate Legendre polynomials $\{p_{\boldsymbol{\alpha}}\}_{\boldsymbol{\alpha}\in\mathcal{A}_r^p}$, and the signal is the vector of gPC coefficients. Its rows are point evaluations of the basis functions at the points $\boldsymbol{\xi}_1, \ldots, \boldsymbol{\xi}_m$. (A careful reader will notice that $A$ is in fact a composition of a point measurement matrix and a sparsifying set of basis functions). Since the observations are computer simulations, we do not have noise (in the statistical sense) but rather error from the terms not in $\mathcal{A}_r^p$; i.e. truncation error. Under certain conditions on $\boldsymbol{a}$ and $A$, $(P_1^\eta)$ is guaranteed to yield the true solution. This remarkable result allows one to considerably reduce the number of evaluations when estimating expansions with large number of terms, an unavoidable consequence in problems of high dimension. In the next section, we review some general conditions for which this holds. We then give the main results in the specific case of estimating univariate and multivariate Legendre chaos expansions.

### RIP-based undersampling limits

In addition to sparsity or near sparsity in the solution vector, the success of recovering the solution in extremely underdetermined systems relies on the properties of the measurement matrix. Namely, the columns of the matrix cannot be too "similar". Researchers have identified several different versions of this notion (e.g. spark, mutual coherence, null space property) and corresponding conditions they must satisfy. This work utilizes the most common among them: the Restricted Isometry Property [13].

**Theorem 3.2.1.** Restricted isometry constant. [13, 12, 14] *Let $A \in \mathbb{R}^{m\times M}$. For $s \leq M$, the restricted isometry constant $\delta_s$ associated to $A$ is the smallest number for*

*which*

$$(1-\delta_s)\|\boldsymbol{a}\|_2^2 \leq \|A\boldsymbol{a}\|_2^2 \leq (1+\delta_s)\|\boldsymbol{a}\|_2^2 \tag{3.6}$$

*for all s-sparse vectors* $\boldsymbol{a} \in \mathbb{R}^M$.

We can view this constant as a bound on the eigenvalues of the Grammians for all possible submatrices formed by taking $s$ columns of $A$. The size of this bound determines whether or not a coefficient is recoverable when "measured" by $A$. The next theorem gives a a sufficient condition on the RIP constant such that $\boldsymbol{a}$ is recoverable via $(P_1^\eta)$.

**Theorem 3.2.2.** Recovery conditions for $A$ [12, 41, 10]. *Let* $A \in \mathbb{R}^{m\times M}$ *and assume that the restricted isometry constant of A satisfies*

$$\delta_{2s} < 3/(4+\sqrt{6}) \tag{3.7}$$

*Let* $\boldsymbol{a} \in \mathbb{R}^M$ *and assume noisy measurements* $\boldsymbol{y} = A\boldsymbol{a} + \boldsymbol{\epsilon}$ *are given with* $\|\boldsymbol{\epsilon}\|_2 \leq \eta$. *Then, the solution to* $(P_1^\eta)$ *satisfies*

$$\|\boldsymbol{a} - \hat{\boldsymbol{a}}\|_2 \leq C_1 \frac{\sigma_s(\boldsymbol{a})_1}{\sqrt{s}} + C_2\eta \tag{3.8}$$

*where*

$$\sigma_s(\boldsymbol{z})_p = \inf_{\boldsymbol{y}:\|\boldsymbol{y}\|_0\leq s} \|\boldsymbol{y} - \boldsymbol{z}\|_p$$

*is the best s-term approximation.* $C_1, C_2$ *only depend on* $\delta_{2s}$. *If* $\boldsymbol{a}$ *is s-sparse and the measurements are noiseless, then recovery is exact i.e.* $\hat{\boldsymbol{a}} = \boldsymbol{a}$.

This result states that Grammians of all $2s$ submatrices of $A$ must be well conditioned in order to accurately an $s$-sparse vector. For a general matrix, it is not possible to determine $\delta_{2s}$, and deterministic constructions are not known for an arbitrary set of basis functions. Instead, the current approach is to generate matrices randomly and satisfy the condition with high probability. One class of structured

random matrices arises from *bounded orthonormal systems* to which the system of Legendre polynomials belongs.

**Definition 3.2.3.** Bounded orthonormal systems. *Let $\phi_j$, $j \in [N]$ be an orthonormal system of functions with respect to the measure $\nu(\xi)$ on $\mathcal{D}$*

$$\int_{\mathcal{D}} \phi_j(\xi)\phi_k(\xi)d\nu(\xi) = \delta_{jk}, \quad j,k \in [N] \tag{3.9}$$

*If this system is uniformly bounded*

$$\sup_{j\in[N]} \|\phi_j\|_\infty = \sup_{j\in[N]} \sup_{\xi\in\mathcal{D}} |\phi_j(\xi)| \leq K \tag{3.10}$$

*for some constant $K \geq 1$, then the system $\{\phi_j\}$ is a bounded orthonormal system.*

For such systems, we can give a precise undersampling rate for which the coefficients vector can be recovered with high probability when we solve $(P_1^\eta)$.

**Theorem 3.2.4.** Recovery for bounded orthonormal systems. [70] *Consider the matrix $A \in \mathcal{C}^{m\times M}$ with entries*

$$A_{i,j} = \phi_j(\xi_i), \quad j \in [M], i \in [m] \tag{3.11}$$

*formed by i.i.d. samples $\xi_i$ drawn from the orthogonalizing measure $\nu$ with uniform bound $K \geq 1$. Assuming that*

$$m \geq C\delta^{-2}K^2 s \log^3(s)\log(M) \tag{3.12}$$

*then with probability at least $1 - M^{-\gamma\log^3(s)}$, the restricted isometry constant $\delta_s$ of $\frac{1}{\sqrt{m}}A$ satisfies $\delta_s \leq \delta$. The constants $C, \gamma > 0$ are universal. Further, the coefficient $\boldsymbol{a}$ is recoverable up to a factor of its best s-term approximation and a factor of its noise level $\frac{1}{\sqrt{m}}\|\boldsymbol{\epsilon}\|_2 \leq \eta$ by solving $(P_1^\eta)$ as given in (3.8).*

Theorem 3.2.4 tells us that for an arbitrary bounded orthonormal system, the allowable degree of undersampling is determined by the system bound $K$. In the next

section, we apply this result to systems of univariate and tensor product Legendre polynomials.

### Recovery of sparse Legendre polynomials

For a given set of basis functions, it remains only to choose the evaluation points $\boldsymbol{\xi}_i$, $i = 1, \ldots, m$. In one dimension, Rauhut [69] gave the optimality of randomly drawing the evaluation points according to the Chebyshev measure and solving the $(P_1^\eta)$ problem for the modified system of equations.

**Theorem 3.2.5.** Noise stable recovery of Legendre-sparse polynomials [69]. *Suppose $m$ evaluation points $\xi_1, \xi_2, \ldots, \xi_m \in [-1, 1]$ are drawn from the Chebyshev measure $d\mu(\xi) = \pi^{-1}(1 - \xi^2)^{-1/2} d\xi$. Consider the $m \times M$ Legendre Matrix $A_{jk} = p_{k-1}(\xi_j)$ for $k = 1, \ldots M$, the $m \times m$ diagonal matrix $D$ with entries $D_{jj} = \sqrt{\frac{\pi}{2}}(1 - \xi_j^2)^{1/4}$, and $m$-vector of simulations $y_j = f(\xi_j)$, $j = 1, \ldots, m$. Let $\frac{1}{\sqrt{m}}\|D\boldsymbol{\epsilon}\|_2 \leq \eta$ and set $\boldsymbol{y} := \frac{1}{\sqrt{m}}\boldsymbol{y}$ and $A := \frac{1}{\sqrt{m}}DA$. If*

$$m \geq Cs \log^3(s) \log(M) \tag{3.13}$$

*then with probability exceeding $1 - M^{-\gamma \log^3(s)}$ the coefficient $\boldsymbol{a}$ is recoverable up to a factor of its best $s$-term approximation and a factor of its noise level $\eta$ by solving $(P_1^\eta)$ as given in (3.8).*

The "pre-conditioning" performed by $D$ ensures the resulting system is bounded orthonormal when sampled under the Chebyshev measure. More importantly, the preconditioning produces a bounding constant that does not scale with $M$, unlike sampling on the uniform measure. Recovery of multi-variate tensor product Legendre polynomials is simply the tensor product analogue of the univariate case.

**Theorem 3.2.6.** Recovery of multivariate Legendre polynomials via preconditioned Chebyshev sampling [94]. *Suppose $m$ evaluation points $\boldsymbol{\xi}_1, \boldsymbol{\xi}_2, \ldots, \boldsymbol{\xi}_m \in [-1, 1]^p$ are*

*drawn from the product Chebyshev measure,*

$$d\mu(\boldsymbol{\xi}) = \prod_{i=1}^{p} \pi^{-1}(1-\xi_i^2)^{-1/2} d\xi_i \tag{3.14}$$

*Consider the $m \times M$ Legendre Matrix $A$ which has columns $A_{jk} = p_{\boldsymbol{\alpha}_k}(\boldsymbol{\xi}_j)$, for $k = 1, \dots M$ and $\boldsymbol{\alpha}_k \in \mathbb{N}_0^p$, the $m \times m$ diagonal matrix $D$ with entries $D_{jj} = \prod_{i=1}^{p} \sqrt{\frac{\pi}{2}}(1-\xi_{ji}^2)^{1/4}$, and $m$-vector of simulations $y_j = f(\boldsymbol{\xi}_j)$. Let $\frac{1}{\sqrt{m}}\|D\boldsymbol{\epsilon}\|_2 \leq \eta$ and set $\boldsymbol{y} := \frac{1}{\sqrt{m}}\boldsymbol{y}$ and $A := \frac{1}{\sqrt{m}}DA$. If*

$$m \geq 3^p C s \log^3(s) \log(M) \tag{3.15}$$

*then with probability exceeding $1 - M^{-\gamma \log^3(s)}$ the coefficient $\boldsymbol{a}$ is recoverable up to a factor of its best $s$-term approximation and a factor of its noise level $\|\boldsymbol{\epsilon}\|_\infty \leq \eta$ by solving $(P_1^\eta)$ as given in (3.8).*

Notice that we are free to use any degree $p$-variate Legendre polynomial $p_{\boldsymbol{\alpha}}$. We can obtain an improved result if we define the spanning subspace. When $p > r$, and we limit the basis functions by total degree $\{p_{\boldsymbol{\alpha}}\}_{\boldsymbol{\alpha} \in \mathcal{A}_r^p}$, Yan et al [94] gives a better approach for selecting evaluation points. Namely, if the evaluation points are selected uniformly random over the hypercube $[-1,1]^p$, then RIP-based undersampling limit scales independently of dimension.

**Theorem 3.2.7.** Recovery of multivariate Legendre polynomials via uniform sampling [94]. *Let $p \geq r$. Suppose $m$ evaluation points $\boldsymbol{\xi}_1, \boldsymbol{\xi}_2, \dots, \boldsymbol{\xi}_m \in [-1,1]^p$ are drawn from the product uniform measure,*

$$d\mu(\boldsymbol{\xi}) = \prod_{i=1}^{p} 1/2 d\xi_i \tag{3.16}$$

*Consider the $m \times M$ Legendre Matrix $A$ which has columns $A_{jk} = p_{\boldsymbol{\alpha}_k}(\boldsymbol{\xi}_j)$ for $\boldsymbol{\alpha}_k \in \mathcal{A}_r^p$, and $m$-vector of simulations $y_j = f(\boldsymbol{\xi}_j)$. Let $\frac{1}{\sqrt{m}}\|\epsilon\|_2 \leq \eta$ and set $\boldsymbol{y} := \frac{1}{\sqrt{m}}\boldsymbol{y}$ and*

$A := \frac{1}{\sqrt{m}} A$. *If*

$$m \geq 3^r C s \log^3(s) \log(M) \tag{3.17}$$

*then with probability exceeding* $1 - M^{-\gamma \log^3(s)}$ *the coefficient* $\boldsymbol{a}$ *is recoverable up to a factor of its best s-term approximation and a factor of its noise level* $\|\boldsymbol{\epsilon}\|_\infty \leq \eta$ *by solving* $(P_1^\eta)$ *as given in (3.8).*

*Proof.* The Legendre polynomials are bounded by the relation

$$\|p_{\alpha_k}\|_\infty = \sqrt{2\alpha_k + 1} \tag{3.18}$$

where the supremum occurs at the end points of the domain $[-1, 1]$. Equivalently, the a $p$-variate tensor product Legendre polynomials satisfy

$$\|p_{\boldsymbol{\alpha}}\|_\infty = \prod_{k=1}^{p} \sqrt{2\alpha_k + 1} \tag{3.19}$$

For $p \geq r$, the supremum for the set of restricted set of polynomials $\{p_{\boldsymbol{\alpha}}\}_{\boldsymbol{\alpha} \in \mathcal{A}_r^p}$ is attained for those polynomials whose multi-index has $r$ ones and $p - r$ zeros. It follows from (3.19) that

$$\sup_{\boldsymbol{\alpha} \in \mathcal{A}_r^p} \|p_{\boldsymbol{\alpha}}\|_\infty = 3^{r/2} \tag{3.20}$$

□

## 3.3 Gauss quadrature

The orthonormal system formed by the set of multivariate Legendre polynomials and the scaled Lebesgue measure can be transformed into a discrete orthogonal system by Gauss quadrature following the discrete orthogonality property [43]. It is shown that the resulting discrete system is also suitable as a measurement matrix for the estimation of gPC coefficients through compressed sensing.

Numerical quadrature is the approximation of integrals using finite sums. Quadrature rules are defined by the choice of nodes and weights that characterize the terms of the finite sum. We are primarily interested in the use of Gauss quadrature rules.

**Theorem 3.3.1.** Gauss quadrature [81, 43]. *Let $[a, b]$ be a bounded real interval and $\mu(\xi)$ to be a probability measure supported on $[a, b]$. The $n$-point Gauss quadrature rule defined by the nodes $G_n = \{\xi_j^n\}$ and weights $W_n = \{w_j^n\}$ is written in the form*

$$\int_{[a,b]} f(\xi) d\mu(\xi) = \sum_{j=1}^{n} f(\xi_j^n) w_j^n + R_n(f) \tag{3.21}$$

*and has the following properties*

1. *The nodes $\{\xi_j^n\}$ are the zeros of the degree $n$ polynomial $p_n$ of the sequence of monic polynomials $\{p_k\}$ orthogonal w.r.t. $\mu(\xi)$. Further, they are mutually distinct and contained in the interior of $[a, b]$.*

2. *The weights $\{w_j^n\}$ are positive and $\sum_{j=1}^{n} w_j^n = \int_{[a,b]} d\mu(\xi)$ [Theorem 1.46, Gautschi]*

3. *For any $f$ which is integrable in the Riemann-Stieltjes sense the quadrature approximation converges*

$$\lim_{n\to\infty} R_n(f) = 0 \tag{3.22}$$

4. *Let $\mathbb{P}_{2n-1}$ to be the space of polynomials of degree $\leq 2n - 1$. Then, $R_n(f) = 0$ for all $f \in \mathbb{P}_{2n-1}$*

5. *Let $f \in C^{2n}([a, b])$ and the degree $n$ polynomial $p_n$ of the sequence of monic polynomials $\{p_k\}$ orthogonal w.r.t. $\mu(\xi)$. Then the remainder $R_n(f)$ can be expressed as*

$$R_n(f) = \frac{f^{(2n)}(\tau)}{(2n)!} \int_{[a,b]} p_n(\xi)^2 d\mu(\xi), \quad \tau \in (a, b) \tag{3.23}$$

As the rule depends on the measure, the nodes and the weights are related to the orthogonal polynomials associated to the same measure. We will consider the case $a = -1, b = 1$ and $d\mu(\xi) = 1/2\, d\xi$; this is known as the Gauss-Legendre quadrature. Taking Cartesian products of one dimensional rules, these results can be extended to the multi-dimensional case. Let $\boldsymbol{n} = (n_1, \ldots, n_p) \in \mathbb{N}^p$ be the multi-index that gives the number points for each of the $p$ univariate rules. Then, define

$$\mathcal{I}_{\boldsymbol{n}} = \{\boldsymbol{i} \ : \ \boldsymbol{i} \in \mathbb{N}^p,\, 1 \leq i_k \leq n_k,\, k = 1, \ldots, p\} \tag{3.24}$$

as the multi-indices that enumerate the nodes and weights on the tensor product rule. Similarly, define $G_{\boldsymbol{n}}$ to be the quadrature nodes,

$$G_{\boldsymbol{n}} = \left\{\boldsymbol{\xi_i} = \left(\xi_{i_1}^{n_1}, \xi_{i_2}^{n_2}, \ldots, \xi_{i_p}^{n_p}\right) \ : \ \boldsymbol{i} \in \mathcal{I}_{\boldsymbol{n}}\right\} \tag{3.25}$$

and $W_{\boldsymbol{n}}$ to be the set of weights

$$W_{\boldsymbol{n}} = \left\{ w_{\boldsymbol{i}} = \prod_{k=1}^{p} w_{i_k}^{n_k} \ : \ \boldsymbol{i} \in \mathcal{I}_{\boldsymbol{n}} \right\}. \tag{3.26}$$

Then, the quadrature-based estimate of the chaos coefficients (3.3) can be written as

$$a_{\boldsymbol{\alpha}}^{\boldsymbol{n}} = Q_{\boldsymbol{n}}(f) = \sum_{\boldsymbol{i} \in \mathcal{I}_{\boldsymbol{n}}} f(\boldsymbol{\xi_i}) p_{\boldsymbol{\alpha}}(\boldsymbol{\xi_i}) w_{\boldsymbol{i}} \tag{3.27}$$

Following Theorem 3.3.1, we can achieve an arbitrarily small error for a sufficiently large $n_i$, $i = 1, \ldots, p$. For a finite set of polynomials $\{\boldsymbol{\alpha}\}_{j=1}^{M}$, the coefficients in (3.27) can be compactly written in matrix notation.

**Definition 3.3.2.** Discrete Legendre Matrix (DLM). *Given an $n$-point Gauss Legendre with nodes $G_n = \{\xi_i^n\}$ and weights $W_n = \{w_i^n\}$, define the $n \times n$ diagonal matrix $\Sigma_n$ to have entries $\Sigma_{ii} = nw_i$ and the $n \times n$ matrix $\Phi_n$ whose columns are the orthonormal, Legendre polynomials $\{p_j\}_{j=0}^{n-1}$ evaluated at the quadrature nodes, $[\Phi_n]_{ij} = p_j(\xi_i)$.*

*Then, the univariate Discrete Legendre Matrix is given by*

$$L_n = \Sigma_n^{1/2} \Phi_n \tag{3.28}$$

*Further, given a multi-index* $\boldsymbol{n} = (n_1, n_2, \ldots, n_p)$*, define the* $p$*, univariate matrix pairs* $(\Sigma_{n_1}, \Phi_{n_1})$*,* $(\Sigma_{n_p}, \Phi_{n_p})$*, . . . ,* $(\Sigma_{n_p}, \Phi_{n_p})$ *as above. Then, the* $N \times N$ *multivariate Discrete Legendre Matrix is given by*

$$L_{\boldsymbol{n}} = \Sigma_{\boldsymbol{n}}^{1/2} \Phi_{\boldsymbol{n}} \tag{3.29}$$

*where*

$$\Sigma_{\boldsymbol{n}} = \bigotimes_{i=1}^{p} \Sigma_{n_i}, \quad \Phi_{\boldsymbol{n}} = \bigotimes_{i=1}^{p} \Phi_{n_i} \tag{3.30}$$

*and* $\otimes$ *denotes the Kronecker product.*

The definition of the DLM relates the choice of quadrature order $n$ to the set of polynomials $\{p_i\}_{i=0}^{n-1}$, and it follows from (4) of Theorem 3.3.1 that $L_n^T L_n = I_n$ where $I_n$ is the $n \times n$ identity matrix; it follows that $L_{\boldsymbol{n}}^T L_{\boldsymbol{n}} = I_N$ where $N = \prod_{i=1}^{p} n_i$ The columns of the DLM are given by the polynomials $\{p_{\boldsymbol{\alpha}_k}\}_{\boldsymbol{\alpha}_k \in \mathcal{Z}_p^{n-1}}$ sampled at the quadrature points $\boldsymbol{\xi_i} \in G_n$, and

$$\mathcal{Z}_p^{n-1} = \{\boldsymbol{\alpha} \in \mathbb{N}_0^p \, : \, \|\boldsymbol{\alpha}\|_\infty \leq n-1\} \tag{3.31}$$

The choice $r_i = n_i - 1$ is a convenient for this work, but in general, the quadrature order and the maximal polynomial order of the basis set need not be coupled. So long as $n_i \geq r + 1$, we have an orthonormal system. Let $\boldsymbol{y}$ be the vector of simulations evaluated at the quadrature nodes $y_i = f(\boldsymbol{\xi}_i)$ $i = 1, \ldots, |\mathcal{I}_{\boldsymbol{n}}|$. Then, the vector of Legendre polynomial chaos coefficients (3.27) is related to the DLM by

$$\boldsymbol{a^n} = L_{\boldsymbol{n}}^T \Sigma^{1/2} \boldsymbol{y} = \Phi_{\boldsymbol{n}}^T \Sigma_{\boldsymbol{n}} \boldsymbol{y} \tag{3.32}$$

Note that the operator $L_{\boldsymbol{n}}^T \Sigma^{1/2}$ is conceptually analogous to the discrete Fourier transform. It takes elements from a nominal space (time domain for the Fourier and $L^2$ for the DLM) and maps it onto the "frequency" space. Further, if $f$ is in the span of $\{p_{\boldsymbol{\alpha}} : \alpha_i < n_i,\, i = 1, \ldots, p\}$ and $\boldsymbol{n}$ is chosen according to the definition of the DLM, then the quadrature estimate (3.27) is exact.

The columns of the DLM are simply weighted versions of the Legendre polynomials evaluated at a finite set of points. Because the points correspond to quadrature nodes, they induce a sequence of discrete bounded orthonormal systems index by $\boldsymbol{n}$. We begin by establishing the bounding constant of the system.

**Lemma 3.3.3.** Asymptotic distribution of Gauss quadrature weights [81]. *Let $w_i^n \in W_n$, $x_i^n \in G_n$ be the weights and nodes to the n-point Gauss-Legendre quadrature rule. Then, the weights have a limiting distribution given by*

$$\lim_{n\to\infty} w_i^n = \frac{\pi}{2n}\sqrt{1-(x_i^n)^2} \tag{3.33}$$

*Further, the weights are bounded above by the limiting distribution*

$$\frac{w_i^n}{\frac{\pi}{2n}\sqrt{1-(x_i^n)^2}} \uparrow 1 \quad \text{as } n \to \infty \tag{3.34}$$

Relating the quadrature points to a limiting distribution, we can establish the bounding constant on the univariate DLM.

**Lemma 3.3.4.** Bound on univariate DLM. *For the univariate DLM, $L_n$, the magnitudes of its entries are bounded above*

$$\sup_{1\le i,j\le n} |[L_n]_{i,j}| < \sqrt{3} \tag{3.35}$$

*Proof.* Using the inequality from Theorem 7.3.3 of [81]

$$(1-x^2)^{1/4}|p_k(x)| < 2\pi^{-1/2}\left(1+\frac{1}{2k}\right)^{1/2}, \quad -1 \le x \le 1 \tag{3.36}$$

for $k \in \mathbb{N}$. Combining with Lemma (3.3.3), it follows that

$$\sup_{1\leq i,k<n} \sqrt{nw_i}|p_{k-1}(x_i)| \lesssim \sup_{1\leq i,k<n} \sqrt{\frac{\pi}{2}}(1-(x_i^n)^2)^{1/4}|p_{k-1}(x_i^n)| < \sqrt{3} \tag{3.37}$$

□

Now we are ready to give the bounds on the multivariate DLM.

**Lemma 3.3.5.** Bound on multivariate DLM. *For the multi-index $\boldsymbol{n} \in \mathbb{N}^p$ and $n_k < \infty$, $k = 1, \ldots, p$, let $N = |\mathcal{I}_{\boldsymbol{n}}|$. Then the elements of the $N \times N$ multivariate DLM have the property*

$$\sup_{1\leq i,j\leq N} |[L_{\boldsymbol{n}}]_{i,j}| < 3^{\frac{p}{2}} \tag{3.38}$$

*Proof.* The multivariate DLM is just a Kronecker product of univariate DLMs, and thus, it is bounded by the product of the univariate bound given in Lemma 3.3.4, $\prod_{i=1}^{p} \sqrt{3}$. □

**Theorem 3.3.6.** *Given a multi-index $\boldsymbol{n}$, let $\mathcal{I}_{\boldsymbol{n}}$ be the enumerating set over the associated quadrature nodes and weights. The columns of the DLM $L_{\boldsymbol{n}}$ form a discrete bounded orthonormal system under the uniform orthogonalizing measure*

$$\nu_u(\boldsymbol{\xi}) = |\mathcal{I}_{\boldsymbol{n}}|^{-1} \sum_{\boldsymbol{i}\in\mathcal{I}_{\boldsymbol{n}}} \delta(\boldsymbol{\xi} - \boldsymbol{\xi}_{\boldsymbol{i}}) \tag{3.39}$$

*where $\delta$ is the Dirac delta function and the system is uniformly bounded by the constant $K = 3^{\frac{p}{2}}$.*

*Proof.* The DLM bounding constant $K = 3^{\frac{p}{2}}$ was established in Lemma 3.3.5. It remains to show columns are orthogonal with respect to $\nu_u$. Let $l_k$ be the $k$-th column of $L_{\boldsymbol{n}}$. and $\Phi$ as in (3.30). Let $\phi_k$ denote the $k$-th column of $\Phi$. Then, the system $\{\phi_k\}$ is an orthogonal system with respect to the measure

$$\nu_w(\boldsymbol{\xi}) = \sum_{\boldsymbol{i}\in\mathcal{I}_{\boldsymbol{n}}} \delta(\boldsymbol{\xi} - \boldsymbol{\xi}_{\boldsymbol{i}}) w_{\boldsymbol{i}} \tag{3.40}$$

by orthogonality of the Legendre polynomials and result *(4)* of Theorem 3.3.1. Given the orthogonality property

$$\langle \phi_k, \phi_j \rangle_{\nu_w} = \sum_{\boldsymbol{i} \in \mathcal{I}_{\boldsymbol{n}}} p_k(\boldsymbol{\xi_i}) p_j(\boldsymbol{\xi_i}) w_{\boldsymbol{i}} \tag{3.41}$$

perform a change of measure by multiplying the right hand side by $|\mathcal{I}_{\boldsymbol{n}}|/|\mathcal{I}_{\boldsymbol{n}}|$

$$\langle \phi_k, \phi_j \rangle_{\nu_w} = |\mathcal{I}_{\boldsymbol{n}}|^{-1} \sum_{\boldsymbol{i} \in \mathcal{I}_{\boldsymbol{n}}} \sqrt{|\mathcal{I}_{\boldsymbol{n}}| w_{\boldsymbol{i}}} p_k(\boldsymbol{\xi_i}) \sqrt{|\mathcal{I}_{\boldsymbol{n}}| w_{\boldsymbol{i}}} p_j(\boldsymbol{\xi_i}) \tag{3.42}$$

$$= \langle l_k, l_j \rangle_{\nu_u} \tag{3.43}$$

□

We note that the limiting distribution corresponds to the "preconditioner" used for Chebyshev sampling in Theorem 3.2.5. This implies that the two systems should converge as $n \to \infty$. However, for finite $n$, there exists a considerable gap as evidenced in Figure 3.1a. The difference becomes more pronounced in high dimensions as evidenced by the comparative performance of the two systems, as shown in Section 3.5.

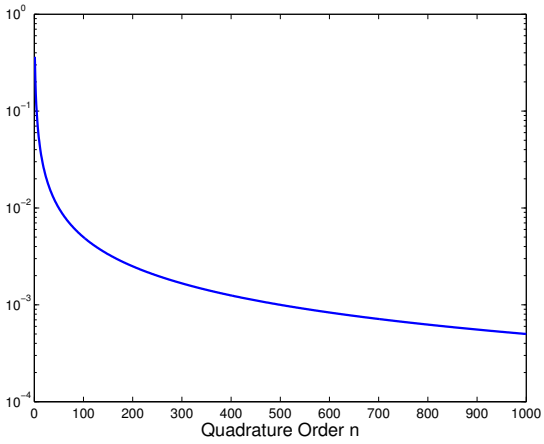


(a) $1 - \sup_{1 \le i \le n} \frac{w_i^n}{\frac{\pi}{2n}(1-(x_i^n)^2)^{1/2}}$

Figure 3.1: Convergence of quadrature weights to limiting distribution

## 3.4 Subsampling the Discrete Legendre Matrix

We propose an alternative approach to generating measurement matrix $A$. Since the DLM is a bounded orthogonal system, we can draw evaluation points according to the orthogonalizing measure $\nu_u$. Since the measure is distributed uniformly over the nodes, we can simply draw rows of the DLM randomly. We denote this randomly chosen matrix the partial DLM and give its recovery properties.

**Definition 3.4.1.** Partial DLM. *Let $L_{\boldsymbol{n}}$ be the $N \times M$ multivariate DLM. Also, let $\Omega \subset [N]$ be a subset of indices and $m = |\Omega| \leq N$. Define $R_\Omega$ as the operator that selects the $m$ rows indexed by $\Omega$. Then, the $m \times M$ partial DLM, $L_n^\Omega$, is defined as*

$$L_{\boldsymbol{n}}^\Omega = R_\Omega(L_{\boldsymbol{n}}) \tag{3.44}$$

**Theorem 3.4.2.** Recovery via partial DLM by independent row draws. *Suppose we take $m$ independent, random draws from $[N]$ and define this set to be $\Omega$. Since some samples may be repeated, $|\Omega| \leq m$. Additionally, let $\boldsymbol{y}$ be the vector simulations evaluated at the quadrature nodes $y_i = f(\boldsymbol{\xi}_{\boldsymbol{i}_1})$, $i = 1, \dots N$ and $\boldsymbol{\epsilon}$ to be the vector of errors $\epsilon_i = \phi_i^T \boldsymbol{a} - \boldsymbol{y}_i$, $i = 1, \dots, N$. If*

$$m \geq 3^p C s \ln^3(s) \ln(M), \tag{3.45}$$

*then with probability at least $1 - M^{-\gamma \ln^3(s)}$ the coefficient vector $\boldsymbol{a}$ is recovered via $(P_1^\eta)$ where $\boldsymbol{y} := \frac{1}{\sqrt{m}} R_\Omega(\Sigma_{\boldsymbol{n}}^{1/2} \boldsymbol{y})$, $A := \frac{1}{\sqrt{m}} L_{\boldsymbol{n}}^\Omega$ up to a factor if its best $s$-term approximation and a factor of its noise level $\| \frac{1}{\sqrt{m}} R_\Omega(\Sigma_{\boldsymbol{n}}^{1/2} \boldsymbol{\epsilon}) \|_2 \leq \eta$ by solving $(P_1^\eta)$ as given in (3.8).*

*Proof.* We have already established that the columns of the DLM form a bounded orthonormal system in Theorem 3.3.6. Then, the result follows directly from the Theorem 3.2.4. □

As a consequence of the finiteness of the system, randomly drawn evaluation points may selected more than once. Ideally, we resolve this issue by sampling without replacement. Unfortunately, under this model, the samples are no longer independent. Instead, consider drawing $m$ samples from all subsets of size $m$ uniformly at random.

This is known as simple random sampling [72] and is commonly used for sampling finite populations. We show that the recovery properties are preserved under this model.

**Theorem 3.4.3.** Recovery via partial DLM by simple random sampling. *Suppose we draw $m$ rows randomly from all the $m$-element subsets of $[N]$ and denote this set $\Omega$. Additionally, let $\boldsymbol{y}$ be the vector simulations evaluated at the quadrature nodes $y_i = f(\boldsymbol{\xi}_{\boldsymbol{i}_1})$, $i = 1, \dots N$ and $\boldsymbol{\epsilon}$ to be the vector of errors $\epsilon_i = \phi_i^T \boldsymbol{a} - \boldsymbol{y}_i$, $i = 1, \dots, N$. If*

$$m \geq 3^p C s \ln^3(s) \ln(M), \tag{3.46}$$

*then with probability at least $1 - M^{-\gamma \ln^3(s)}$ the coefficient vector $\boldsymbol{a}$ is recovered via $(P_1^\eta)$ where $\boldsymbol{y} := \frac{1}{\sqrt{m}} R_\Omega(\Sigma_{\boldsymbol{n}}^{1/2} \boldsymbol{y})$, $A := \frac{1}{\sqrt{m}} L_{\boldsymbol{n}}^\Omega$ up to a factor if its best $s$-term approximation and a factor of its noise level $\| \frac{1}{\sqrt{m}} R_\Omega(\Sigma_{\boldsymbol{n}}^{1/2} \boldsymbol{\epsilon}) \|_2 \leq \eta$ by solving $(P_1^\eta)$ as given in (3.8).*

*Proof.* Suppose the rows were selected as described in Theorem 3.4.2 and define this set to be $\Omega_0$. Then, $|\Omega_0| \leq |\Omega| = m$. Using Theorem 4.5 of [40], the probability of recovery by selecting the rows in $\Omega$ is bounded below by the probability of recovery for $\Omega_0$, $\Omega_0 \subset \Omega$ which is given in Theorem 3.4.2. Informally, the probability of recovery is nondecreasing as we add measurements. □

For $m = N$, the difference between the BPDN estimate and the quadrature estimate is given by $\eta$.

**Corollary 3.4.4.** Deviation from $\boldsymbol{a^n}$ for orthonormal design. *Let $m = N$ and $\boldsymbol{a^n} \in \mathbb{R}^N$ be the quadrature estimate using the $n$-point tensor product rule. Then, $\|\boldsymbol{a^n} - \hat{\boldsymbol{a}}\|_2^2 \leq \eta^2$. Namely, if $\eta = 0$, then the two estimates are equivalent.*

*Proof.* For $\boldsymbol{y} := \frac{1}{\sqrt{N}} \Sigma_{\boldsymbol{n}}^{1/2} \boldsymbol{y}$, $A := \frac{1}{\sqrt{N}} L_{\boldsymbol{n}}$, and $\boldsymbol{a^n} = A^T \boldsymbol{y}$, we can write the $(P_1^\eta)$ constraint as

$$\|A\hat{\boldsymbol{a}} - \boldsymbol{y}\|_2^2 = \hat{\boldsymbol{a}}^T A^T A \hat{\boldsymbol{a}} - 2\hat{\boldsymbol{a}}^T A^T \boldsymbol{y} + \boldsymbol{y}^T \boldsymbol{y} \leq \eta^2$$

Since $A^TA = I_N$, we can rewrite the constraint as

$$\begin{aligned}\|A\hat{\boldsymbol{a}} - \boldsymbol{y}\|_2^2 &= \hat{\boldsymbol{a}}^T A^T A\hat{\boldsymbol{a}} - 2\hat{\boldsymbol{a}}^T A^T\boldsymbol{y} + \boldsymbol{y}^T A^T A\boldsymbol{y} \\ &= \hat{\boldsymbol{a}}^T\hat{\boldsymbol{a}} - 2\hat{\boldsymbol{a}}^T\boldsymbol{a^n} + \boldsymbol{a^n}^T\boldsymbol{a^n} \\ &= \|\boldsymbol{a^n} - \hat{\boldsymbol{a}}\|_2^2\end{aligned}$$

□

## 3.5 Results to numerical experiments

In this section, we compare the practical performance of the three sampling approaches for problems of various dimensionality $p$ and degree $r$. In particular, we wish to understand the extreme cases when $p \gg r$ and $p \ll r$. We do this in two ways. First, we investigate the ability of each method to exactly recover purely sparse, finite polynomial expansions. This is shown using *phase diagrams* [32], which give the precise undersampling-sparsity trade off curve for each sampling method. Then, as more traditional in numerical analysis, we show detailed convergence plots of $\hat{\boldsymbol{a}}$ for various analytical functions. We include functions that cannot be expressed as a finite expansion and thus incurring an nonzero noise term. The numerical experiments were conducted in the MATLAB [59] computing environment and $(P_1^\eta)$, $(P_1)$ are solved using the convex optimization solver PDCO [76]. In what follows, we use the short hand notation of $\mathcal{S}_C$, $\mathcal{S}_U$, $\mathcal{S}_D$ to denote sampling from the Cheybshev measure (with pre-conditioning), sampling from uniform measure, and simple random sampling from the rows of the DLM, respectively.

### 3.5.1 Recovery of purely sparse functions via phase diagrams

Consider functions of the form $f(\boldsymbol{\xi}) = \sum_{j=1}^M a_{\boldsymbol{\alpha}_j} p_{\boldsymbol{\alpha}_j}(\boldsymbol{\xi})$ and suppose $\boldsymbol{a} \in \mathbb{R}^M$ is $s$-sparse. Drawing $m$ points from the orthogonalizing measure, we wish to know if it is possible to recover the true solution by solving $(P_1)$. Parameterize this problem instance by $\rho = s/m$ (sparsity) and $\delta = m/M$ (undersampling), and consider pairs

$(\delta, \rho)$ on the unit square $[0,1]^2$. In the seminal papers of Donoho and Tanner [30, 33, 28] and works following [31, 27], the authors show that the square partitions into a region in which the true solution can be recovered with nearly probability one, a region in which it cannot with nearly probability one, and a thin transition region. The width of the transition region converges to zero in the large system limit $s, m, M \to \infty$, and the transition from success to failure occurs sharply at a precise undersampling rate $\rho_{CG}(\delta)$, known as the *phase transition curve*. That is, it is not possible to recover $\boldsymbol{a}$ from $(P_1)$ for $(\delta, \rho)$ that lie above this curve, and recovery is guaranteed below it. This curve is shown in Figure 3.2.

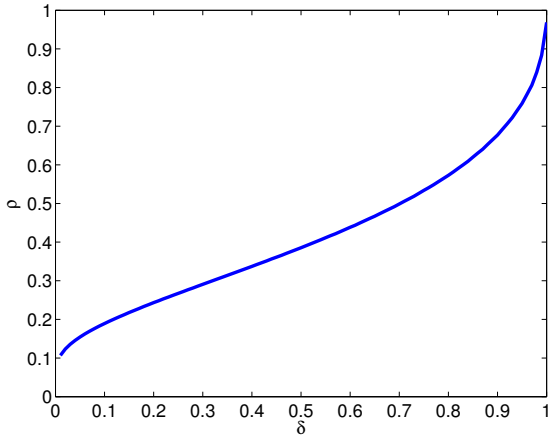


Figure 3.2: Asymptotic phase transition curve for $(P_1)$

This curve was derived assuming the measurement matrix is a Gaussian random matrix but has shown to apply for a variety of structured random matrices through extensive empirical testing [32, 61]. We compare the pure sparse recovery performance of the three sampling strategies by estimating their respective phase transition curves. For a given order and dimension, $(r, p)$, we consider sparse combinations of the polynomials $\{p_{\boldsymbol{\alpha}_k}\}_{\boldsymbol{\alpha}_k \in \mathcal{A}_p^r}$. Each instance $(\delta, \rho)$ is solved fifty times. For each instance, we randomly generate an $s$-sparse $\boldsymbol{a}$ whose nonzero entries are assigned according to the standard normal, draw the appropriate number of samples randomly and solve $(P_1)$. We consider a recovery "exact" if it satisfies $\|\boldsymbol{a} - \hat{\boldsymbol{a}}\|_2 \leq 10^{-5}$. Recording the number

of exact recoveries for each problem instance gives us a grid of "counts" from which we can estimate the phase transition curve. As consistent with the literature, the curve is estimated to be the set of points for which the probability of exact recovery is 0.5. We estimate this point for a fixed $\delta$ by fitting a two parameter logistic regression curve over $\rho$.

Let us consider the $p \leq r$ case. From the theorems above, we expect $\mathcal{S}_C$ to generally outperform $\mathcal{S}_U$ in this regime. Furthermore, we expect $\mathcal{S}_D$ to outperform $\mathcal{S}_C$ but have similar asymptotic performance $r \to \infty$; i.e. $\mathcal{S}_C$ is dominated by $\mathcal{S}_D$. The phase transition curves for $p$ and $r$ that satisfy this condition are given in Figure 3.3. For a fixed $p$ and increasing $r$, $\mathcal{S}_U$ diverges from the other curves towards poorer recovery. In contrast, aside from the $p = 1$ case, the curve for $\mathcal{S}_C$ is mostly unchanged and follows the theoretical curve closely. $\mathcal{S}_D$ is consistently the best performing but degrades for increasing $r$. This is consistent with the theoretical result that $\mathcal{S}_D$ has a smaller bounding constant, and thus better recovery performance, than $\mathcal{S}_C$ for finite $n$ but have the same performance as $r \to \infty$. For $p = 1$, $\delta = 1$ corresponds to the orthonormal design condition when samples are drawn according to $\mathcal{S}_D$. As expected, we observe exact recovery for the 50 out of 50 trials, independent of $r$. Surprisingly, $\mathcal{S}_C$ does not follow the theoretical performance as we'd expect, but this seems consistent with other investigations of $\mathcal{S}_C$ in the literature [69, 71].

Now let's consider the $p \geq r$ cases shown in Figure 3.4. For a fixed $r$ and increasing $p$, the trends of $\mathcal{S}_U$ and $\mathcal{S}_C$ are reversed. Notably, it becomes virtual impossible to recover the solution with $\mathcal{S}_C$ when $p > 80$; the effect of "preconditioning" produces a bounding constant that overwhelms the undersampling ability of compressed sensing. In contrast, $\mathcal{S}_U$ follows the theoretical curve increasingly closely as $p$ increases and is the only sampling method to do so as we approach very large dimensions. Interestingly, $\mathcal{S}_D$ has near theoretical performance even in this very different regime. Outside of very large dimension where performance begins to degrade slightly, $\mathcal{S}_D$ is competitive and occasionally better than $\mathcal{S}_U$, especially for $p \approx r$. More surprisingly, it is vastly better than $\mathcal{S}_C$. This highlights the significance of the gap between the bounding constants of the two sampling schemes for finite $n$ as described in Lemma 3.3.3. Unlike $\mathcal{S}_C$, the DLM allows us to prescribe the "right" amount of preconditioning

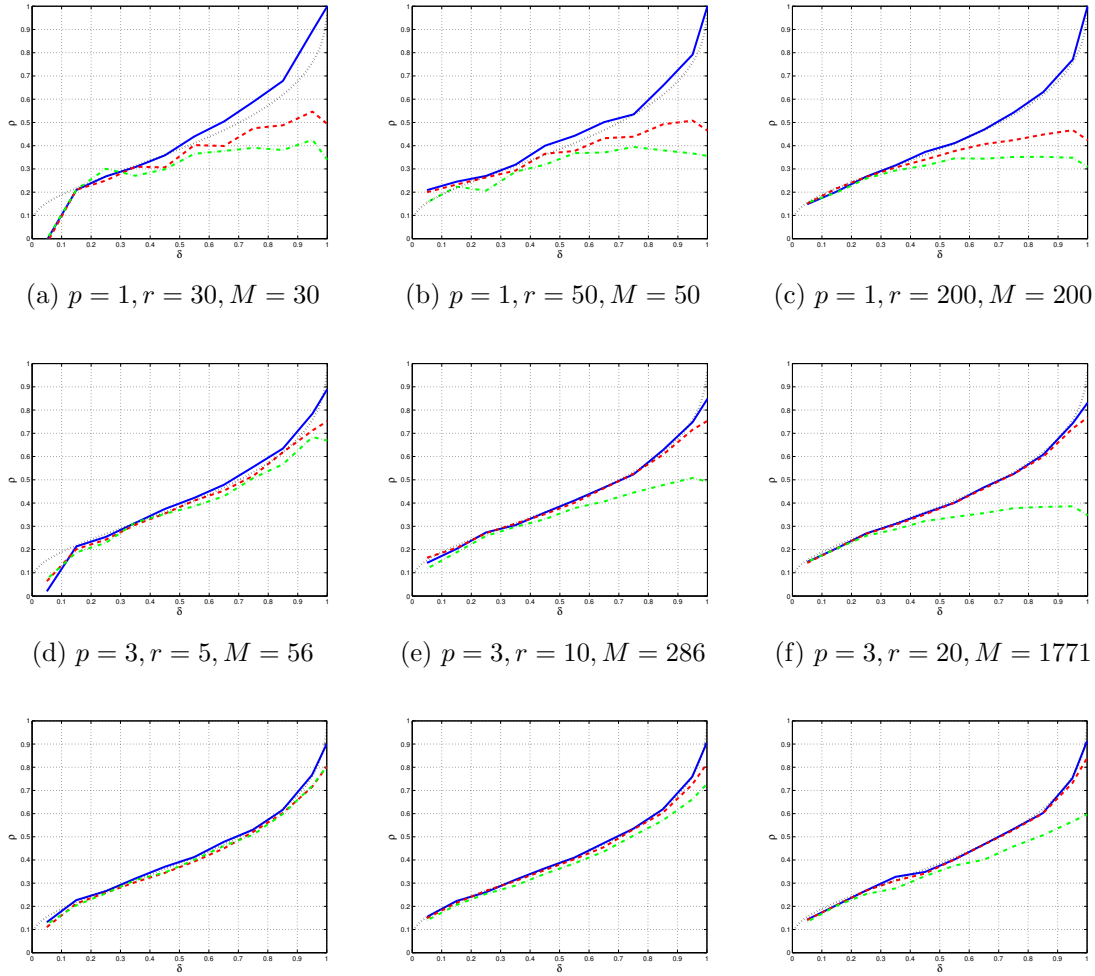

(a) $p = 1, r = 30, M = 30$ (b) $p = 1, r = 50, M = 50$ (c) $p = 1, r = 200, M = 200$

(d) $p = 3, r = 5, M = 56$ (e) $p = 3, r = 10, M = 286$ (f) $p = 3, r = 20, M = 1771$

(g) $p = 5, r = 5, M = 252$ (h) $p = 5, r = 7, M = 792$ (i) $p = 5, r = 10, M = 3003$

Figure 3.3: $p \leq r$. Empirical phase transition curves for sampling based on Chebyshev measure (dotted red), uniform measure (dotted green), and DLM (solid blue) compared to asymptotic phase transition curve (dotted black)

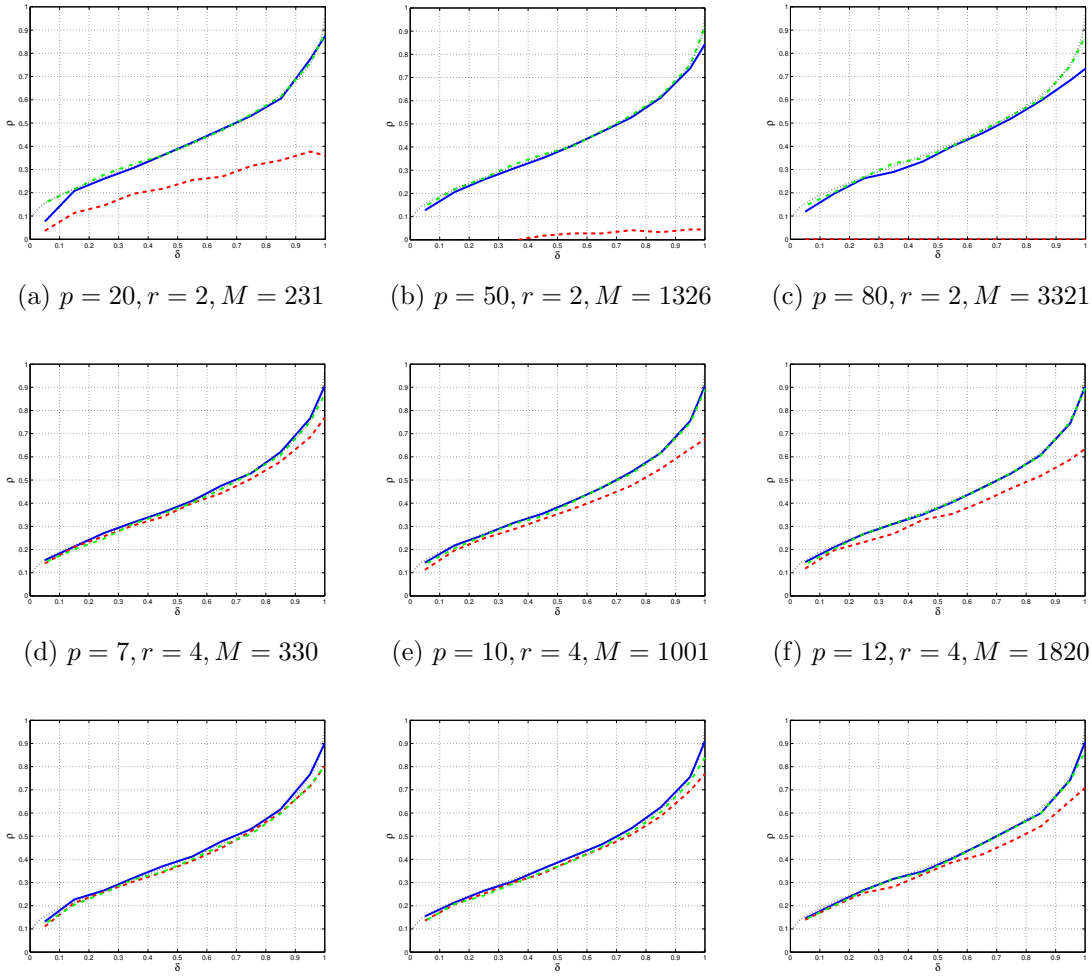

(a) $p = 20, r = 2, M = 231$ (b) $p = 50, r = 2, M = 1326$ (c) $p = 80, r = 2, M = 3321$

(d) $p = 7, r = 4, M = 330$ (e) $p = 10, r = 4, M = 1001$ (f) $p = 12, r = 4, M = 1820$

(g) $p = 5, r = 5, M = 252$ (h) $p = 7, r = 5, M = 792$ (i) $p = 10, r = 5, M = 3003$

Figure 3.4: $p \geq r$. Empirical phase transition curves for sampling based on Chebyshev measure (dotted red), uniform measure (dotted green), and DLM (solid blue) compared to asymptotic phase transition curve (dotted black)

through $\boldsymbol{n}$ for a given value of $r$ and results in a much smaller bounding constant in high dimensions. This gives $\mathcal{S}_D$ robustness across a variety of problem settings and is the only sampling scheme that does not have a pronounced difference in performance in the two regimes.

| Name | Definition | $p$ | $r$ | $n$ | $M$ |
|---|---|---|---|---|---|
| High-degree monomial | $x_1^{10}x_2^{10}$ | 2 | 20 | 21 | 231 |
| Rational Function | $\frac{1}{2+16(x_1-0.1)^2+25(x_2+0.1)^2}$ | 2 | 50 | 51 | 1326 |
| Generalized Rosenbrock | $\sum_{i=1}^{p}(1-x_i)^2+100(x_{i+1}-x_i^2)^2$ | 10 | 4 | 5 | 1001 |
| Sphere Function | $\sum_{i=1}^{p}x_i^2$ | 50 | 2 | 3 | 1326 |

Table 3.1: Analytical function definitions and parameters

### 3.5.2 Recovery of analytical functions

In general, functions do not have a finite representation in the Legendre polynomial basis. Here, we consider a few example functions of this form. Again we consider the two regimes of $p \gg r$ and $p \ll r$. The function definitions and the basis set $\mathcal{A}_r^p$ are given in Table 3.1. We use an *isotropic* DLM i.e. $\boldsymbol{n} = (n, n, \ldots, n)$ and specify the $n$ used for each function. Since the methods are inherently probabilistic, we give the *average case* error convergence by taking the sample average over a set of convergence curves. That is, given a function to estimate and a proposed sampling scheme, $(P_1^\eta)$ is solved for evaluation points of various sizes $m_1, m_2, \ldots$, generating an convergence curve for the error. Letting the corresponding sets of evaluation points to be $\Omega_1, \Omega_2, \ldots$, we enforce nestedness of the evaluation points $\Omega_1 \subset \Omega_2 \subset \ldots$. This mimics the manner in which estimation is done in practice. For each function, $n_{MC} = 50$ such curves are computed and their averages are given in Figure 3.5. For test functions not in the span of $\{p_{\boldsymbol{\alpha}}\}_{\boldsymbol{\alpha}\in\mathcal{A}_r^p}$, they may have a nonzero $\eta$. We assume this value is not known *a priori* and is estimated by five-fold cross-validation [35, 49].

The first two functions represent the $p \leq r$ case and their convergence plots are shown in Figure 3.5. The high-degree monomial can be expanded exactly in a finite Legendre chaos expansion but the convergence plot gives us a different look than that

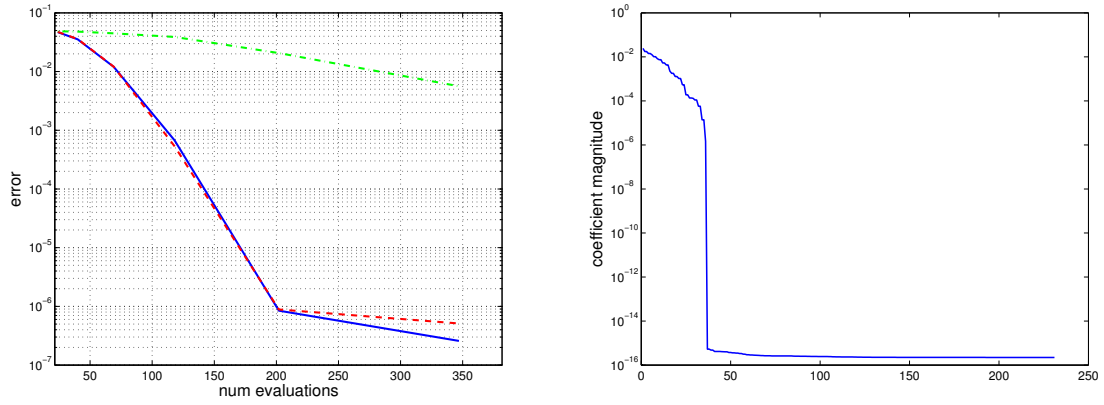


(a) High-degree monomial

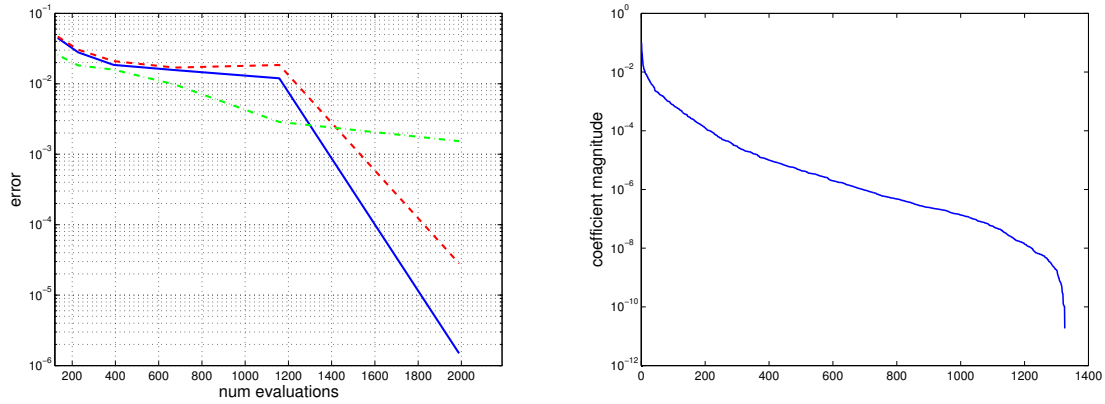


(b) Rational Function

Figure 3.5: $p \leq r$. **Left:** $\ell_2$ error $\|\boldsymbol{a} - \hat{\boldsymbol{a}}\|_2$ for sampling based on Chebyshev measure (dotted red), uniform measure (dotted green), and DLM (solid blue). **Right:** Coefficient magnitudes sorted in order of decreasing size.

offered by the phase diagram. We see that $\mathcal{S}_D$ and $\mathcal{S}_C$ converge smoothly and rapidly while $\mathcal{S}_U$ converges at a significantly slower rate, as expected in this regime. The rational function cannot be exactly represented by a sparse Legendre chaos expansion and has a nonzero noise $\hat{\eta}$. In addition, the coefficients are significantly less sparse and decay slowly. The result is a convergence plot that has a slow convergence region and rapid convergence region when sampling via $\mathcal{S}_C$ or $\mathcal{S}_D$. In contrast, $\mathcal{S}_U$ converges slowly throughout, slowing slightly in the region where the others accelerate.

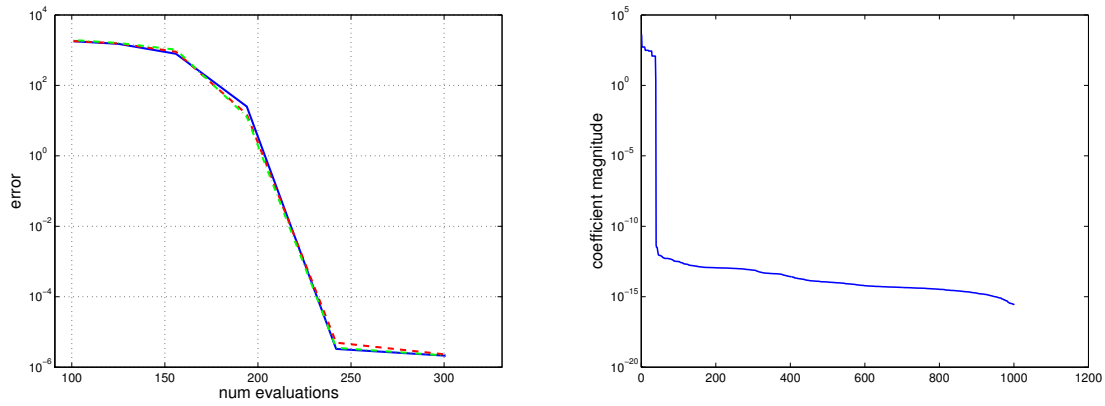


(a) Generalized Rosenbrock Function

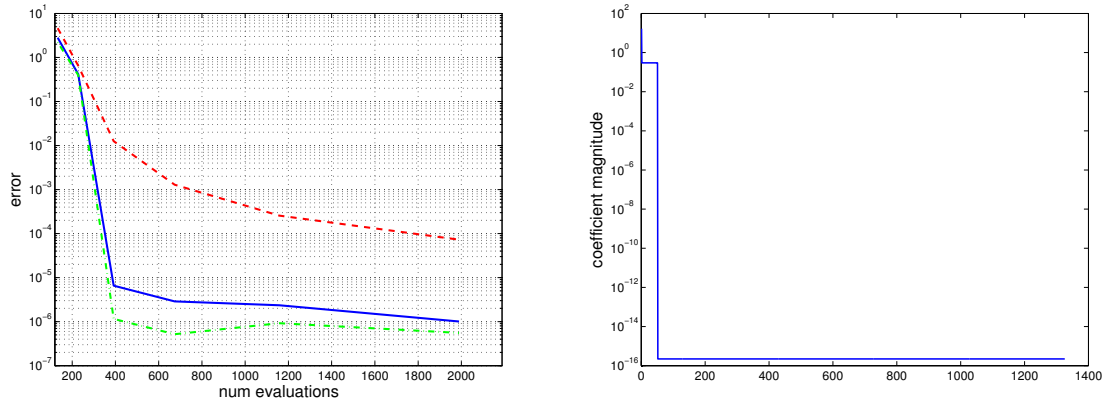


(b) Sphere Function

Figure 3.6: $p \geq r$. **Left:** $\ell_2$ error $\|\boldsymbol{a} - \hat{\boldsymbol{a}}\|_2$ for sampling based on Chebyshev measure (dotted red), uniform measure (dotted green), and DLM (solid blue). **Right:** Coefficient magnitudes sorted in order of decreasing size.

The next two functions represent the $p \geq r$ case and their convergence plots are given in Figure 3.6. From the phase diagrams, we'd expect $\mathcal{S}_C$ to slightly underperform the other two sampling methods in this regime, but the convergence plots are nearly identical across all methods. The sphere function is set in very high dimensions and the difference between the methods reveal themselves as expected from theory. Namely, $\mathcal{S}_U$ has the fastest convergence with $\mathcal{S}_D$ following closely and $\mathcal{S}_C$ converging at a much slower rate.

## 3.6 Discussion

In this work, we proposed a novel approach to estimating Legendre polynomial chaos expansions by solving the basis pursuit denoising problem on points subsampled from a tensor product quadrature rule or equivalently, forming the linear system by drawing rows from the partial DLM. We showed that it has asymptotic performance equal to another approach proposed in the literature where one samples from the Chebyshev distribution and applies a preconditioning on the basis pursuit denoising constraint. In the non-asymptotic regime, sampling from the rows of the DLM is shown to be better across all problem settings parameterized by dimension $p$ and maximal polynomial degree $r$. That is, it *dominates* the Chebyshev strategy in the decision theoretic sense. Furthermore, while sampling uniformly on the hypercube remains optimal for polynomial chaos expansions restricted to the span of $\mathcal{A}_r^p$, our approach remains competitive even for very high dimensions. Unlike the other two sampling approaches mentioned here, its performance is robust to the regimes of $p \gg r$ *and* $p \ll r$. Our sampling approach also has the advantage that sample space is finite and corresponds to the set evaluation points required for tensor product quadrature. This is important for practitioners who have already accrued a set of function responses evaluated at quadrature nodes and wish to use the compressed sensing methodology. While our work only involves Legendre chaos, many of the above results can be extended to the family of Jacobi polynomial chaos, of which Legendre is member.

# Chapter 4

# Derivative enhanced sparse estimation

The availability of derivative values can greatly enhance the construction of surrogates especially if those derivatives can be obtained inexpensively. For example, the full gradient for many CFD applications can be obtained for about the cost of an additional simulation run by solving the associated adjoint equations [55]. The utility of the gradient in high dimensional surrogate construction cannot be understated. pieces of information can dramatically reduce the computational cost required for a desired level of accuracy.

A direct application of derivatives for polynomial surrogates is through Hermite interpolation [48], where no estimation is required. The use of derivatives in parameter estimation is most common for Kriging, or more broadly, Gaussian process response surfaces [25, 57]. Chung and Alonso [21, 20, 22] explored the use of derivatives to estimate co-Kriging models for aerodynamic applications. Van Keulen and Vervenne used derivatives for polynomial regression models in formulations that included weighted least squares and multi-objective optimization [89, 91, 90].

In this chapter, we review some common approaches for incorporating derivative information in regression based estimation. Then, we introduce a naive sparse estimator by extending the basis pursuit denoising formulation to include derivatives and demonstrate some theoretical and practical deficiencies. We propose an alternative

sparse estimator that remedies the defects and has the ability to exploit sparsity in the derivatives. Finally, we address the larger question of whether derivative information is *as useful* as function information in estimating the polynomial approximation.

## 4.1 Augmenting ordinary least squares

The ordinary least squares (OLS) formulation is the most common way to estimate the coefficients $\{\alpha_j\}_{j=0}^{M}$. The OLS estimate minimizes the fitting error in the $\ell_2$ norm $F(\cdot) = \|\cdot\|_2$ without additional constraints $G(\cdot) = 0$. Formally, it is the solution to

$$\min_{\boldsymbol{\alpha}} \|\Phi\boldsymbol{\alpha} - \boldsymbol{y}\|_2 \tag{OLS}$$

For an "accurate" estimate, the standard rule of thumb is to *oversample* at a ratio of at least 2 [54]. That is, $m > 2(M+1)$. This corresponds to an overdetermined system and for a reasonable set of design points (e.g. in general position) the solution is unique (i.e. $\Phi$ has full column rank) and is available in closed form. However, $M$ grows rapidly in $p$ and for high dimensional UQ problems, $2(M+1)$ may be an infeasible number of samples. Suppose that in addition to the function values, the gradient vector were also given at each sample point. Then, following the previous rule of thumb, we could could potentially reduce the necessary number of samples by a factor of $p+1$.

### 4.1.1 Stacked ordinary least squares

One simple approach is to take the derivative (or in the case of multivariate approximation, the partial derivatives) of the truncated expansion and fit it to the point evaluation of the derivative. Let the derivative matrix $D^{(k)}$ be the partial derivative of $\Phi$ with respect to $x_k$ evaluated at the sample points

$$D_{ij}^{(k)} = \frac{\partial \phi_j}{\partial x_k}(\boldsymbol{x}_i), \quad D^{(k)} \in \mathbb{R}^{m\times(M+1)},\ k \in [p] \tag{4.1}$$

For directional derivatives, we have a slightly more complicated form

$$D_{ij}^{(v)} = \nabla \phi_j(\boldsymbol{x}_i)^T v, \quad v \in \mathbb{R}^p, \, \|v\|_1 = 1. \tag{4.2}$$

In this work, we assume we have knowledge of the partial derivatives at each sample point (i.e. directional derivatives along the standard basis). Collecting the matrices $D^{(k)}$ into the matrix $D$, we have

$$D = \left[ {D^{(1)}}^T \, {D^{(2)}}^T \, \cdots \, {D^{(p)}}^T \right]^T, \quad D \in \mathbb{R}^{pm \times (M+1)}. \tag{4.3}$$

Similarly, define the vector of partial derivatives with respect to $x_k$ evaluated at the sample points to be

$$\boldsymbol{g}^{(k)} = \left[ \tfrac{\partial f}{\partial x_k}(x_1), \ldots, \tfrac{\partial f}{\partial x_k}(x_m) \right]^T \tag{4.4}$$

and the collected form $\boldsymbol{g}$ to be

$$\boldsymbol{g} = \left[ {\boldsymbol{g}^{(1)}}^T, \ldots, {\boldsymbol{g}^{(p)}}^T \right]^T, \quad \boldsymbol{g} \in \mathbb{R}^{pm} \tag{4.5}$$

Modifying the data fit of OLS to include this information, we define the *stacked ordinary least squares* problem to be

$$\min_{\boldsymbol{\alpha}} \left\| \begin{bmatrix} \Phi \\ D \end{bmatrix} \boldsymbol{\alpha} - \begin{bmatrix} \boldsymbol{y} \\ \boldsymbol{g} \end{bmatrix} \right\|_2 \tag{S-OLS}$$

However, this simple extension implies a possibly spurious model assumption. Namely, it suggests the truncation error in the function is equal to the truncation error in the derivatives. In reality, if the derivative error is much higher than the error in the function, then S-OLS estimate will attempt to fit the derivatives at the expense of fitting the function values. Since the goal is to approximate the function response, this approach may lead to undesirable solutions.

### 4.1.2 Equality constrained least squares

Another possibility is to modify OLS to be an *equality constrained least squares problem*. In order to prevent misfitting of the function responses, we explicitly force the approximation to pass through the function values exactly and use the remaining degrees of freedom to minimize the error in the derivatives.

$$\begin{aligned} \min_{\boldsymbol{\alpha}} \quad & \|D\boldsymbol{\alpha} - \boldsymbol{g}\|_2 \\ \text{s.t.} \quad & \Phi\boldsymbol{\alpha} = \boldsymbol{y} \end{aligned} \tag{EC-LS}$$

However, there are practical limitations to this approach. Assuming $\Phi$ is full rank, this optimization problem is only feasible for $m \leq M$ since the equality constraint cannot, in general, be satisfied for an overdetermined set of equations. This implies that we may not oversample at a ratio greater than one without needing to throw away function values. While this may not be an issue for high dimensional problems, unless $f(\boldsymbol{x})$ is exactly in the span of the basis polynomials i.e. there is no truncation error, we are introducing bias in the estimation of $\boldsymbol{\alpha}$ by enforcing this unsatisfiable condition. Furthermore, suppose that the coefficients are sparse or nearly sparse as is common in high dimensional problems. Then, as we explained in previous chapters, if the objective in EC-LS is underdetermined, the least squares estimate will not have a sparse form. In contrast, the $\ell_1$ regularized solution can potential yield the exact solution. In the next section, we describe how derivative information can be used in the regularized setting and its implication for undersampling using derivatives.

## 4.2 Derivatives in $\ell_1$ regularized least squares

Consider the underdetermined setting where $mp + m < (M + 1)$. That is, even with the gradient information, the data fit problem remains underdetermined. As we did in the S-OLS model, we could simply incorporate the derivative information in the system of equations describing the data fit. In order to account for possible differences in the order of error in the function and order of error in the derivative, the two linear systems are partitioned and controlled by two independent parameters $\eta_y$ and $\eta_g$.

This modified form defines the *stacked basis pursuit (denoising)* problems

$$\begin{aligned} \min \quad & \|\boldsymbol{\alpha}\|_1 \\ \text{s.t.} \quad & \Phi\boldsymbol{\alpha} = \boldsymbol{y} \\ & D\boldsymbol{\alpha} = \boldsymbol{g} \end{aligned} \tag{S-BP}$$

and

$$\begin{aligned} \min \quad & \|\boldsymbol{\alpha}\|_1 \\ \text{s.t.} \quad & \|\Phi\boldsymbol{\alpha} - \boldsymbol{y}\|_2 \leq \eta_y \\ & \|D\boldsymbol{\alpha} - \boldsymbol{g}\|_2 \leq \eta_g \end{aligned} \tag{S-BPDN}$$

While columns of $\Phi$ are uncorrelated when the sample points are drawn uniformly from $[-1, 1]^p$, this is not true of the columns of $D$. That is, the derivatives of the Legendre polynomials are not generally orthogonal to each other with respect to the Lebesgue measure. The resulting polynomials are theoretically linearly independent in the infinite dimensional sense [16], but for a finite number of evaluations, this may not be true. In our experience, $D$ can become ill-conditioned and is especially apparent in high dimensions as shown in Figure 4.1. The lack of full row rank implies

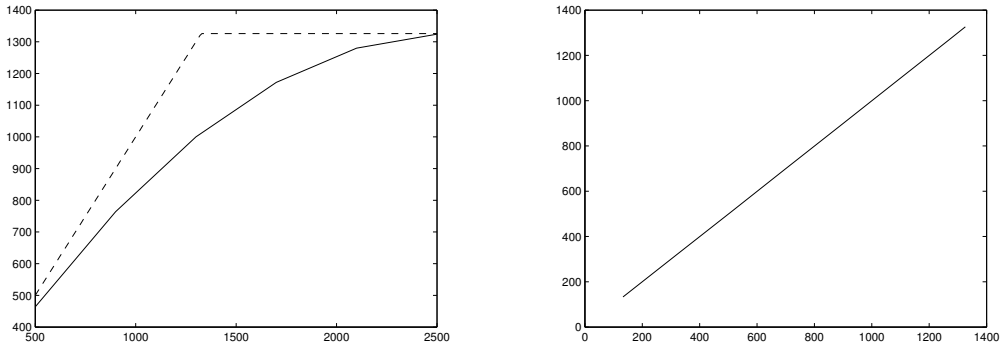


(a) $D$ (b) $\Phi$

Figure 4.1: Rank of matrix as a function of number of rows with $M = 1326$ columns. Ideal (dashed) and true (solid) for tensor product Legendre basis functions $\Lambda_{50}^2$

that some of the linear conditions imposed by $D$ are redundant. Informally, this means the information content generated by the derivatives may be destroyed by expressing them in terms of polynomials represented in the columns of $D$. Furthermore, high correlation between columns of the matrix introduces noise and can lead to the wrong solution even in the asymptotic limit $m \to \infty$ [97].

Suppose that the (partial) derivatives also belonged to the space $L^2[-1,1]^p$. For the sake of clarity, let's consider the $p = 1$ case. Let $P_M$ be the operator that projects a function onto the Legendre polynomials of degree $\leq M$. Then for a polynomial approximation $P_M f = f_M(x)$, we can express its derivative by $P_{M-1} f'$.

$$P_{M-1} f' = \sum_{j=0}^{M-1} \alpha_j^{(1)} \phi_j(x) \tag{4.6}$$

Note that, in general, this is not the same as differentiating the polynomial approximation $(P_M f)'$ which is given by $D\boldsymbol{\alpha}$. This is known as the *Legendre projection derivative (LPD)*. That is, differentiation and truncation do not commute in the Legendre series expansion.

$$(P_M f)' \neq P_{M-1} f' \tag{4.7}$$

To see this, recall the following identity of [2.3.21 Canuto][1] between $\alpha_k$ and $\alpha_k^{(1)}$

$$\alpha_k = \frac{\alpha_{k-1}^{(1)}}{\sqrt{(2k-1)(2k+1)}} - \frac{\alpha_{k+1}^{(1)}}{\sqrt{(2k+3)(2k+1)}}, \quad k \geq 1. \tag{4.8}$$

Inverting the identity, we have the corresponding result in terms of $\alpha_k$ (Section 2.3.18 [16])

$$\alpha_k^{(1)} = \sqrt{(2k+1)(2k+5)} \sum_{p=k+1,\, p+k \text{ odd}}^{\infty} \theta_p \alpha_p, \quad k \geq 0 \tag{4.9}$$

[1] modified for *orthonormal* Legendre polynomials

where

$$\theta_p = \prod_{j=k+1,\, j+k \text{ odd}}^{p-2} \sqrt{\frac{2j+7}{2j+1}} \tag{4.10}$$

Since the coefficients $\alpha_k^{(1)}$ are equal to an infinite sum of $\alpha_k$, (4.7) follows. Furthermore, when $f$ has finite regularity i.e. not infinitely differentiable, $(P_M f)'$ is an asymptotically a worse approximation to $f'$ than $P_{M-1} f'$ as $M \to \infty$. Further details on how the two differ can be found in (Section 5.4.2 [16]). Thus, we expect an estimator that uses the LPD to be worse than an estimator that uses the more accurate estimate.

### 4.2.1 Exploiting sparsity in $f$, $\nabla f$

This result suggests that we should construct a separate polynomial approximation for the derivative $P_{P-1} f'$ and connect the two approximations using (4.8). First we assume that $f$ has square integrable derivative $f' \in L^2[-1, 1]$. Further, at the moment, assume that $f \in W_1^M$. Then, $f'$ can be represented exactly by the $P-1$ order approximation

$$f'(x) = \sum_{j=0}^{M-1} \alpha_j^{(1)} \phi_j(x) \tag{4.11}$$

Then for a set of sample points, function values, and derivatives $\{(x_i, y_i, g_i)\}_{i=1}^m$ we have the following system of equations

$$\Phi_M \boldsymbol{\alpha} = \boldsymbol{y} \tag{4.12}$$

$$\Phi_{M-1} \boldsymbol{\alpha}^{(1)} = \boldsymbol{g} \tag{4.13}$$

$$H \boldsymbol{\alpha}^{(1)} = I \boldsymbol{\alpha} \tag{4.14}$$

where we've used the subscript on $\Phi$ to denote its set of basis functions $\Phi_{M-1} \implies \Phi_{ij} = \phi_{j-1}(x_i)$, $j = 1, \ldots, M$, $H$ is the $M \times M$ representing the linear relation (4.8), and $I$ is the $M \times (M+1)$ matrix that selects all $\alpha_j$, $j \neq 0$. That is, $\alpha_0$ is independent

of $\boldsymbol{\alpha}^{(1)}$. Rewriting in block matrix notation, we have

$$\begin{bmatrix} \Phi_M & 0 \\ 0 & \Phi_{M-1} \\ -I & H \end{bmatrix} \begin{bmatrix} \boldsymbol{\alpha} \\ \boldsymbol{\alpha}^{(1)} \end{bmatrix} = \begin{bmatrix} \boldsymbol{y} \\ \boldsymbol{g} \\ 0 \end{bmatrix}. \tag{4.15}$$

Since the relations (4.8) allow us to go from $\{\alpha_j\}_{j=1}^{\infty}$ to $\{\alpha_j^{(1)}\}_{j=0}^{\infty}$, and vice versa, the matrix $H$ is invertible. Thus, we can rewrite the system of equations as

$$A\boldsymbol{\alpha} = \begin{bmatrix} \Phi_M & \\ 0 & \Phi_{M-1}H^{-1}I \end{bmatrix} \boldsymbol{\alpha} = \begin{bmatrix} \boldsymbol{y} \\ \boldsymbol{g} \end{bmatrix} \tag{4.16}$$

When $A$ has rank less than $M$, there are infinitely many solutions for $\boldsymbol{\alpha}$. Naturally, we can impose regularization on this system to reduce the degrees of freedom. Using the $\ell_1$ penalty, $G(\cdot) = \|\cdot\|_1$, we have the following optimization problem (can be expressed as a linear program)

$$\begin{aligned} \min \quad & \|\boldsymbol{\alpha}\|_1 + \gamma\|\boldsymbol{\alpha}^{(1)}\|_1 \\ \text{s.t.} \quad & \Phi_M\boldsymbol{\alpha} = \boldsymbol{y} \\ & \Phi_{M-1}\boldsymbol{\alpha}^{(1)} = \boldsymbol{g} \\ & H\boldsymbol{\alpha}^{(1)} = I\boldsymbol{\alpha} \end{aligned} \tag{F-BP}$$

Here, we have applied regularization on both $\boldsymbol{\alpha}$ and $\boldsymbol{\alpha}^{(1)}$ with the hyper-parameter $\gamma$ controlling the sparsity trade-off. The utility of this formulation is that if either $f$ *or* $f'$ are sparse, then that function can be recovered quickly and imposed on $\boldsymbol{\alpha}$. Identifying which of the two functions, if any, are sparse is role of $\gamma$. For example, if $\boldsymbol{\alpha}$ is sparse, then a small value for $\gamma$ will allow $\boldsymbol{\alpha}^{(1)}$ to be whatever it needs to be in order to satisfy (4.8). However, if $\boldsymbol{\alpha}^{(1)}$ is sparse, then a large $\gamma$ will force $\boldsymbol{\alpha}^{(1)}$ to be sparse and allow $\boldsymbol{\alpha}$ to satisfy (4.8) with little regularization. In general, this parameter must be estimated through a cross validation procedure [49]. This is described in more detail in Section 4.2.2. When $f$ is not exactly representable by $span(\Lambda_1^P)$, we

have the noise aware variant

$$\begin{aligned} \min \quad & \|\boldsymbol{\alpha}\|_1 + \gamma\|\boldsymbol{\alpha}^{(1)}\|_1 \\ \text{s.t.} \quad & \|\Phi_M\boldsymbol{\alpha} - \boldsymbol{y}\|_2 \leq \eta_y \\ & \|\Phi_{M-1}\boldsymbol{\alpha}^{(1)} - \boldsymbol{g}\|_2 \leq \eta_g \\ & \|H\boldsymbol{\alpha}^{(1)} - I\boldsymbol{\alpha}\|_2 \leq \eta_c \end{aligned} \tag{F-BPDN}$$

Here, we have introduced a new parameter $\eta_c$ that controls the error between the two sets of coefficients, in addition to the ones introduced in S-BPDN. From (4.9), we see that when the truncation error in $f_M$ is small, $\eta_c$ will be small. This problem is convex and can be efficiently solved.

The extension to $p > 1$ is straight forward. Now the function lies in the space $H^1[-1,1]^p$ where

$$\begin{aligned} H^m[-1,1]^p = \{v \in L^2[-1,1]^p \ &: \text{for each multi-index } \boldsymbol{\beta} \in \mathbb{N}^p \\ &\text{with } |\beta_k| \leq m \text{ the distributional derivative} \\ &\frac{D^{\boldsymbol{\beta}} v}{\partial^{\beta_1} x_1 \dots \partial^{\beta_j} x_p} \text{ belongs to } L^2[-1,1]^p\} \end{aligned} \tag{4.17}$$

Equipped with the appropriate inner product, $H^m$ is the Hilbert Sobolev space [16]. For our purposes, we need only the $L^2$ inner product. Let $\boldsymbol{j} = (j_1, \dots, j_p)$, $j_k \in \mathbb{N}$ be the multi-index identifying the order of the tensor product polynomial $\phi_{\boldsymbol{j}}$. Furthermore, let $\{\alpha_{\boldsymbol{j}}^{(1),k}\}_{\boldsymbol{j}\in\mathbb{N}^p}$ be the coefficients associated to the expansion of partial derivative $\frac{\partial f}{\partial x_k}$.

$$\frac{\partial f}{\partial x_k}(\boldsymbol{x}) = \sum_{\boldsymbol{j}\in\mathbb{N}^p} \alpha_{\boldsymbol{j}}^{(1),k} \phi_{\boldsymbol{j}}(\boldsymbol{x}), \quad k = 1, \dots, p \tag{4.18}$$

It is simple to show that the multivariate analog of (4.8).

**Proposition 4.2.1.** *Consider the coefficients $\{\alpha_{\boldsymbol{j}}^{(1),k}\}_{\boldsymbol{j}\in\mathbb{N}^p}$ corresponding to the expansion of the partial derivative $\frac{\partial f}{\partial x_k}(\boldsymbol{x})$ and denote $\boldsymbol{j}_{-k}$ to be the multi-index $\boldsymbol{j}$ without*

$j_k$. *Then, letting* $\boldsymbol{j} = (\boldsymbol{j}_{-k}, j_k) \in \mathbb{N}^{p-1} \times \mathbb{N}\backslash 0$ *we have the identity*

$$\alpha_{(\boldsymbol{j}_{-k}, j_k)} = \frac{\alpha^{(1),k}_{(\boldsymbol{j}_{-k}, j_k - 1)}}{\sqrt{(2j_k - 1)(2j_k + 1)}} - \frac{\alpha^{(1),k}_{(\boldsymbol{j}_{-k}, j_k + 1)}}{\sqrt{(2j_k + 3)(2j_k + 1)}} \tag{4.19}$$

*Proof.* For any $f \in H^1[-1,1]^p$, its admits a series representation in the tensor product Legendre polynomials

$$f(\boldsymbol{x}) = \sum_{\boldsymbol{j} \in \mathbb{N}^p} \alpha_{\boldsymbol{j}} \phi_{\boldsymbol{j}}(\boldsymbol{x}), \quad \boldsymbol{x} \in [-1,1]^p. \tag{4.20}$$

Additionally, its partial derivatives also admit such a representation

$$\begin{aligned} \frac{\partial f}{\partial x_k}(\boldsymbol{x}) &= \sum_{\boldsymbol{j} \in \mathbb{N}^p} \alpha^{(1),k}_{\boldsymbol{j}} \phi_{\boldsymbol{j}}(\boldsymbol{x}), \quad \boldsymbol{x} \in [-1,1]^p \\ &= \sum_{\boldsymbol{j} \in \mathbb{N}^p} \alpha^{(1),k}_{\boldsymbol{j}} \prod_{\ell=1 \neq k}^{p} \phi_{j_\ell}(x_\ell) \cdot \phi_{j_k}(x_k). \end{aligned} \tag{4.21}$$

Recall the property of orthonormal Legendre polynomials $\phi_j$ (Section 2.3.19 [16])

$$\phi_j = c_j \phi'_{j+1} - d_j \phi'_{j-1}, \quad j \geq 0. \tag{4.22}$$

where

$$c_j = \frac{1}{\sqrt{(2j+1)(2j+3)}}, \quad d_j = \frac{1}{\sqrt{(2j+1)(2j-1)}} \tag{4.23}$$

Then substituting into (4.21),

$$\begin{aligned}
\frac{\partial f}{\partial x_k}(\boldsymbol{x}) &= \sum_{\boldsymbol{j}\in\mathbb{N}^p} \alpha_{\boldsymbol{j}}^{(1),k} \prod_{\ell=1\neq k}^{p} \phi_{j_\ell}(x_\ell) \left[c_{j_k}\phi'_{j_k+1}(x_k) - d_{j_k}\phi'_{j_k-1}(x_k)\right] \\
&= \sum_{(\boldsymbol{j}_{-k},j_k)\in\mathbb{N}^p} \alpha_{(\boldsymbol{j}_{-k},j_k)}^{(1),k} \prod_{\ell=1\neq k}^{p} \phi_{j_\ell}(x_\ell) c_{j_k}\phi'_{j_k+1}(x_k) \\
&- \sum_{(\boldsymbol{j}_{-k},j_k)\in\mathbb{N}^p} \alpha_{(\boldsymbol{j}_{-k},j_k)}^{(1),k} \prod_{\ell=1\neq k}^{p} \phi_{j_\ell}(x_\ell) d_{j_k}\phi'_{j_k-1}(x_k) \\
&= \sum_{(\boldsymbol{j}_{-k},j_k)\in\mathbb{N}^{p-1}\times\mathbb{N}\setminus 0} \alpha_{(\boldsymbol{j}_{-k},j_k-1)}^{(1),k} \prod_{\ell=1\neq k}^{p} \phi_{j_\ell}(x_\ell) c_{j_k-1}\phi'_{j_k}(x_k) \\
&- \sum_{(\boldsymbol{j}_{-k},j_k)\in\mathbb{N}^{p-1}\times\mathbb{N}\cup\{-1\}} \alpha_{(\boldsymbol{j}_{-k},j_k+1)}^{(1),k} \prod_{\ell=1\neq k}^{p} \phi_{j_\ell}(x_\ell) d_{j_k+1}\phi'_{j_k}(x_k) \\
&= \sum_{\boldsymbol{j}\in\mathbb{N}^{p-1}\times\mathbb{N}\setminus 0} \left[c_{j_k-1}\alpha_{(\boldsymbol{j}_{-k},j_k-1)}^{(1),k} - d_{j_k+1}\alpha_{(\boldsymbol{j}_{-k},j_k+1)}^{(1),k}\right] \prod_{\ell=1\neq k}^{p} \phi_{j_\ell}(x_\ell)\phi'_{j_k} \qquad (4.24)
\end{aligned}$$

where we've used the fact $\phi'_{-1} = \phi'_0 = 0$. On the other hand, differentiating (4.20) gives

$$\frac{\partial f}{\partial x_k}(\boldsymbol{x}) = \sum_{\boldsymbol{j}\in\mathbb{N}^{p-1}\times\mathbb{N}\setminus 0} \alpha_{(\boldsymbol{j}_{-k},j_k)} \prod_{\ell=1\neq k}^{p} \phi_{j_\ell}(x_\ell)\phi'_{j_k}. \qquad (4.25)$$

Since $\phi'_j$ are linearly independent, we have our result. □

Again, let's consider functions of finite Legendre expansions. Let $f \in W_p^P$. Then, its partial derivatives are in $W_p^{P-1}$.

**Proposition 4.2.2.** *If $f \in W_p^P$, then $\frac{\partial f}{\partial x_k} \in W_p^{P-1}$ for $k = 1, \ldots, p$.*

*Proof.* For each polynomial $\phi_{\boldsymbol{j}} \in \Lambda_p^P$, consider the two cases:
$j_k = 0$. Then, the polynomial in $x_k$ is a constant and

$$\frac{\partial \phi_{\boldsymbol{j}}}{\partial x_k} = 0 \in span(\Lambda_p^{P-1}) \qquad (4.26)$$

$j_k > 0$. By the definition $\sum_{q=1}^{p} j_q \leq P$. Then,

$$\frac{\partial \phi_{\boldsymbol{j}}}{\partial x_k} = \prod_{q \neq k} \phi_{j_q}(x_q) \frac{\partial \phi_{j_k}}{\partial x_k} \tag{4.27}$$

which has total order $\sum_{q \neq k} j_q + (j_k - 1) \leq P - 1$. □

Since $|\mathcal{A}_p^P| \geq |\mathcal{A}_p^{P-1}| + 1$, with equality only holding for $p = 1$, not all $\boldsymbol{\alpha}$ are dependent on $\boldsymbol{\alpha}^{(1),k}$.

**Proposition 4.2.3.** *Let $M = |\Lambda_p^P|$ and $M' = |\Lambda_p^{P-1}|$. For $f \in W_p^P$, let $\boldsymbol{\alpha} = \{\alpha_{\boldsymbol{j}}\}_{\boldsymbol{j} \in \mathcal{A}_p^P}$ be its coefficients in the tensor product Legendre polynomials. For $k \in [p]$, if the coefficients $\boldsymbol{\alpha}^{(1),k} = \{\alpha_{\boldsymbol{j}}^{(1),k}\}_{\boldsymbol{j} \in \mathcal{A}_p^{P-1}}$ are known, then exactly $M'$ entries of $\boldsymbol{\alpha}$ can be determined.*

*Proof.* Observe that the basis functions $\phi_{\boldsymbol{j}} \in \Lambda_p^P$, $\boldsymbol{j} = (\boldsymbol{j}_{-k}, 0)$ are independent of $x_k$ and thus cannot be known from $\frac{\partial f}{\partial x_k}$. Since there are

$$q = \binom{P + (p-1)}{(p-1)}$$

such polynomials (since we are effectively fixing one $j$ to be zero, we are seeking the set of all $\boldsymbol{j}$ such that the remaining $p - 1$ indices sum to $\leq P$), by the binomial coefficient identity

$$\binom{n}{k} = \binom{n-1}{k-1} + \binom{n-1}{k}. \tag{4.28}$$

there are at most $M' = M - q$ remaining cofficients. It remains to show that all of these coefficients can be determined from $\boldsymbol{\alpha}^{(1),k}$. Let these entries of $\boldsymbol{\alpha}$ be represented by the indices $\boldsymbol{J} = \{\boldsymbol{j} : \boldsymbol{j} \in \mathcal{A}_p^P,\, j_\ell \neq 0\}$. Consider the expanded set of coefficients

$$\mathfrak{A}_k = \{\alpha_{\boldsymbol{j}}^{(1),k}\}_{j \in \mathbb{N}^p} = \{\alpha_{\boldsymbol{j}}^{(1),k}\}_{\boldsymbol{j} \in \mathcal{A}_p^{P-1}} \cup \{\alpha_{\boldsymbol{j}}^{(1),k} = 0\}_{\boldsymbol{j} \notin \mathcal{A}_p^P}.$$

From Proposition 4.2.1, for any $(\boldsymbol{j}_{-k}, j_k) \in \boldsymbol{J}$, and $1 \leq j_k \leq P$, then $\alpha^{(1),k}_{(\boldsymbol{j}_{-k}, j_k-1)}$, $\alpha^{(1),k}_{(\boldsymbol{j}_{-k}, j_k+1)} \in \mathfrak{A}_k$. □

**Corollary 4.2.4.** *The coefficients* $\{\alpha_{\boldsymbol{j}}\}_{\boldsymbol{j}\in\mathcal{A}_p^P\setminus\mathbf{0}}$ *are completely determined by the coefficients of the partial derivatives* $\{\alpha^{(1),k}_{\boldsymbol{j}}\}_{\boldsymbol{j}\in\mathcal{A}_p^{P-1}}$, $k = 1, \ldots, p$.

*Proof.* We only need to show that for any $\boldsymbol{j} \in \mathcal{A}_p^P\setminus\mathbf{0}$, $\alpha_{\boldsymbol{j}} \in \mathfrak{A}_k$ for some $k \in [p]$. For any such $\boldsymbol{j}$, there is at least one $j_\ell \neq 0$ by definition. Denote this index to be $\ell^*$. Since $\alpha^{(1),\ell^*}_{(\boldsymbol{j}_{-\ell^*}, j_{\ell^*}-1)}$, $\alpha^{(1),\ell^*}_{(\boldsymbol{j}_{-\ell^*}, j_{\ell^*}+1)} \in \mathcal{A}_{\ell^*}$, $\alpha_{\boldsymbol{j}}$ can be determined. □

This implies that with an exact representation of the partial derivatives, we can recover a function $f \in W_p^P$ up to a constant. Again, the utility of this formulation is that if any $\frac{\partial f}{\partial x_k}$ are sparse, it can be found quickly by the *basis pursuit* formulation and imposed on the coefficients $\boldsymbol{\alpha}$. Now we are ready to present the multivariate version of F-BP. Define $\Phi_M$ as the matrix corresponding to the set of polynomials $\Lambda_p^P$ evaluated at the sample points $\{\boldsymbol{x}_i\}_{i=1}^m$ and $\Phi_{M'}$ as the matrix corresponding to the set of polynomials $\Lambda_p^{P-1}$ evaluated at the same sample points. Further, let $\boldsymbol{\alpha}^{(1),k} \in \mathbb{R}^{M'}$, $k = 1, \ldots, p$ are the vector of coefficients associated to the polynomial approximation to the partial derivative $\frac{\partial f}{\partial x_k}$ and $H_k$, $I_k$ be the matrices that enforce the system of relations in Proposition 4.2.1.

$$
\begin{aligned}
\min \quad & \|\boldsymbol{\alpha}\|_1 + \gamma \sum_{k=1}^{p} \|\boldsymbol{\alpha}^{(1),k}\|_1 && \text{(F-BP)}\\
\text{s.t.} \quad & \Phi_M \boldsymbol{\alpha} = \boldsymbol{y} \\
& \Phi_{M'} \boldsymbol{\alpha}^{(1),k} = \boldsymbol{g}^{(k)}, \quad k = 1, \ldots, p \\
& H_k \boldsymbol{\alpha}^{(1),k} = I_k \boldsymbol{\alpha}, \quad k = 1, \ldots, p && (4.29)
\end{aligned}
$$

For $f$ that are not finite expansions in the Legendre polynomials, we have the corresponding noise-aware variant

$$\begin{aligned} \min \quad & \|\boldsymbol{\alpha}\|_1 + \gamma \sum_{k=1}^{p} \|\boldsymbol{\alpha}^{(1),k}\|_1 \\ \text{s.t.} \quad & \|\Phi_M \boldsymbol{\alpha} - \boldsymbol{y}\|_2 \leq \eta_y \\ & \sum_{k=1}^{p} \|\Phi_{M'} \boldsymbol{\alpha}^{(1),k} - \boldsymbol{g}^{(k)}\|_2^2 \leq \eta_g^2 \\ & \sum_{k=1}^{p} \|H_k \boldsymbol{\alpha}^{(1),k} - I_k \boldsymbol{\alpha}\|_2^2 \leq \eta_c^2 \end{aligned} \tag{F-BPDN}$$

(4.30)

Arguing as before, one could extend this model by having a separate $\gamma$, $\eta_g$ or $\eta_c$ for each partial derivative constraint. However, in practice, one observes some robustness in the solution to the exact choice of parameters. In the interest of balancing complexity with degrees of freedom, we only use the parameterization given above. In the next section, we discuss how we choose the *hyperparameters*[2] $\gamma$, $\eta_y$, $\eta_g$, and $\eta_c$

### 4.2.2 Choosing hyper-parameters via cross validation

In general, we do not know the truncation error of a particular approximation *a priori*, and as a consequence, we do not know the appropriate values for $\eta_y$, $\eta_g$, and $\eta_c$; similarly for $\gamma$. One common approach to determining these hyper-parameters is to employ cross validation. In principle, the goal is to get a good fitting approximation without *overfitting* i.e. fitting too closely to the observed data. Since we are generally operating in the undersampling regime $m+pm < M$ (more unknowns than equations), we can always achieve arbitrarily low error. For example, the least squares solution in an undetermined problem has zero error. This is known as *training error*, or the error of the approximation on the data points used to estimate the model parameters. Instead, one could split the data into a *training set* $\Theta_{tr}$ and *test set* $\Theta_{te}$, fitting the data (e.g. via F-BPDN) on the training set and then estimating the error of the approximation on the test set i.e. *test error*. When these sets are chosen randomly,

[2] to distinguish between *parameters* $\boldsymbol{\alpha}$, $\boldsymbol{\alpha}^{(1),k}$

the test error gives us an unbiased estimate of the true error.

In our case, for a given training set and a fixed value for the hyper-parameters $\boldsymbol{\tau}' = (\eta_y', \eta_g', \eta_c', \gamma')$, we will have an estimate of $\boldsymbol{\alpha}, \boldsymbol{\alpha}^{(1),k}$, $k = 1, \ldots, p$. Using this estimate, we the evaluate the approximation at points in the test set and compare the error to true value. Let $\hat{f}$ denote this approximation. Then, the test error is computed by

$$\hat{\epsilon} = \frac{1}{|\Theta_{te}|} \sum_{\boldsymbol{x}_i \in \Theta_{te}} (\hat{f}(\boldsymbol{x}_i; \boldsymbol{\tau}') - \boldsymbol{y}_i)^2 \tag{4.31}$$

where $\mathbb{E}[\hat{\epsilon}] = \|\hat{f} - f\|_2^2$. Since we are primarily concerned with error in the function values, we do not split the derivative data into to training and test sets. Instead, all of the derivative data is used with $\eta_g$ modulating their influence. The goal is to minimize error on the training data with respect to the parameters $\boldsymbol{\tau}$

$$\min_{\boldsymbol{\tau}} \frac{1}{|\Theta_{te}|} \sum_{\boldsymbol{x}_i \in \Theta_{te}} (\hat{f}(\boldsymbol{x}_i; \boldsymbol{\tau}) - \boldsymbol{y}_i)^2 \tag{4.32}$$

In general this can be solved like any other optimization problem. However, the objective can be quite noisy and thus traditional gradient-based optimization methods are not used. Instead, we perform a basic *grid search* where we define a grid over the parameter space, evaluate the approximation $\hat{f}$ at the parameter values, and record the resulting test error $\hat{\epsilon}$. Then, the parameter values corresponding to the lowest test error is selected. In practice, the parameter space is relatively flat and thus the error is robust to the exact choice of parameter values.

### $k$-fold cross validation

We can take the ideas of the previous section further by defining an ensemble of training and test sets for a given data set. In $k$-fold cross validation, the data set is partitioned into $k$ disjoint sets. A training set is defined on $k-1$ of those sets, and the remaining set is used as the test set. $k$ unique test and training sets can be created from this procedure, and an estimate for the test error can be obtained by

taking the mean of the $k$ test errors.

$$\hat{\epsilon} = \frac{1}{k} \sum_{i=1}^{k} \hat{\epsilon}_i \tag{4.33}$$

$k$-fold cross validation ensures greater randomization in choice of training and test sets and further reduces the bias of the test error $\hat{\epsilon}$. This is particularly important when the data size $m$ is small and the test error is highly dependent on the few points in the test set. In our numerical experiments, we use this form of cross validation with $k = \min(10, m)$.

## 4.3 Numerical experiments

In this section, we give the convergence of the Legendre polynomial approximation for functions with zero truncation error $f \in W_p^P$ and those with nonzero truncation error $f \notin W_p^P$. We expect that the two gradient enhanced methods, F-BPDN and S-BPDN, perform equally well when $f \in W_p^P$ but differently when $f \notin W_p^P$ according to (4.7). Further, we investigate the degree of undersampling achievable by F-BPDN when both $f$ and $f'$ are sparse (e.g. Giunta). The optimization problems were solved using the CVX MATLAB toolbox [47] with some solution tolerance above machine zero. As a consequence, we do not expect the estimates to converge to machine zero. For the non-polynomial functions, there is an additional error incurred by truncation which further limits the ability to estimate the coefficients to machine zero. Each method is repeated $n_{MC} = 5$ times to alleviate dependence on the particular sample points drawn. The graphs in the subsequent figures are the average errors of those $n_{MC}$ instances.

### 4.3.1 Polynomial functions

**Sphere function.** $P = 2$, $p = 15$

$$f(\boldsymbol{x}) = \sum_{k=1}^{p} x_k^2 \tag{4.34}$$

The sphere function represents a "low complexity" i.e. small $P$, high dimensional

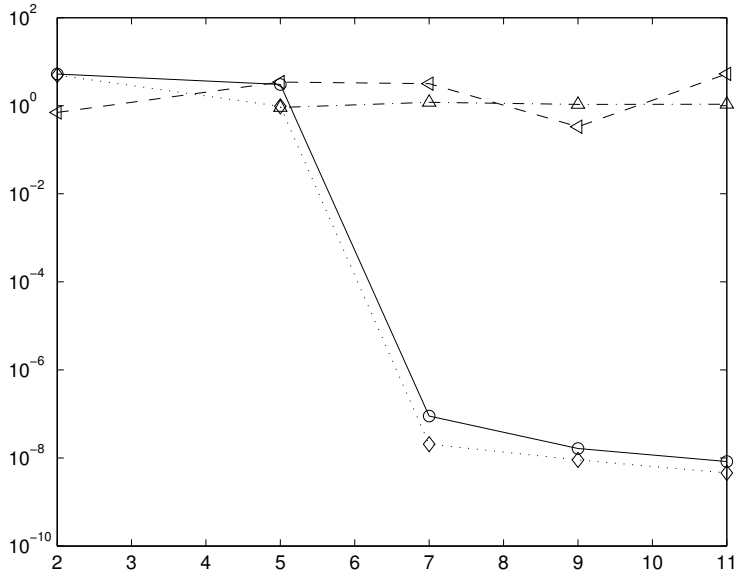


Figure 4.2: *Sphere function.* Error $\|\boldsymbol{\alpha} - \hat{\boldsymbol{\alpha}}\|_2$ vs number of data points $m$. for F-BPDN (diamond), S-BPDN (circle), $P_1^{\eta}$ (upward facing triangle), and S-OLS (left facing triangle)

problem to assess the information gained in high dimensions by adding derivative information. This function has $M = 136$ unknowns and a sparsity of $s = 16$. The function is also sparse in its derivatives; $s = 1$ in each partial derivative. Figure 4.2 shows the tremendous power provided by derivatives in the high dimensional setting. While the error of $P_1$ is effectively unchanged up to eleven evaluations, we see that with only seven "evaluations," both gradient enhanced methods achieve an error at

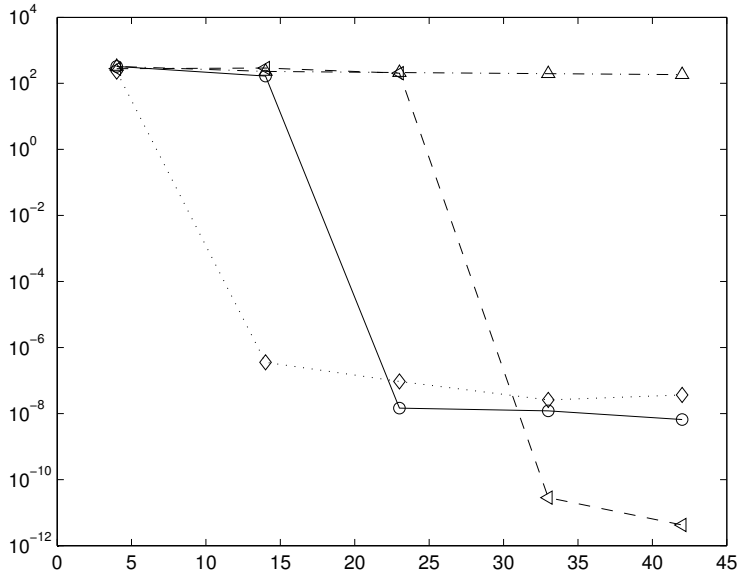


Figure 4.3: *Generalized Rosenbrock function.* Error $\|\boldsymbol{\alpha} - \hat{\boldsymbol{\alpha}}\|_2$ vs number of data points $m$. for F-BPDN (diamond), S-BPDN (circle), $P_1^\eta$ (upward facing triangle), and S-OLS (left facing triangle)

order of the solver tolerance. As expected, the performance of S-BP and F-BP are nearly identical.

**Generalized Rosenbrock.** $P = 4$**,** $p = 6$

$$f(\boldsymbol{x}) = \sum_{k=1}^{p-1} (1 - x_k)^2 + 100(x_{k+1} - x_k^2)^2 \tag{4.35}$$

The Generalized Rosenbrock function is of lower dimension, but also sparse and contains two-way interactions. In Figure 4.3, we see that $P_1^\eta$ achieves no meaningful decrease in error for this few number of sample points $m$ where the two gradient enhanced methods were able to converge the solution with $15 - 25$ data points with F-BP performing slightly better.

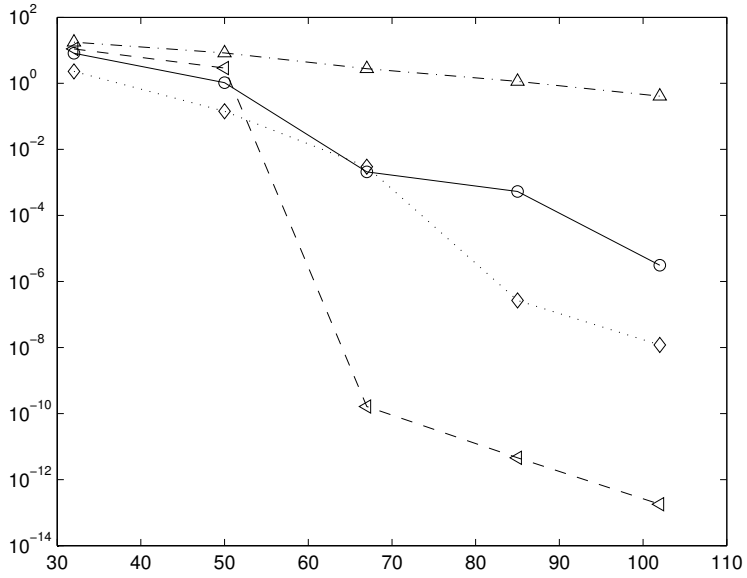


Figure 4.4: *Legendre-dense polynomial.* Error $\|\boldsymbol{\alpha} - \hat{\boldsymbol{\alpha}}\|_2$ vs number of data points $m$. for F-BPDN (diamond), S-BPDN (circle), $P_1^{\eta}$ (upward facing triangle), and S-OLS (left facing triangle)

**Legendre-dense polynomial.** $P = 18$, $p = 2$

$$f(\boldsymbol{x}) = \sum_{i=1}^{15} \sum_{j=1}^{15-i} x_1^i x_2^j + x_1^i + x_2^j \tag{4.36}$$

The Legendre-dense polynomial test function has a nonzero value for nearly two thirds of the entries in coefficient $\boldsymbol{\alpha}$. Since the basis pursuit solution can have at most $m$ nonzero coefficients values [64], it can have slow convergence when the coefficient vector $\boldsymbol{\alpha}$ is dense. The goal of this function is to study its effect on the gradient enhanced methods. One complication arises in the formulation of S-BP. As defined, it can accept at most $M$ data points (i.e. function values or derivatives) without becoming overdetermined. Thus, despite knowing that $f \in W_p^P$, we have to use the noise-aware variant S-BPDN in order to add additional points, necessarily degrading our estimate by the noise parameters $\eta_f$ and $\eta_g$. F-BP does not have this issue as

it has $M + 2M'$ nominal degrees of freedom. The first instance of $m(p+1) > M$ occurs at $m = 67$ and we see that the convergence of S-BPDN is slowed compared to F-BP. Nonetheless, both estimates still improve upon the nominal estimate $P_1$. Comparing the solutions at $m_1 = 32$ to $m_4 = 85$, we see that the error for the two gradient enhanced methods at $m_1$ are comparable to that of $P_1$ at $m_4$. Since the gradient enhancement is a $p + 1 = 3$ multiplier in this case, we can conclude that estimates using of derivatives and function values is similar to estimates that just use the function values. We also note that the density of the solution is particularly well suited for S-OLS, and it performs the best for this problem.

### 4.3.2 Functions of nonzero truncation error

In this section, we'll investigate functions with a nonzero truncation error. Following (4.7), we expect that the approximation to the derivatives using the LPD and having a separate expansion in the Legendre polynomials will be different. When the function is infinitely differentiable, as is the case in the first two test functions, the estimators should be of similar order of accuracy. However, when the function has finite regularity, the LPD is asymptotically a worse estimate to the true derivatives than a Legendre projection of the derivative.

**Sum of polynomial sinusoids [46].** $P = 10$**,** $p = 3$

$$f(\boldsymbol{x}) = \sum_{k=1}^{p} 0.3 + \sin\left(\frac{16}{15}x_k - 0.7\right) + \sin^2\left(\frac{16}{15}x_k - 0.7\right) \tag{4.37}$$

Since this function is infinitely differentiable, the two derivative approximations are of similar accuracy, and thus we expect no meaningful difference in the abilities of S-BPDN and F-BPDN to utilize the derivative information. However, Figure 4.5 shows a $O(10^2)$ error gap between the two estimates. Examining the optimal parameters $\hat{\tau}^*$ for F-BPDN, we see a large value for $\hat{\gamma}^*$ indicating the preference for sparse solutions of $\hat{\boldsymbol{\alpha}}^{(1),k}$ in the cross validation procedure. In fact, the sparsity $\boldsymbol{\alpha}^{(1),k}$ is less than half of $\boldsymbol{\alpha}$ and thus the F-BPDN is able to identify this through the cross validation

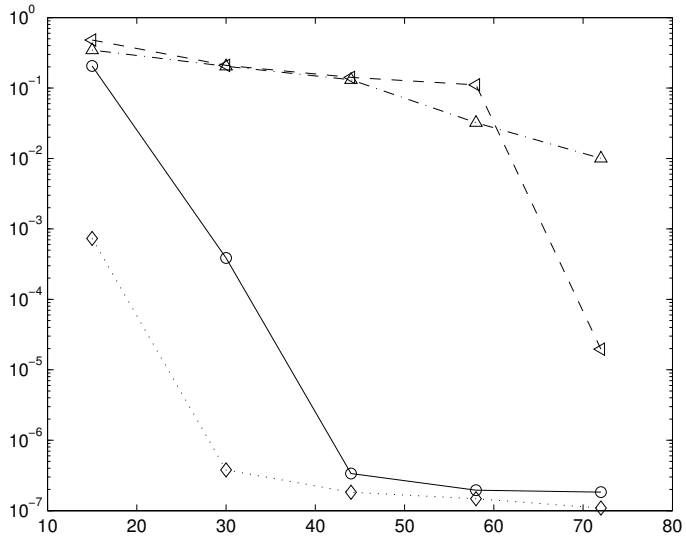


(a) $\|\boldsymbol{\alpha} - \hat{\boldsymbol{\alpha}}\|_2$ vs $m$

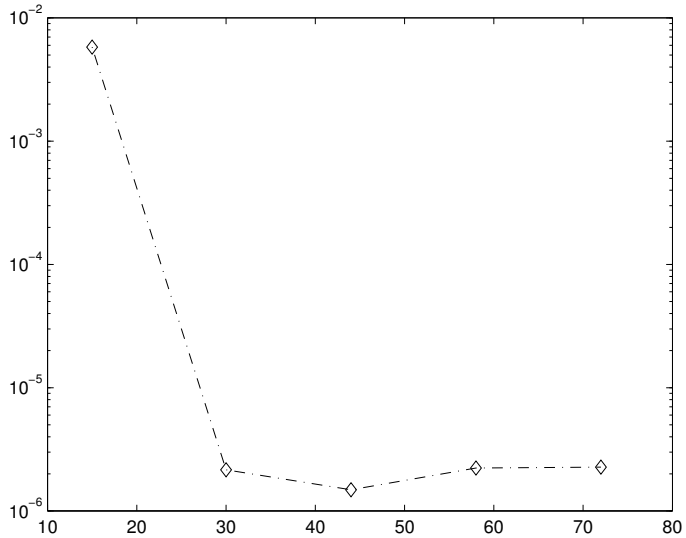


(b) $\left(\sum_{k=1}^{p} \|\boldsymbol{\alpha}^{(1),k} - \hat{\boldsymbol{\alpha}}^{(1),k}\|_2^2\right)^{1/2}$ vs $m$

Figure 4.5: *Sum of polynomial sinusoids.* F-BPDN (diamond), S-BPDN (circle), $P_1^{\eta}$ (upward facing triangle), and S-OLS (left facing triangle)

procedure and take advantage of the sparsity in the derivative to obtain a better estimate for $\boldsymbol{\alpha}$. Note that this type of information cannot be utilized by S-BPDN. Similarly, since $P_1^\eta$ does not utilize derivative information, its performance is solely tied to the sparsity in $\boldsymbol{\alpha}$. Therefore, for even for the same number of points (e.g. solutions at $m_1$ and $m_4$), it is not able to match the accuracy of F-BPDN.

**Ishigami Function [79].** $P = 12$**,** $p = 3$

$$f(\boldsymbol{x}) = \left(1 + 0.1\left(\frac{\pi}{2}x_3 - \frac{\pi}{2}\right)^4\right)\sin\left(\frac{\pi}{2}x_1 - \frac{\pi}{2}\right) + 7\sin^2\left(\frac{\pi}{2}x_2 - \frac{\pi}{2}\right) \tag{4.38}$$

Again, we have an infinitely differentiable function so S-BPDN and F-BPDN will have comparable approximations to the derivatives. Since there is significant sparsity in the derivatives, the F-BPDN outperforms S-BPDN as expected. Compare estimates of F-BPDN and $P_1^\eta$ at $m_1$ and $m_4$, we notice that the *efficiency* of the derivative information is not as pronounced as it was for Function 4.37. That is, for a similar number of data points, the two estimates have comparable accuracy. This can be explained by the difference in decay rates of the entries in $\boldsymbol{\alpha}$. While both functions are sparse, Function 4.38 is sparser and decays more smoothly. This is shown in Figure 4.7. Therefore, $P_1^\eta$ is able to give a better estimate than it could for Function 4.37.

**Rational Function [24].** $P = 200$**,** $p = 1$

$$f(x) = \frac{1}{2 + 25x^2} \tag{4.39}$$

Rational functions are poorly approximated by polynomial functions. As a result, the coefficients decay slowly and $\boldsymbol{\alpha}$ is relatively dense. In Figure 4.8, we see this adversely affects the convergence of the $P_1^\eta$ estimate. However, the effect is alleviated in the two gradient enhanced estimates. Once again, we observe a nonzero error gap that persists between F-BPDN and S-BPDN but its much smaller than observed in the previous functions. The coefficient profiles of the function and derivative are shown

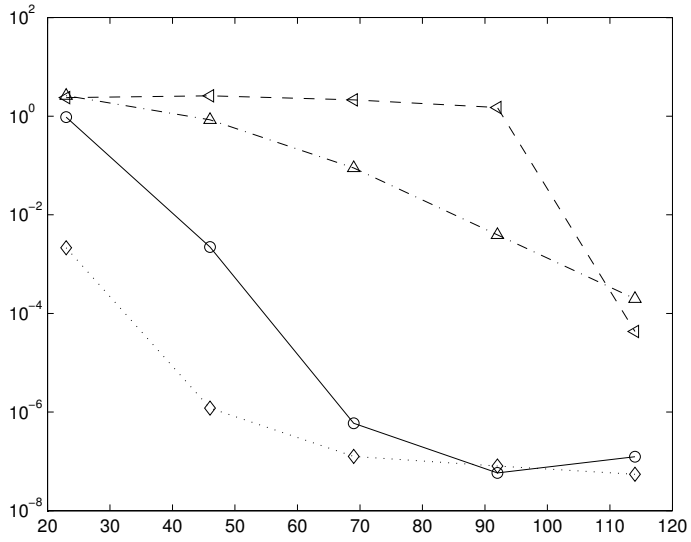


(a) $\|\boldsymbol{\alpha} - \hat{\boldsymbol{\alpha}}\|_2$ vs $m$

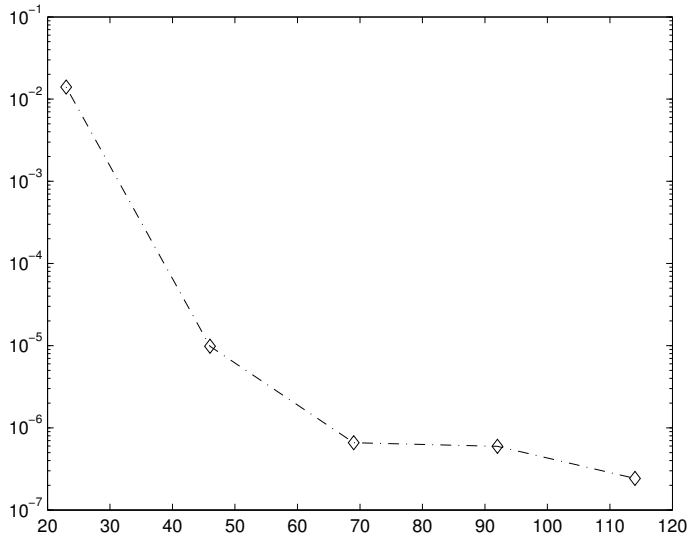


(b) $\left(\sum_{k=1}^{p} \|\boldsymbol{\alpha}^{(1),k} - \hat{\boldsymbol{\alpha}}^{(1),k}\|_2^2\right)^{1/2}$ vs $m$

Figure 4.6: *Ishigami function.* F-BPDN (diamond), S-BPDN (circle), $P_1^{\eta}$ (upward facing triangle), and S-OLS (left facing triangle)

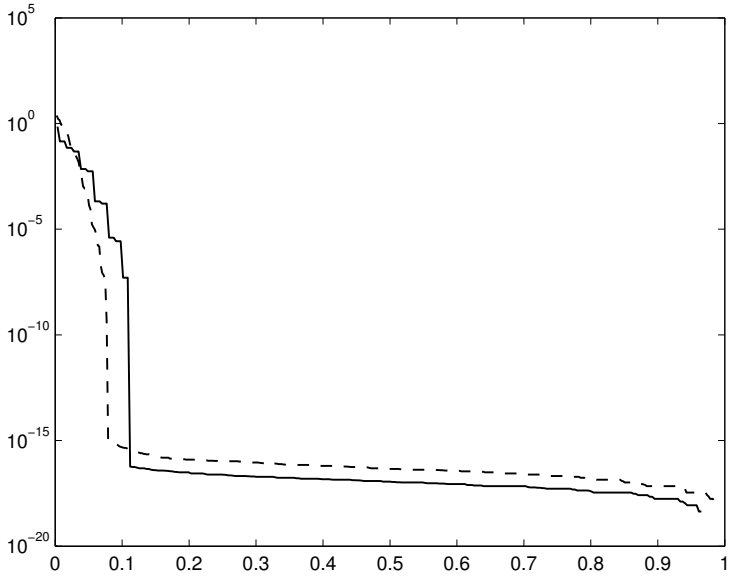


Figure 4.7: Magnitudes of entries of $\boldsymbol{\alpha}$ sorted by size. *Ishigami function* (dashed) and *sum of polynomial sinusoids* (solid)

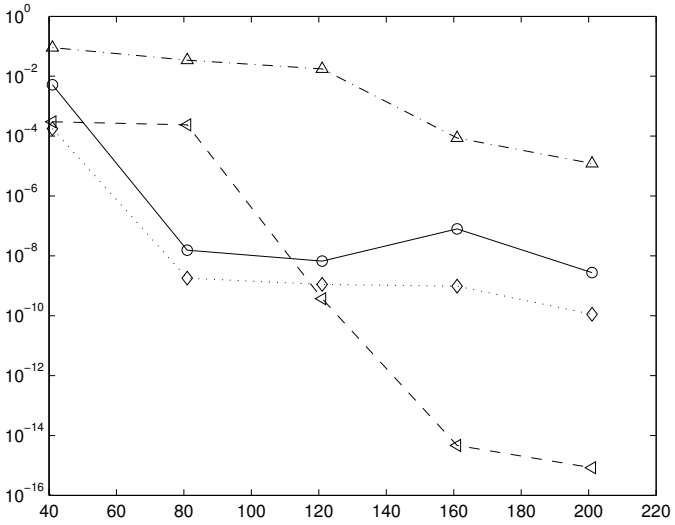


(a) $\|\boldsymbol{\alpha} - \hat{\boldsymbol{\alpha}}\|_2$ vs $m$

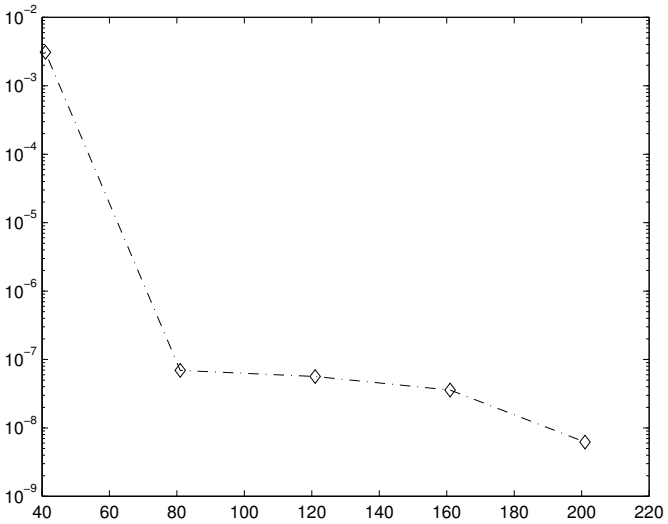


(b) $\left(\sum_{k=1}^{p} \|\boldsymbol{\alpha}^{(1),k} - \hat{\boldsymbol{\alpha}}^{(1),k}\|_2^2\right)^{1/2}$ vs $m$

Figure 4.8: *Rational function.* Error $\|\boldsymbol{\alpha} - \hat{\boldsymbol{\alpha}}\|_2$ vs number of data points $m$. for F-BPDN (diamond), S-BPDN (circle), $P_1^{\eta}$ (upward facing triangle), and S-OLS (left facing triangle)

in FIgure 4.9. Since the sparsity and coefficient decay in the derivative is comparable

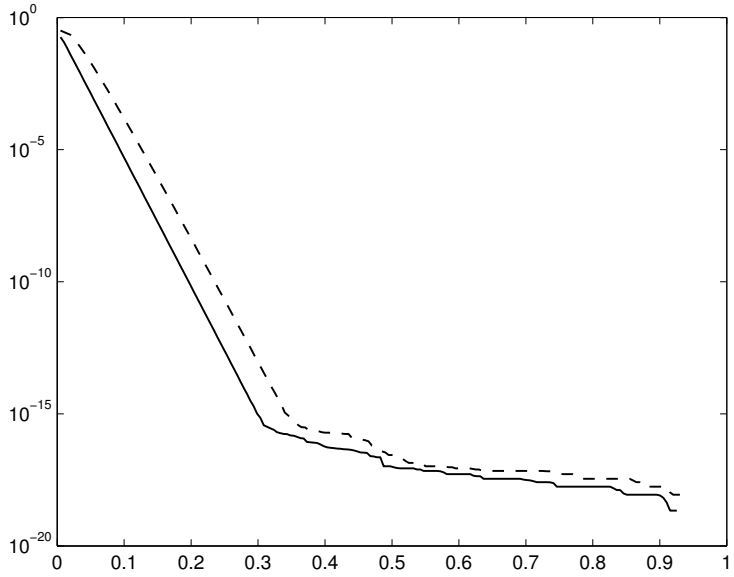


Figure 4.9: Magnitudes of coefficients for *rational function*. $\boldsymbol{\alpha}$ (solid) and $\boldsymbol{\alpha}^{(1)}$ (dashed)

to that of the function, the F-BPDN estimate is not dramatically better than the S-BPDN estimate.

**$C^1$ function [16].** $P = 150$**,** $p = 1$

$$f(x) = |x|^{3/2} \tag{4.40}$$

For our last test function, we choose one with finite regularity. The function $g(z) = |z|^{\beta}$ is not differentiable at $z = 0$ for $\beta \leq 1$ and is not twice differentiable for $\beta \leq 2$. Hence, we expect that approximation quality to the derivative using F-BPDN will be better than that of S-BPDN. The exact coefficients of the orthonormal Legendre

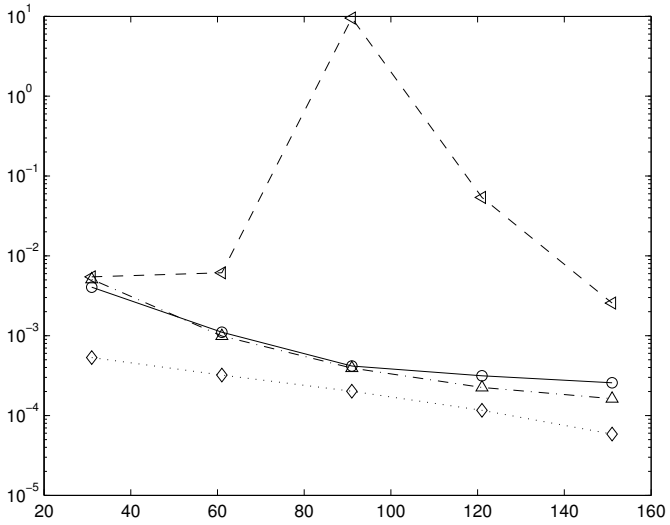


(a) $\|\boldsymbol{\alpha} - \hat{\boldsymbol{\alpha}}\|_2$ vs $m$

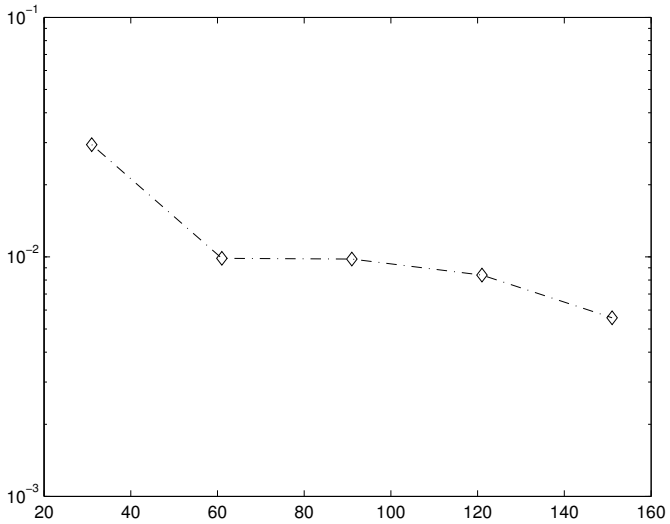


(b) $\left(\sum_{k=1}^{p} \|\boldsymbol{\alpha}^{(1),k} - \hat{\boldsymbol{\alpha}}^{(1),k}\|_2^2\right)^{1/2}$ vs $m$

Figure 4.10: $C^1$ *function.* Error $\|\boldsymbol{\alpha} - \hat{\boldsymbol{\alpha}}\|_2$ vs number of data points $m$. for F-BPDN (diamond), S-BPDN (circle), $P_1^{\eta}$ (upward facing triangle), and S-OLS (left facing triangle)

expansion are given in closed form

$$\alpha_j = \begin{cases} 0, & j \text{ odd}, \\ \frac{1}{a+1}, & j = 0, \\ \frac{\sqrt{2j+1}a(a-1)(a-2)\ldots(a-j+2)}{(a+1)(a+3)\ldots(a+j+1)} & \text{otherwise} \end{cases} \tag{4.41}$$

where $a = 3/2$. These coefficients converges *algebraically* and thus we expect a significant truncation error, directly affecting the quality of approximation. Figure 4.10 shows slow convergence across all estimators. Due to poor quality of LPD approximation to the derivative, the S-BPDN estimate essentially adds no information to the $P_1^\eta$ estimate and in fact, seems to degrade the estimate beginning at $m_3$. However, the F-BPDN estimate remains stable and offers an estimation accuracy that is consistent with $P_1^\eta$ for the same number of data points.

### 4.3.3 Remark on exchangeability of of $\boldsymbol{y}$ and $\boldsymbol{g}$

One important question that motivated this study is whether the function information is exchangeable with derivative information. That is, are the pairs $(\boldsymbol{x}_i, y_i)$ and $(\boldsymbol{x}_i, g_i^{(k)})$ equally useful for estimating $\boldsymbol{\alpha}$? Intuitively, we may think that they should. For example, we could create an artificial function value by applying Taylor's theorem to a collocated point value and derivative by simply taking a small step $\Delta x$ from the collocation point. However, from our experiments, we conclude that this answer is dependent on both the function and the estimator used. If the function exhibits sparsity in its partial derivatives, F-BPDN not only *enhances* the estimate but *accelerates* it towards the true value. In these instances, it has a higher efficiency than $P_1^\eta$. When the derivatives are less favorable (equally or more dense than the function in the Legendre expansion), it exhibits an efficiency that is at least as good as the $P_1^\eta$ estimate. For functions with high regularity, S-BPDN generally gives an estimate that is equally efficient to the $P_1^\eta$ but maybe worse when this condition is not satisfied even when both estimates share the same function values.

## 4.4 Summary

We've developed and tested several new gradient enhanced estimators for high dimensional estimation. S-BPDN is a natural extension of $P_1^\eta$ which performs well for most function of interest but is limited by the poor approximation quality in its derivative fit. The F-BPDN estimator aimed to resolve this deficiency while adding the capability to exploit sparsity in the derivatives. Experimental results show that this can lead to extremely low under sampling rates and achieve efficiencies even better than that of $P_1^\eta$. Furthermore, since this estimator gives an accurate approximation to the derivatives, one could utilize this surrogate inside of a surrogate based optimization framework. The possible downside to this estimator is a potentially large ($M + M'p$ variables) optimization problem. However, this can be overcome using parallel algorithms such as ADMM [[Boyd]] since objective is separable in $\boldsymbol{\alpha}$ and $\boldsymbol{\alpha}^{(1),k}$, $k = 1, \ldots, p$. Future work includes analysis of the estimator consistency and theoretical undersampling rates when there is sparsity in both function and derivatives.

# Chapter 5

# Variable importance by sensitivity analysis

With the advances in sparse representations, we are tempted to define an exaggerated UQ problem that includes all possible uncertainties and simply let the $\ell_1$ machinery sort it out. However, the ability to identify the most important variables or rank their importance remains invaluable. Firstly, it offers critical insight to modelers and engineers responsible for understanding the physical system and its behavior. Secondly, the presence of many unimportant or *nuisance* variables degrades estimation quality by adding superfluous parameters to be estimated. The ability to rank variables by importance would allow us to judiciously remove unimportant inputs, thereby reducing the dimensionality of the problem.

Informally, sensitivity analysis is study of methodologies used to identify important variables from unimportant variables. We will use the terms *sensitivity* and *importance* interchangeably when describing the impact of a variable on the response. A good introduction is given by Saltelli [75]. This topic also goes by the aliases subset selection, model selection, and variable screening. We are particularly interested in the subfield, *variance-based global sensitivity analysis*. These methods rank parameter importance with respect to a response by its contribution to the variance of the response.In this section, we will review the functional ANOVA (analysis-of-variance) decomposition and how it applies to the polynomial surrogates under consideration.

We'll discuss Sobol' definition for sensitivity and common approaches for computing this quantity. We then show the effectiveness of $\ell_1$ methods to identify important variables even when the estimation error is not small.

## 5.1 ANOVA Decomposition

### 5.1.1 Background

The functional ANOVA decomposition is a widely used tool for exploratory analysis of functions. It allows us to quantify the characteristics of a function based on the number of important dimensions, the degree of interaction between dimensions, its *effective dimensionality* and more. The decomposition is composed of $2^p - 1$ effects and corresponding variance contributions. Naturally, estimating these all effects are extremely difficult to do in high dimensions without further assumptions on $f$. The ANOVA decomposition of $L^2[0,1]^p$ was first presented by Hoeffding [51] in 1948 for his analysis of $U$-statistics, Sobol' used it for multidimensional integration by Haar functions [78] in 1969 and Efron and Stein [36] used it to study the jacknife in 1981. In the sequel, we mostly retain the notation of Owen [65].

### 5.1.2 Notation

For subsets $u \subseteq \mathcal{D} = \{1, \ldots, p\}$, let $|u|$ denote the cardinality of $u$ and let $v - u$ denote the set difference $\{j : j \in v, j \notin u\}$ and let $-u$ denote the complement $\mathcal{D} - u$. Using a slightly different notation for the variables $\boldsymbol{x} = (x^1, x^2, \ldots, x^2)$, denote $\boldsymbol{x}^u$ to be the $|u|$-tuple of components $x^j$ $j \in u$ where $\boldsymbol{x}^u$ lives in a copy of $[-1,1]^{|u|}$.

### 5.1.3 Definitions and properties

Let $f \in L^2(\Omega)$ where the domain is the centered hypercube $\Omega = [-1,1]^p$, $\boldsymbol{x} \in \Omega$. Denote its mean $\mu$ to be $\mu(f) = 2^{-p} \int_\Omega f(\boldsymbol{x}) d\boldsymbol{x}$ and variance $\sigma^2 < \infty$ to be $\sigma^2(f) = 2^{-p} \int_\Omega (f(\boldsymbol{x}) - \mu(f))^2 d\boldsymbol{x}$ where $d\boldsymbol{x} = dx_1 dx_2 \cdots dx_p$ is the product Lebesgue measure.

Then, $f$ has the following decomposition

$$f(\boldsymbol{x}) = \sum_{u \subseteq \mathcal{D}} f_u(\boldsymbol{x}) \tag{5.1}$$

where $f_u(\boldsymbol{x}) = f_u(\boldsymbol{x}^u)$ depends on $\boldsymbol{x}$ only through $\boldsymbol{x}^u$. The function $f_u$ is defined recursively by:

$$\begin{aligned} f_u(\boldsymbol{x}) &= 2^{-p} \int \left( f(\boldsymbol{x}) - \sum_{v \subset u} f_v(\boldsymbol{x}) \right) d\boldsymbol{x}^{-u} \\ &= 2^{-p} \int f(\boldsymbol{x}) d\boldsymbol{x}^{-u} - \sum_{v \subset u} f_v(\boldsymbol{x}) \end{aligned} \tag{5.2}$$

We can interpret this as the function that remains after subtracting attribution to proper subsets of $u$ and then averaged over the values of $\boldsymbol{x}^{-u}$. It follows that this decomposition has the properties

$$\int f_u(\boldsymbol{x}) d\boldsymbol{x}^u = 0 \tag{5.3}$$

$$\int f_u(\boldsymbol{x}) f_v(\boldsymbol{x}) d\boldsymbol{x} = 0, \quad u \neq v. \tag{5.4}$$

It can be shown [53] that the functional decomposition of form (5.1) is unique when the functions $f_u$ satisfy the properties in (5.3). By orthogonality, the variance $\sigma^2$ decomposes additively according to $u$

$$\sigma^2 = \sigma^2(f) = \sum_{u \subseteq \mathcal{D},\, u \neq \emptyset} \sigma^2(f_u) \tag{5.5}$$

That is, the function $f$ has an orthogonal decomposition in the $2^p$ functions $f_u$ and has variance which is the sum of the individual variances $\sigma^2(f_u)$. Tang [82] shows that by applying the orthogonality property, the partial variances $\sigma^2(f_u)$ simply to

$$\sigma^2(f_u) = 2^{-p} \int \left( \int f(\boldsymbol{x}) d\boldsymbol{x}^{-u} \right)^2 d\boldsymbol{x}^u - 2^{-p} \sum_{v \subset u} \int f_v(\boldsymbol{x})^2 d\boldsymbol{x}^u \tag{5.6}$$

## 5.2 Sobol' indices

Sobol' [77] introduced the partial effect indices $S_u$ that measures the variance contribution of $f_u$ to $f$ by

$$S_u = \frac{\sigma^2(f_u)}{\sigma^2} \tag{5.7}$$

In addition, he presented two ways to quantify the importance of a subset $u$ of variables by

$$\underline{S}_u = \sum_{v \subseteq \mathcal{D},\, v \subset u} S_v \tag{5.8}$$

$$\overline{S}_u = \sum_{v \subseteq \mathcal{D},\, v \cap u \neq \emptyset} S_v \tag{5.9}$$

When $u$ is a singleton $u = j$, $\underline{S}_j = S_j$ is defined to be the *main effect* of variable $x^j$ and $\overline{S}_j$ is defined to be the *total effect* of variable $x^j$. The main effect only measures the direct impact of $x^j$ while ignoring interactions with other variables while the total effect includes interactions as well. Comparing the main and total effect indices allow us to rank the relative importance of each variable to the response.

### 5.2.1 Estimating $S_u$ using polynomial surrogates

Sobol' [77] also gave several clever Monte Carlo algorithm to compute the indices $S_u$. For some advances see [75, 66]. Seeking to avoid Monte Carlo, we are interested in cheaply and accurately computing the sensitivity indices when a polynomial surrogate is available. To be sure, we could simply apply the Monte Carlo algorithms proposed by Sobol' on the surrogates to obtain an estimate efficiently and cheaply. However, since the surrogates are polynomials we can use Gauss quadrature to obtain the exact sensitivity indices of the surrogates. Furthermore, the form of Legendre polynomial expansion allows for a natural approximation of the functions $f_u$.

### Lagrange polynomials

For a set of sample points and function values $(\boldsymbol{x}_i, y_i)$, $y_i = f(\boldsymbol{x}_i)$, $i = 1, \ldots, m$, the Lagrange polynomial approximation of a function has the form

$$f_L(\boldsymbol{x}) = \sum_{i=1}^{m} f(\boldsymbol{x}_i) L_i(\boldsymbol{x}) \tag{5.10}$$

where $L_i(\boldsymbol{x})$ is the multivariate Lagrange polynomial that satisfies $L_i(\boldsymbol{x}_j) = \delta_{ij}$; i.e. the Lagrange polynomial approximation interpolates the function $f$ at the sample points $\boldsymbol{x}_i$. The explicit form of $L_i(\boldsymbol{x})$ can be found in any elementary numerical analysis text such as [48]. Since the Lagrange polynomial interpolates the true function at the sample points, it is intuitive that a quadrature estimate of the Sobol' indices $\hat{S}_u$ using the points $(\boldsymbol{x}_i, f(\boldsymbol{x}_i))$, $i = 1, \ldots, m$ is equivalent to the Sobol' indices that result from performing quadrature over $f_L(\boldsymbol{x})$ at the same points. An explicit expression for this estimate is given in [82]. However, the structure of this polynomial approximation does not lend to an obvious estimate of the functions $f_u(\boldsymbol{x})$.

### Legendre polynomial expansions

The ANOVA decomposition of Legendre polynomial expansions is particularly simple. Sudret [80] gives results for more general orthogonal expansions. For a choice of basis functions $\Lambda$, the basis functions $\phi_{\boldsymbol{j}} \in \Lambda$ naturally partition into variable subsets $u \subseteq \mathcal{D}$ according to their multi-index $\boldsymbol{j} = (j_1, \ldots, j_p)$. Namely, $\phi_{\boldsymbol{j}}(\boldsymbol{x})$ depends on $\boldsymbol{x}$ only through $\boldsymbol{x}^u$ for $u = \{k : j_k > 0, \boldsymbol{j} = (j_1, \ldots, j_p)\}$. Define the set of multi-indices $\mathcal{J}_u = \{\boldsymbol{j} : j_k > 0, k \in u, j_k = 0, k \notin u, k = 1, \ldots, p\}$ to be a partition of $\lambda_p^P$ by subsets $u \subset \mathcal{D}$. Since the Legendre polynomial basis functions have mean zero and are mutually orthogonal, it follows from uniqueness of the decomposition that the constituent functions of a Legendre polynomial expansion is defined as

$$f_u(\boldsymbol{x}; \Lambda) = \sum_{\boldsymbol{j} \in \mathcal{J}_u} \alpha_{\boldsymbol{j}} \phi_{\boldsymbol{j}}(\boldsymbol{x}) \tag{5.11}$$

Define the *maximal univariate degree* set $\Theta_p^P = \{\phi_{\boldsymbol{j}} : j_k \leq P, \boldsymbol{j} = (j_1, \ldots, j_p) \in \mathbb{N}^p\}$. Suppose $\Lambda = \Theta_p^P$. If the coefficients $\alpha_{\boldsymbol{j}}$ are computed using Gauss quadrature points, and the number of quadrature points $m$ exceeds the number of terms in the expansion $|\Theta_p^P|$, the Legendre polynomial expansion is equivalent to the interpolating Lagrange polynomial 5.10 constructed from the same quadrature points [24]. In other words, the Legendre expansion is interpolatory at the quadrature points and the equivalence of quadrature estimates follow from the Lagrange polynomial. More generally, for an arbitrary choice of $\Lambda$, it follows from Equation (5.11) that

$$S_u(\Lambda) = \sum_{\boldsymbol{j} \in \mathcal{J}_u} \alpha_{\boldsymbol{j}}^2 \tag{5.12}$$

## 5.3 Fast variable ranking by $\ell_1$-methods

While the accurate estimate $S_u$ allows us to ask precise questions such as "what is the minimum amount of variation lost by fixing this variable," often times it is merely used as a tool to rank the importance of the inputs. In particular, if the goal is to obtain a truncated expansion in the top $k$ inputs, it may suffice to simply know the ordering of quantities such as the total effect $\overline{S}_j$.

Recall from Theorem 3.2.4 that for a fixed value of $m$, $P_1^\eta$ gives us an estimate that is close to the best $k$-term approximation modulo a factor of the truncation error where where $k = k(m, M)$. Intuitively, the probability of incorrectly ranking the variables depends both on the rate at which correlations between basis functions go to zero and the rate at which quantities such as $\overline{S}_j$ decay. For example, if the coefficients $\alpha_{\boldsymbol{j}}$ decay rapidly, we may obtain the correct ranking of variables with far fewer points than would be necessary to get an accurate estimate. The theoretical developments are the focus of ongoing work. We present a few numerical experiments as a proof of concept.

## 5.4 Numerical experiments

The goal of the experiments is to determine the quality of the estimates $\hat{\bar{S}}_k$, $k = 1, \ldots, p$ for extremely under-sampled and inaccurate estimates $\hat{\boldsymbol{\alpha}}$. For each function, we compute the total effect indices $\hat{\bar{S}}_k$ from $\hat{\alpha}$ for a sequence of small sample sizes and compare their ranking to the ranking given by the true indices $\bar{S}_k$. The degree of undersampling (i.e. inaccuracy of the estimates) is represented by the error of $\hat{\boldsymbol{\alpha}}$ corresponding to those sample sizes. For some functions, we will add nuisance variables (variables that are independent of the function) to mimic the effect of including uncertainties that do not affect the quantity of interest. We denote the $p$ to be the *total* number of variables, which includes the nuisance variables and is the dimension used to determine the set of basis functions in the truncated series $\Lambda_p^P$.

Ishigami Function: $p = 3$, $P = 12$

$$f(\boldsymbol{x}) = \left[1 + 0.1\left(\frac{\pi}{2}x_3 - \frac{\pi}{2}\right)^4\right]\sin\left(\frac{\pi}{2}x_1 - \frac{\pi}{2}\right) + 7\sin\left(\frac{\pi}{2}x_2 - \frac{\pi}{2}\right)^2 \tag{5.13}$$

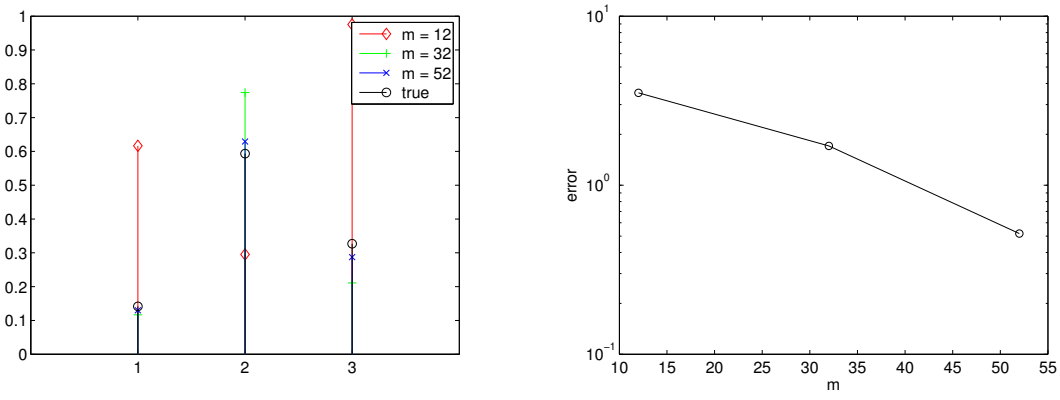


(a) Total effect indices $\hat{\bar{S}}_k$ vs $x_k$

(b) $\|\boldsymbol{\alpha} - \hat{\boldsymbol{\alpha}}\|_2$ vs $m$

Figure 5.1: Ishigami function

Gerstner Function: $p = 3$, $P = 10$

$$f(\boldsymbol{x}) = \exp(x_1) + \exp(x_2) + 10\exp(x_1 x_2) \tag{5.14}$$

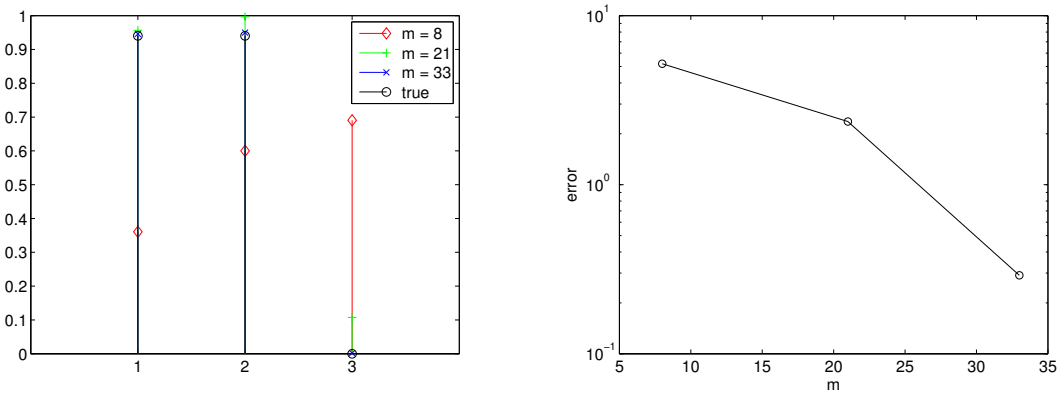


(a) Total effect indices $\hat{\tilde{S}}_k$ vs $x_k$

(b) $\|\boldsymbol{\alpha} - \hat{\boldsymbol{\alpha}}\|_2$ vs $m$

Figure 5.2: Gerstner function

Sobol G-Function: $p = 4$, $P = 12$

$$f(\boldsymbol{x}) = \prod_{k=1}^{4} \frac{|4x_k - 2| + a_k}{1 + a_k}, \quad \boldsymbol{a} = (0, 0.5, 1, 1.5) \tag{5.15}$$

Weighted sphere function: $p = 50$, $P = 2$

$$f(\boldsymbol{x}) = \sum_{k=1}^{50} a_k x_k^2, \quad a_k = \begin{cases} 10 - k + 1 & \text{for } k \leq 10 \\ 0 & \text{otherwise} \end{cases} \tag{5.16}$$

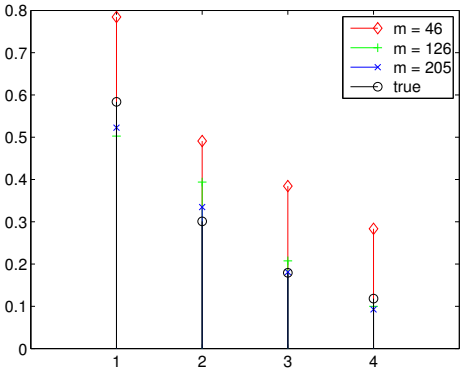


(a) Total effect indices $\hat{\tilde{S}}_k$ vs $x_k$

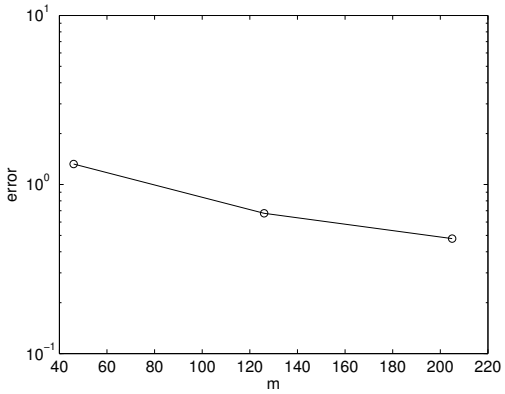


(b) $\|\boldsymbol{\alpha} - \hat{\boldsymbol{\alpha}}\|_2$ vs $m$

Figure 5.3: Sobol G-function

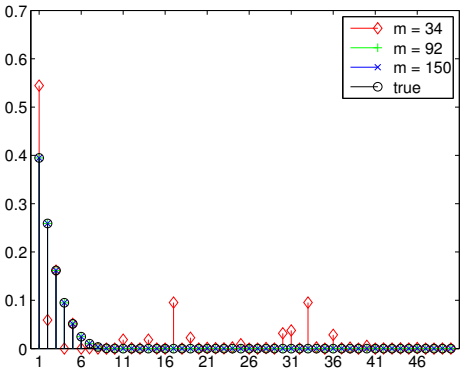


(a) Total effect indices $\hat{\tilde{S}}_k$ vs $x_k$

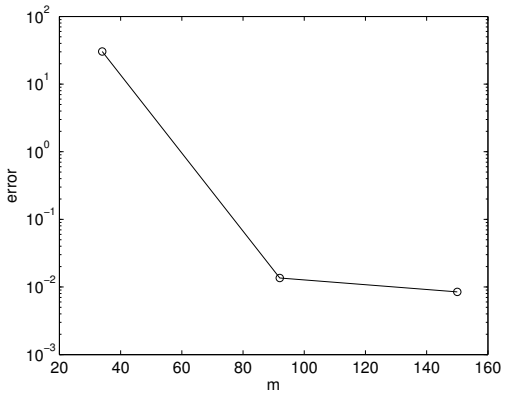


(b) $\|\boldsymbol{\alpha} - \hat{\boldsymbol{\alpha}}\|_2$ vs $m$

Figure 5.4: Weighted sphere function

Sphere function: $p = 50$, $P = 2$

$$f(\boldsymbol{x}) = \sum_{k=1}^{50} a_k x_k^2, \quad a_k = \begin{cases} 1 & \text{for } k \leq 10 \\ 0 & \text{otherwise} \end{cases} \tag{5.17}$$

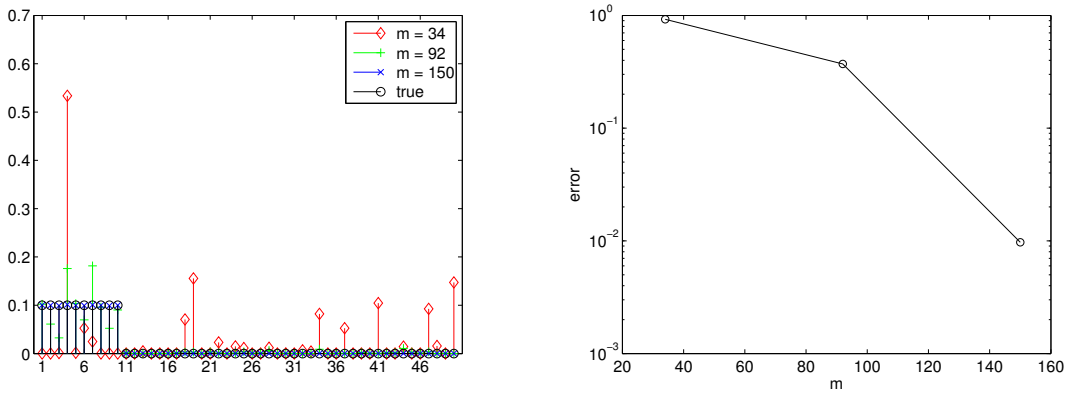


(a) Total effect indices $\hat{\bar{S}}_k$ vs $x_k$

(b) $\|\boldsymbol{\alpha} - \hat{\boldsymbol{\alpha}}\|_2$ vs $m$

Figure 5.5: Sphere function

## 5.5 Discussion

The numerical experiments on a variety test functions show that even for fairly inaccurate estimates $\hat{\boldsymbol{\alpha}}$, the corresponding total effect estimates $\hat{\bar{S}}_k$ can reliably rank variable importance. The proper ranking of the first three functions is obtained despite errors on the order $\approx 1$. The last two functions show that the ranking of $\hat{\bar{S}}_k$ is robust even in the presence of many nuisance parameters. The small sample analyses proposed here can give the UQ practitioner insight into significant and negligible uncertainties and enables one to design a more tailored basis set $\Lambda$ and sampling scheme.

## 5.6 Future work

The goal of this work is to identify important uncertainties without needing to construct a surrogate over full set of nominal uncertainties. However, in the extremely high dimensional case, there may be so many parameters such that starting an $\ell_1$ procedure would be infeasible. El Ghaoui [37] shows how one can use the KKT conditions governing the estimates $\hat{\boldsymbol{\alpha}}$ can be used to automatically detect which coefficients will

be exactly zero. The idea is to perform a screening step before an $\ell_1$ estimate is computed. When the basis functions are properly scaled, it can be shown [37] that this is equivalent to standard correlation-based feature selection [50]. However, these conditions only describe sparsity in the *basis functions*. What we'd prefer is conditions that describes sparsity in the *variables* i.e. whether an uncertainty variable $x_k$ can be determined to have zero or nearly zero [85] effect. A possible direction of future research would utilize a more general notion of sparsity that is well described by the Group Lasso [96]. For example, one could construct groups (even overlapping groups) based on the ANOVA decomposition and the definition for $\bar{S}_k$. From the (overlap) Group Lasso setting, one could construct test based on the KKT conditions that would determine whether or not an entire group of basis functions would be exactly zero.

# Chapter 6

# UQ analysis of vertical axis wind turbines

We consider a UQ analysis of a notional 5MW, offshore, vertical-axis wind turbine (VAWT). Pacquette and Barone [67] explore the use of VAWTs in resource-rich, deep-water locations where conventional horizontal-axis wind-turbines (HAWT) may not be economically viable. They argue that the three fundamental characteristics of VAWTs: lower turbine center of gravity, simplicity in the machine architecture, and the opportunity for scaling to very large sizes align well with the design constraints for offshore wind.

As a part of a broader feasibility study, these systems must be designed such that they can pass certification tests and withstand real world operating conditions. The scale of the notional design is far too large to construct, and thus, experimentation and preliminary testing must be carried out by numerical simulation. The quantity of interest in this work is the blade load impulse, a time-integrated quantity that serves as a proxy to the maximum blade load experienced by each blade when subject to an extreme gust event. We quantify the uncertainty of this response subject to a stochastic gust profile and geometric variability in the blades. We begin by giving detailed descriptions of the physical system and characterizations of the uncertainties. Then, we outline the solution procedure

## 6.1 Description of physical system

The VAWT being studied is known as a V-VAWT; an example is shown in Figure 6.1. The parameters describing the nominal geometry and operating conditions are given

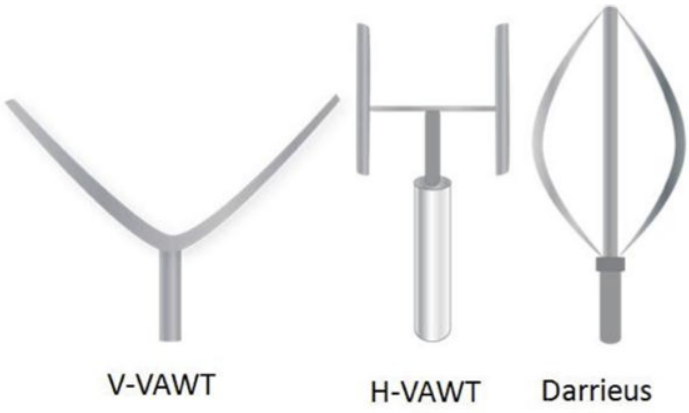


Figure 6.1: VAWT varieties [67]

in Table 6.1. We will not simulate the full three-dimensional geometry but rather a

Table 6.1: VAWT Design parameter

| Design Parameter | Value |
|---|---|
| rotor radius (m) | 74 |
| height from base of rotor (m) | 85 |
| number of blades | 3 |
| blade chord (m) | 1.52 |
| blade attachment point (fraction of chord) | 0.5 |
| rotational speed (rpm) | 7.66 |
| airfoil | SNL0018/50 |
| chord Reynolds number | $5.4 \times 10^6$ |
| tip speed ratio | 4 |

two-dimensional cross-section of the rotors on a plane parallel to the ground. The rotor blades will be represented by three, two-dimensional airfoils that are axially symmetric. In a future study, these airfoils will be allowed to pitch and translate radially to model fluid-structure interaction; a visualization of these systems are given

in Figure 6.2. For the purposes of this work, the structure is assumed to be fixed. For

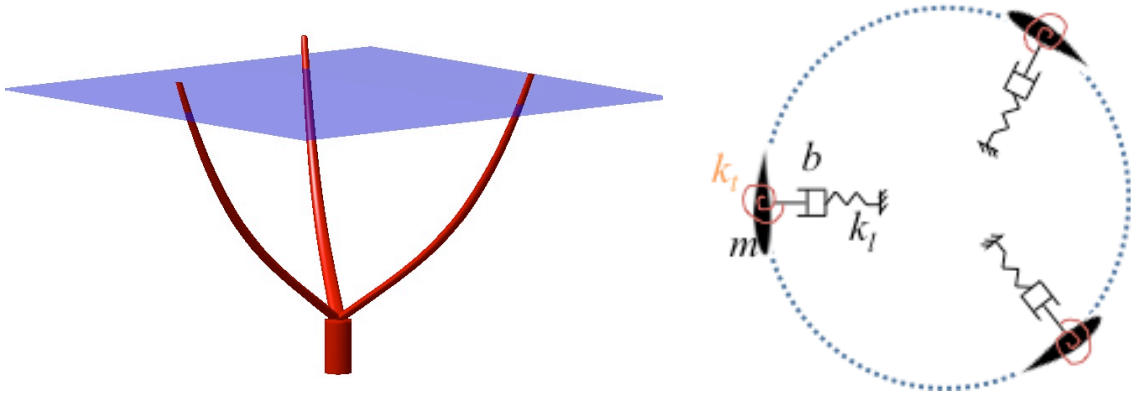


(a) preliminary design and cross-sectional plane (b) rotor cross-section

Figure 6.2: Notional offshore V-VAWT design [63]

the system depicted in Figure 6.2b, the wind travels from left to right and produces aerodynamic loads on the airfoils; the local velocity and resultant loads are shown in Figure 6.3. The maximum normal blade load $F_N$ experienced by the turbine blades is a key constraint in the structural design of the VAWT. We use a proxy metric, the blade load impulse, $f_0$, as our quantity of interest.

$$f_0 = \int_{t_1}^{t_2} |F_N(t)|\, dt \tag{6.1}$$

In most cases, a design with larger blade load impulse will have larger maximum load. We prefer the time-integrated form because it is smoother than the maximum load and thus more amenable to polynomial approximation methods.

## 6.2 Description of computational code: CACTUS

We simulate this two-dimensional system using CACTUS (Code for Axial and Cross-flow Turbine Simulation) [3, 62], a turbine performance simulation code based on a free wake vortex method developed at Sandia National Labs. The physics of the

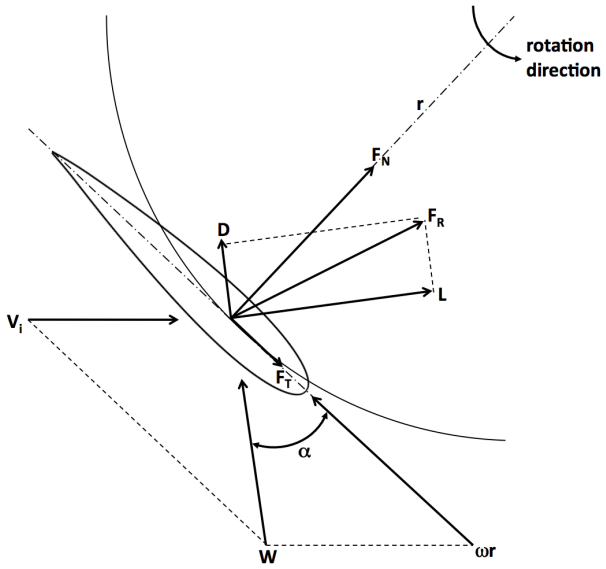


Figure 6.3: Depiction of aerodynamic loading on single airfoil [17]

fluid system is described by potential flow that includes a dynamic wake and models dynamic stall effects. We summarize the detailed description found in [3].

The fluid flow field is represented by a superposition of potential flow elements: a free stream element, a vortex system composed of the trailing and spanwise wake vorticity, and a bound vortex system attached to the blade elements. From the set of potential flow elements, the velocity field can be evaluated using the Bio-Savart law [1]. Given a description of the wake vortex lattice system at any time, the solver determines a set of blade element loads that are consistent with the local flow at each element produced by the current wake, freestream flow, and bound vorticity. This condition and nonlinearities introduced by a dynamic stall model is described by a set of algebraic equations that are solved at each temporal iteration.

The geometry of the blades only affects computation of the flow field through the vorticies attached to the blade elements. Instead of discretizing the surface of the airfoils like most panel methods, CACTUS uses precomputed airfoil polars associated to the blades' cross-section to determine the value of the bound vortex. We mimic the effect of geometric variability by perturbing the polars directly and invoking

the inverse relationship between polar and geometry. The characterization of this perturbation is given in the next section.

## 6.3 Problem description and uncertainty characterization

We are interested in predicting *blade load impulse* for an oncoming gust. Since the same airfoil is used in all three blades, it suffices to predict the blade load impulse for a single blade. The prediction is subject to a non-deterministic gust profile and geometric variability in the airfoils. Denote the ensemble of variables used to characterize those uncertainties to be $\boldsymbol{x} \in \mathbb{R}^p$. We simulate the VAWT system over eleven revolutions which corresponds to an 86.2 second period. Our quantity of interest is given by the following integral

$$f(\boldsymbol{x}) = \int_{t_1}^{t_2} |F_N(t, \boldsymbol{x})| \, dt, \tag{6.2}$$

where $(t_1, t_2) = (53.5, 81.5)$. Now, let us define the uncertainties $\boldsymbol{x}$.

### 6.3.1 Stochastic gust

While we are certain that our VAWT will experience a gust, the exact characterization of that gust profile is stochastic. We've modeled the gust using three parameters describing its arrival time $x_1$ (i.e. the blade orientation when the gust hits), duration $x_2$, and maximum velocity $x_3$. They are described by the following random variables

$$\begin{aligned} x_1 \,(\text{sec}) &\sim U[66.45, 67.32], \\ x_2 \,(\text{sec}) &\sim U[10, 12], \\ x_3 \,(\text{ft/s}) &\sim U[40, 50] \end{aligned} \tag{6.3}$$

The nominal freestream velocity is $U_\infty = 48.69$ (ft/s) which means the incoming velocity is nearly a factor of two larger when exposed to a gust.

### 6.3.2 Geometric variability

In addition to the stochastic gust, we also consider the effect of uncertainty in the geometry of the blades. This can be a consequence of manufacturing, or more commonly, the accretion of foreign substances such as dirt, debris, and bug splatter. Let $a \in [-1, 1]$ be the angle of attack in degrees normalized by 180. Using the Sandia 0018/50 symmetric airfoil's polar $(\bar{C}_L(a), \bar{C}_D(a))$ as the mean, we represent a family of perturbed polars $(C_L(a), C_D(a))$ using a Karhunen-Loeve like expansion of a stationary random field. Define the mean zero random field $W(a)$ to be

$$W(a) = \sum_{j=0}^{\infty} \sqrt{\lambda_j}\psi_j(a)z_j, \quad z_j \sim U[-1, 1], \tag{6.4}$$

where $\psi_j$ and $\lambda_j$ are the eigenfunctions and eigenvalues from the Gaussian correlation function

$$C(a, a') = \sigma_0 \exp\left(-\frac{|a - a'|^2}{2c_0}\right) \tag{6.5}$$

with parameters $c_0 = 4$ and $\sigma_0 = 0.03$. Then, the perturbed polars are define by

$$\begin{aligned} C_L(a) &= \bar{C}_L(a) + \sqrt{0.1|\bar{C}_L(a)|}W(a) \\ C_D(a) &= \bar{C}_D(a) + \sqrt{0.1|\bar{C}_D(a)|}W(a), \end{aligned} \tag{6.6}$$

This formulation creates a direct correlation between the perturbed functions $C_L$ and $C_D$ that implies positive/negative perturbations in $C_L$ result in positive/negative perturbations in $C_D$ and vice versa. Pre-multiplying the random field $W(a)$ by $\sqrt{0.1|\bar{C}_{(\cdot)}(a)|}$ produces a spatially (i.e. angle of attack) dependent variance that is proportional to the nominal magnitude for $\bar{C}_{(\cdot)}(a)$. In order to accommodate some numerical nuances of CACTUS, we augment the expressions in Equation (6.6) to enforce symmetry about $a = 0$. More specifically, Equation (6.6) holds for $a \in [-1, 0)$,

and we enforce

$$C_L(a) = C_L(-a), \quad C_D(a) = C_D(-a), \tag{6.7}$$

for $a \in (0, 1]$. Because the eigenvalues $\lambda_j$ decay rapidly for this correlation function, we only retain the first seven modes of the random field and let

$$(x_4, \ldots, x_{10}) := (z_0, \ldots, z_6). \tag{6.8}$$

Using these seven modes, a few realizations of $(C_L, C_D)$ are given in Figure 6.4. The addition of these seven uncertain variables gives a total of ten input uncertainties in our problem.

## 6.4 Numerical results

### 6.4.1 Estimation

Our polynomial surrogate is the truncated Legendre series represented by the basis functions in the maximal degree set $\Lambda_p^P$, where $p = 10$ and we choose $P = 6$. This set has $M = 8008$ basis functions and coefficients $\boldsymbol{\alpha} \in \mathbb{R}^{8008}$. We perform 10,000 simulations using the DAKOTA framework [38] with CACTUS. From the responses generated from the simulations, we solve the basis pursuit denoising problem $P_1^\eta$ using [76] for a sequence of sample sizes

$$\boldsymbol{m} = [50, 75, 100, 500, 1000, 3000, 6000, 8000].$$

Since the true solution $\boldsymbol{\alpha}$ is not known, we use prediction error,

$$\begin{aligned} PE &= \|f - \hat{f}_M\|_{L^2}^2 \\ &= \sum_{\boldsymbol{j} \in \mathcal{A}_p^P} (\alpha_{\boldsymbol{j}} - \hat{\alpha}_{\boldsymbol{j}})^2 + \sum_{\boldsymbol{j} \notin \mathcal{A}_p^P} \alpha_{\boldsymbol{j}}^2, \end{aligned} \tag{6.9}$$

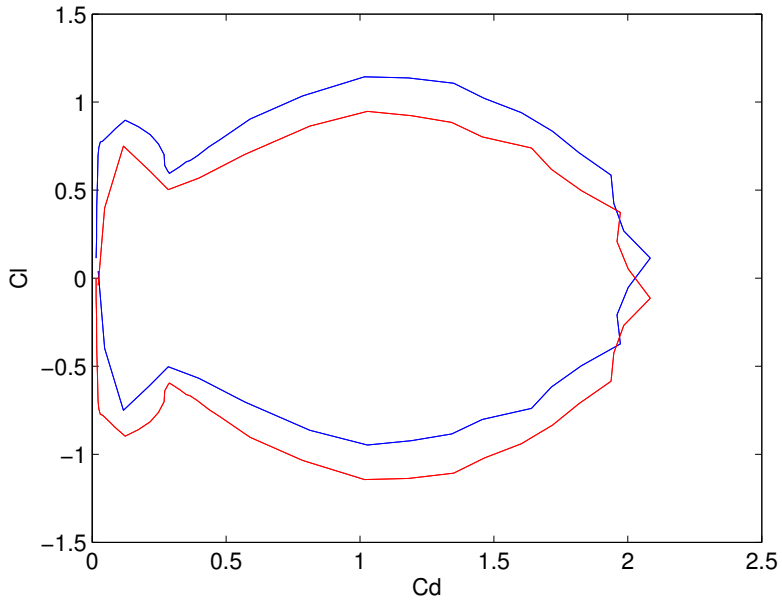


(a) Nominal polar for Sandia 0018/50 airfoil

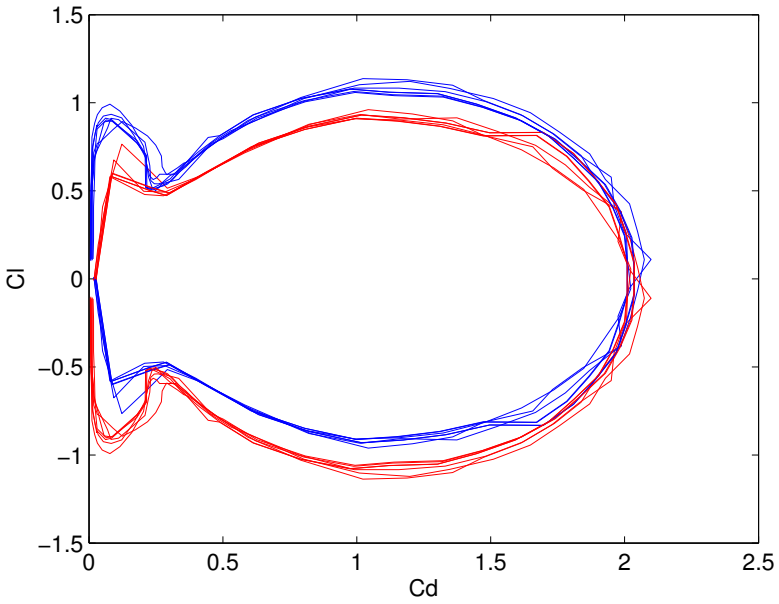


(b) Ten instances of $(C_L, C_D)$

Figure 6.4: Aerodynamic polars at positive (blue) and negative (red) angles of attack

to determine the quality of our approximation. The left term represents the estimation error while the right term represents the truncation error. Once the prediction error ceases to decrease with an increasing number of samples $m$, the estimation error has converged. The error convergence plot for our estimate $\hat{\boldsymbol{\alpha}}$ is given in Figure 6.5. We

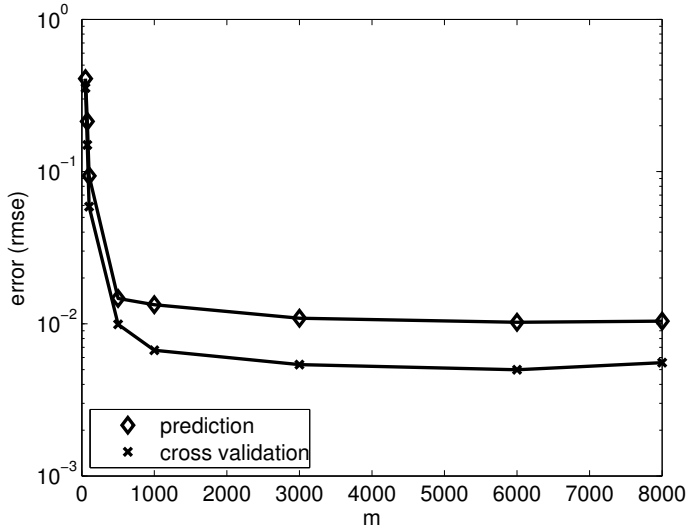


Figure 6.5: Cross validation and prediction error of $\hat{\boldsymbol{\alpha}}$ as a function of samples $m$

see that both $k$-fold cross validation and prediction error curves flatten at around $m = 3000$. This suggests that we are able to converge the estimation error using a number of samples that is less than half the number of unknowns. Furthermore, Figure 6.6 shows that the cumulative distribution function (CDF) of the blade load impulse generated from $m = 10,000$ samples is well approximated by interrogating the surrogate estimated using only $m = 100$ samples; it is nearly identical for $m = 500$ samples.

### 6.4.2 Effect of uncertainty on the blade load impulse

Figure 6.6 shows estimates of the cumulative distribution function (CDF) of the blade load impulse subject to the uncertainties described in previous sections. We see the uncertainties generally have the effect of *decreasing* the blade load impulse

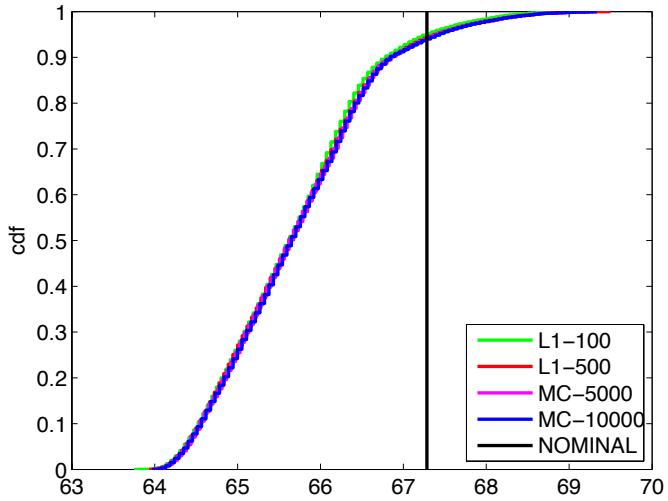


Figure 6.6: CDF of the blade load impulse subject to uncertainty

from its nominal value. Specifically, the blade load impulse is less than the nominal value with probability exceeding 0.9. We understand this to be a result of degraded aerodynamic performance caused by "off design" geometric variation characterized by the perturbed polars. Nonetheless, there is still a non-trivial probability that the impulse exceeds the nominal value and must be accounted for in the design.

### 6.4.3 Sensitivity analysis

Aside from estimating the resultant variation due to uncertainty, an important part of any UQ analysis is identifying the most impactful uncertainties or uncertain parameters (to discern the uncertainties, e.g. gust, from its parameterization, e.g. duration). To identify the most influential variables in $\boldsymbol{x}$, we perform a variance-based sensitivity analysis as described in Chapter 5. Estimates of the total effect Sobol' indices $\hat{\tilde{S}}_k$, $k = 1, \ldots, 10$ are shown in Figure 6.7. We see that the variance in the blade load impulse is dominated by the arrival time and duration of the gust and the first mode in the polar perturbations. In fact, using as few as $m = 50$ sample points, sensitivity analysis via $\ell_1$-methods is able to identify the three important uncertain parameters.

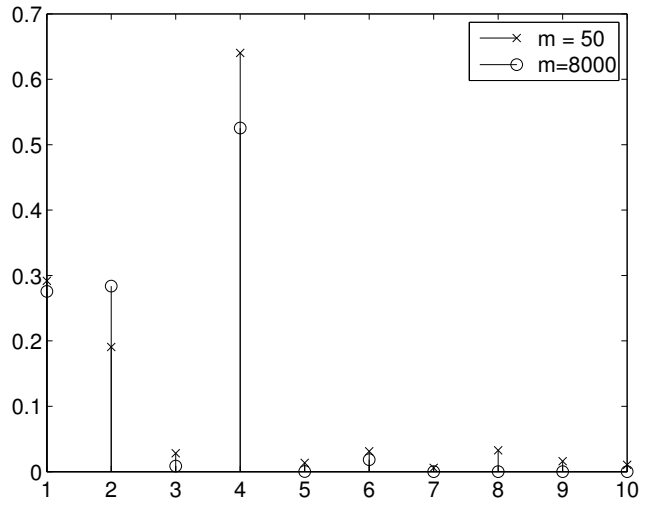


Figure 6.7: Total effect indices $\hat{\bar{S}}_k$ for variables $x_k$

## 6.5 Summary

This chapter described a UQ analysis of a notional vertical axis wind turbine subject to uncertain gust profile and turbine blade geometry. The polynomial surrogate constructed on this ten dimensional input space was efficiently estimated using the noise-aware basis pursuit algorithm $P_1^\eta$. The uncertainties driving the variation in the blade impulse load were determined to be gust arrival, gust duration, and the first mode of random field describing geometric variability. We determined that the uncertainties generally caused the blade load impulse to decrease, albeit with non-trivial probability that the impulse will increase (above the nominal).

The results in the previous section highlight a greater theme regarding $\ell_1$ methods for UQ which is the quality of "intermediate" estimates. UQ practitioners rarely have the luxury of obtaining enough samples to converge statistics, surrogate parameters, etc. Instead, decisions are usually made based on incomplete analyses, and an ideal estimator would produces the best possible estimate for a given sample size $m$. Theorems 3.2.2 and 3.2.4 tell us that the estimates $\hat{\boldsymbol{\alpha}}$ will always be within a factor of the best $k$-term approximations where the relationship $k = k(m)$ is nearly optimal [23].

Figures 6.6 and 6.7 demonstrate the practical significance of this property, which give practitioners the insight to conduct more relevant and informative UQ analyses.

## 6.6 Addendum: approximating non-smooth functions with polynomial methods

The use of the blade load impulse over the more traditional maximum blade load was a deliberate change that made the problem simpler and estimation easier. Preliminary results showed that the maximum blade load calculated using CACTUS exhibited non-smooth behavior, a challenge that is not well suited to polynomial surrogates. The success of $\ell_1$-methods is predicated on the sparsity of the coefficients, which in turn, is dependent on the appropriate choice of basis functions. Global polynomials are an appropriate choice for smooth functions, but not non-smooth or discontinuous functions. Once a function has been determined to be non-smooth, the task shifts from coefficient estimation to basis selection. Some possible directions for future research include mixed global and local basis functions (e.g. Legendre polynomials with Haar wavelets) and adaptive hierarchical basis functions (e.g. multi-wavelets) within an $\ell_1$-regularized regression framework.

# Bibliography


[1] John David Anderson. *Fundamentals of aerodynamics*, volume 2. McGraw-Hill New York, 2001.

[2] Ivo Babuska, Raúl Tempone, and Georgios E Zouraris. Galerkin finite element approximations of stochastic elliptic partial differential equations. *SIAM Journal on Numerical Analysis*, 42(2):800–825, 2004.

[3] Matthew Franklin Barone and Jonathan Murray. The development of cactus: a wind and marine turbine performance simulation code. Technical report, Sandia National Laboratories, 2010.

[4] Marcel Bieri, Roman Andreev, and Christoph Schwab. Sparse tensor discretization of elliptic spdes. *SIAM Journal on Scientific Computing*, 31(6):4281–4304, 2009.

[5] Leo Breiman. Better subset regression using the nonnegative garrote. *Technometrics*, 37(4):373–384, 1995.

[6] Peter Bühlmann. *Statistics for high-dimensional data*. Springerverlag Berlin Heidelberg, 2011.

[7] Robert H Cameron and William T Martin. The orthogonal development of non-linear functionals in series of fourier-hermite functionals. *The Annals of Mathematics*, 48(2):385–392, 1947.

[8] Emmanuel Candes and Justin Romberg. Signal recovery from random projections. In *Proc. SPIE*, volume 5674, pages 76–86, 2005.

[9] Emmanuel Candes and Justin Romberg. Sparsity and incoherence in compressive sampling. *Inverse problems*, 23(3):969, 2007.

[10] Emmanuel J Candès. The restricted isometry property and its implications for compressed sensing. *Comptes Rendus Mathematique*, 346(9):589–592, 2008.

[11] Emmanuel J Candès, Justin Romberg, and Terence Tao. Robust uncertainty principles: Exact signal reconstruction from highly incomplete frequency information. *Information Theory, IEEE Transactions on*, 52(2):489–509, 2006.

[12] Emmanuel J Candes, Justin K Romberg, and Terence Tao. Stable signal recovery from incomplete and inaccurate measurements. *Communications on pure and applied mathematics*, 59(8):1207–1223, 2006.

[13] Emmanuel J Candes and Terence Tao. Decoding by linear programming. *Information Theory, IEEE Transactions on*, 51(12):4203–4215, 2005.

[14] Emmanuel J Candes and Terence Tao. Near-optimal signal recovery from random projections: Universal encoding strategies? *Information Theory, IEEE Transactions on*, 52(12):5406–5425, 2006.

[15] Emmanuel J Candès and Michael B Wakin. An introduction to compressive sampling. *Signal Processing Magazine, IEEE*, 25(2):21–30, 2008.

[16] Claudio Canuto, M Youssuff Hussaini, Alfio Quarteroni, and Thomas A Zang. *Spectral methods*. Springer, 2006.

[17] Travis Justin Carrigan. Aerodynamic shape optimization of a vertical axis wind turbine. Master's thesis, University of Texas Arlington, 2010.

[18] Scott Shaobing Chen, David L Donoho, and Michael A Saunders. Atomic decomposition by basis pursuit. *SIAM journal on scientific computing*, 20(1):33–61, 1998.

[19] Shaobing Chen and David Donoho. Basis pursuit. In *Signals, Systems and Computers, 1994. 1994 Conference Record of the Twenty-Eighth Asilomar Conference on*, volume 1, pages 41–44. IEEE, 1994.

[20] Hyoung-Seog Chung and Juan J Alonso. Design of a low-boom supersonic business jet using cokriging approximation models. *AIAA paper*, 5598:2002, 2002.

[21] Hyoung-Seog Chung and Juan J Alonso. Using gradients to construct cokriging approximation models for high-dimensional design optimization problems. *AIAA paper*, 317:14–17, 2002.

[22] Hyoung-Seog Chung, Seongim Choi, and Juan J Alonso. Supersonic business jet design using knowledge-based genetic algorithm with adaptive, unstructured grid methodology. *AIAA Paper*, 3791:23–26, 2003.

[23] Albert Cohen, Wolfgang Dahmen, and Ronald DeVore. Compressed sensing and best -term approximation. *Journal of the American Mathematical Society*, 22(1):211–231, 2009.

[24] Paul G Constantine, Michael S Eldred, and Eric T Phipps. Sparse pseudospectral approximation method. *Computer Methods in Applied Mechanics and Engineering*, 2012.

[25] Noel Cressie. Statistics for spatial data. *Terra Nova*, 4(5):613–617, 1992.

[26] Philip J Davis and Philip Rabinowitz. *Methods of numerical integration*. Dover Publications, 2007.

[27] David Donoho and Jared Tanner. Observed universality of phase transitions in high-dimensional geometry, with implications for modern data analysis and signal processing. *Philosophical Transactions of the Royal Society A: Mathematical, Physical and Engineering Sciences*, 367(1906):4273–4293, 2009.

[28] David L Donoho. High-dimensional centrally symmetric polytopes with neighborliness proportional to dimension. *Discrete & Computational Geometry*, 35(4):617–652, 2006.

[29] David L Donoho and Michael Elad. On the stability of the basis pursuit in the presence of noise. *Signal Processing*, 86(3):511–532, 2006.

[30] David L Donoho and Jared Tanner. Neighborliness of randomly projected simplices in high dimensions. *Proceedings of the National Academy of Sciences of the United States of America*, 102(27):9452–9457, 2005.

[31] David L Donoho and Jared Tanner. Counting faces of randomly-projected polytopes when the projection radically lowers dimension. *J. Amer. Math. Soc*, 22(1):1–53, 2009.

[32] David L Donoho and Jared Tanner. Precise undersampling theorems. *Proceedings of the IEEE*, 98(6):913–924, 2010.

[33] David Leigh Donoho. Neighborly polytopes and sparse solution of underdetermined linear equations. 2005.

[34] David Leigh Donoho. Compressed sensing. *Information Theory, IEEE Transactions on*, 52(4):1289–1306, 2006.

[35] Alireza Doostan and Houman Owhadi. A non-adapted sparse approximation of pdes with stochastic inputs. *Journal of Computational Physics*, 230(8):3015–3034, 2011.

[36] Bradley Efron and Charles Stein. The jackknife estimate of variance. *The Annals of Statistics*, pages 586–596, 1981.

[37] Laurent El Ghaoui, Vivian Viallon, and Tarek Rabbani. Safe feature elimination for the lasso. *Submitted, April*, 2011.

[38] Michael S Eldred, Anthony A Giunta, Bart G van Bloemen Waanders, Steven F Wojtkiewicz, William E Hart, and Mario P Alleva. *DAKOTA, a multilevel parallel object-oriented framework for design optimization, parameter estimation, uncertainty quantification, and sensitivity analysis: Version 4.1 reference manual*. Sandia National Laboratories Albuquerque, NM, 2007.

[39] Oliver G Ernst, Antje Mugler, Hans-Jörg Starkloff, and Elisabeth Ullmann. On the convergence of generalized polynomial chaos expansions. *ESAIM: Mathematical Modelling and Numerical Analysis*, 46(02):317–339, 2012.

[40] S Foucart and H Rauhut. A mathematical introduction to compressive sensing. *Appl. Numer. Harmon. Anal. Birkhäuser, Boston, in preparation*, 2011.

[41] Simon Foucart and Ming-Jun Lai. Sparsest solutions of underdetermined linear systems via q-minimization for 0¡ q 1. *Applied and Computational Harmonic Analysis*, 26(3):395–407, 2009.

[42] Wenjiang J Fu. Penalized regressions: the bridge versus the lasso. *Journal of computational and graphical statistics*, 7(3):397–416, 1998.

[43] Walter Gautschi. Orthogonal polynomials: applications and computation. *Acta numerica*, 5:45–119, 1996.

[44] Thomas Gerstner and Michael Griebel. Numerical integration using sparse grids. *Numerical algorithms*, 18(3-4):209–232, 1998.

[45] Roger G Ghanem and Pol D Spanos. *Stochastic finite elements: a spectral approach*. Dover publications, 2003.

[46] Anthony A Giunta, Layne T Watson, and J Koehler. A comparison of approximation modeling techniques: polynomial versus interpolating models. In *Proceedings of the 7th AIAA/USAF/NASA/ISSMO Symposium on Multidisciplinary Analysis and Design*, pages 392–404, 1998.

[47] Michael Grant and Stephen Boyd. CVX: Matlab software for disciplined convex programming, version 2.0 beta. http://cvxr.com/cvx, September 2012.

[48] Richard Hamming. *Numerical methods for scientists and engineers*. Courier Dover Publications, 2012.

[49] Trevor Hastie, Robert Tibshirani, Jerome Friedman, and James Franklin. The elements of statistical learning: data mining, inference and prediction. *The Mathematical Intelligencer*, 27(2):83–85, 2005.

[50] Jon Craig Helton, Jay Dean Johnson, Cedric J Sallaberry, and Curt B Storlie. Survey of sampling-based methods for uncertainty and sensitivity analysis. *Reliability Engineering & System Safety*, 91(10):1175–1209, 2006.

[51] Wassily Hoeffding. A class of statistics with asymptotically normal distribution. *The Annals of Mathematical Statistics*, 19(3):293–325, 1948.

[52] Arthur E Hoerl and Robert W Kennard. Ridge regression: Biased estimation for nonorthogonal problems. *Technometrics*, 12(1):55–67, 1970.

[53] Toshimitsu Homma and Andrea Saltelli. Importance measures in global sensitivity analysis of nonlinear models. *Reliability Engineering & System Safety*, 52(1):1–17, 1996.

[54] Serhat Hosder, Robert W. Walters, and Michael Balch. Point-collocation nonintrusive polynomial chaos method for stochastic computational fluid dynamics. *AIAA Journal*, 48(12):2721–2730, 2013/05/28 2010.

[55] Antony Jameson. Aerodynamic design via control theory. *Journal of scientific computing*, 3(3):233–260, 1988.

[56] Keith Knight and Wenjiang Fu. Asymptotics for lasso-type estimators. *Annals of Statistics*, pages 1356–1378, 2000.

[57] JR Koehler and AB Owen. Computer experiments. *Handbook of statistics*, 13(13):261–308, 1996.

[58] David G Luenberger. *Optimization by vector space methods*. Wiley-Interscience, 1997.

[59] MATLAB. *version 7.10.0 (R2010a)*. The MathWorks Inc., Natick, Massachusetts, 2010.

[60] Nicolai Meinshausen and Peter Bühlmann. High-dimensional graphs and variable selection with the lasso. *The Annals of Statistics*, 34(3):1436–1462, 2006.

[61] Hatef Monajemi, Sina Jafarpour, Matan Gavish, David L Donoho, Sivaram Ambikasaran, Sergio Bacallado, Dinesh Bharadia, Yuxin Chen, Young Choi, Mainak Chowdhury, et al. Deterministic matrices matching the compressed sensing phase transitions of gaussian random matrices. *Proceedings of the National Academy of Sciences*, 110(4):1181–1186, 2013.

[62] Jonathan C. Murray and Matthew Barone. *CACTUS User's Manual Version 1.0*. Sandia National Laboratories, Albuquerque, NM 87185-0825.

[63] NREL Workshop. *Computational Strategies for Aero-Mechanical Analysis in the Prescence of Uncertainties*, 2013.

[64] Michael R Osborne, Brett Presnell, and Berwin A Turlach. On the lasso and its dual. *Journal of Computational and Graphical statistics*, 9(2):319–337, 2000.

[65] Art B Owen. Orthogonal arrays for computer experiments, integration and visualization. *Statistica Sinica*, 2(2):439–452, 1992.

[66] Art B. Owen. Variance components and generalized sobol' indices. *SIAM/ASA Journal on Uncertainty Quantification*, 1(1):19–41, 2013.

[67] Joshua Paquette and Matthew Barone. Innovative offshore vertical-axis wind turbine rotor project. *EWEA 2012 Annual Event, Copenhagen, Denmark*, 2012.

[68] Melempati Madhusudana Rao and Randall J Swift. *Probability theory with applications*, volume 2. Springer, 2006.

[69] H Rauhut and R Ward. Efficient and stable recovery of legendre-sparse polynomials. In *Information Sciences and Systems (CISS), 2010 44th Annual Conference on*, pages 1–6. IEEE, 2010.

[70] Holger Rauhut. Compressive sensing and structured random matrices. *Theoretical foundations and numerical methods for sparse recovery*, 9:1–92, 2010.

[71] Holger Rauhut and Rachel Ward. Sparse legendre expansions via 1-minimization. *Journal of Approximation Theory*, 164(5):517–533, 2012.

[72] John A Rice. *Mathematical statistics and data analysis*. Duxbury press, 2007.

[73] Christian P Robert, George Casella, and Chritian P Robert. *Monte Carlo statistical methods*, volume 128. Springer New York, 1999.

[74] Kenneth A Ross. *Elementary analysis: the theory of calculus*. Springer Verlag, 1980.

[75] Andrea Saltelli, Stefano Tarantola, Francesca Campolongo, and Marco Ratto. *Sensitivity analysis in practice: a guide to assessing scientific models*. Wiley, 2004.

[76] Michael A Saunders and Byunggyoo Kim. Pdco: Primal-dual interior method for convex objectives. *Software available at http://www. stanford. edu/group/SOL/software/pdco. html*, 2002.

[77] Ilya M Sobol. Global sensitivity indices for nonlinear mathematical models and their monte carlo estimates. *Mathematics and computers in simulation*, 55(1-3):271–280, 2001.

[78] IM Sobol. Multidimensional quadrature formulas and haar functions. *Izdat" Nauka", Moscow*, 1969.

[79] Curtis B Storlie, Laura P Swiler, Jon C Helton, and Cedric J Sallaberry. Implementation and evaluation of nonparametric regression procedures for sensitivity analysis of computationally demanding models. *Reliability Engineering & System Safety*, 94(11):1735–1763, 2009.

[80] Bruno Sudret. Global sensitivity analysis using polynomial chaos expansions. *Reliability Engineering & System Safety*, 93(7):964–979, 2008.

[81] Gabor Szegö. *Orthogonal polynomials*, volume 23. Amer Mathematical Society, 1939.

[82] Gary Tang, Gianluca Iaccarino, and Michael Eldred. Global sensitivity analysis for stochastic collocation. In *Proceedings 51st AIAA/ASME/ASCE/AHS/ASC Structures, Structural Dynamics, and Materials Conference*. American Institute of Aeronautics and Astronautics, 2010.

[83] Robert Tibshirani. Regression shrinkage and selection via the lasso. *Journal of the Royal Statistical Society. Series B (Methodological)*, pages 267–288, 1996.

[84] Robert Tibshirani. Regression shrinkage and selection via the lasso: a retrospective. *Journal of the Royal Statistical Society: Series B (Statistical Methodology)*, 73(3):273–282, 2011.

[85] Robert Tibshirani, Jacob Bien, Jerome Friedman, Trevor Hastie, Noah Simon, Jonathan Taylor, and Ryan J Tibshirani. Strong rules for discarding predictors in lasso-type problems. *Journal of the Royal Statistical Society: Series B (Statistical Methodology)*, 74(2):245–266, 2012.

[86] Ryan J Tibshirani. The lasso problem and uniqueness. *arXiv preprint arXiv:1206.0313*, 2012.

[87] Radu Alexandru Todor and Christoph Schwab. Convergence rates for sparse chaos approximations of elliptic problems with stochastic coefficients. *IMA Journal of Numerical Analysis*, 27(2):232–261, 2007.

[88] Ewout Van Den Berg and Michael P Friedlander. Probing the pareto frontier for basis pursuit solutions. *SIAM Journal on Scientific Computing*, 31(2):890–912, 2008.

[89] F van Keulen, B Liu, and RT Haftka. Noise and discontinuity issues in response surfaces based on functions and derivatives. In *Proceedings of the 41st AIAA/ASME/ASCE/AHS/ASC Structures, Structural Dynamics, and Materials Conference and Exhibit, Atlanta, GA, USA, pp. Paper AIAA-00-1363.*, 2000.

[90] Fred van Keulen and Koen Vervenne. Gradient-enhanced response surface building. *Structural and Multidisciplinary Optimization*, 27(5):337–351, 2004.

[91] K Vervenne and F Van Keulen. An alternative approach to response surface building using gradient information. In *Proceedings of the 43st AIAA/ASME/ASCE/AHS/ASC Structures, Structural Dynamics, and Materials Conference and Exhibit, Denver, CO, USA, pp. Paper AIAA-2002-1584.*, volume 70, 2002.

[92] Norbert Wiener. The homogeneous chaos. *Amer. J. Math*, 60(4):897–936, 1938.

[93] Dongbin Xiu and George Em Karniadakis. The wiener–askey polynomial chaos for stochastic differential equations. *SIAM Journal on Scientific Computing*, 24(2):619–644, 2002.

[94] Liang Yan, Ling Guo, and Dongbin Xiu. Stochastic collocation algorithms using $\ell_1$-minimization. *International Journal for Uncertainty Quantification*, 2(3), 2012.

[95] Nicholas Young. *An introduction to Hilbert space*. Cambridge university press, 1988.

[96] Ming Yuan and Yi Lin. Model selection and estimation in regression with grouped variables. *Journal of the Royal Statistical Society: Series B (Statistical Methodology)*, 68(1):49–67, 2006.

[97] Peng Zhao and Bin Yu. On model selection consistency of lasso. *The Journal of Machine Learning Research*, 7:2541–2563, 2006.

[98] Hui Zou. The adaptive lasso and its oracle properties. *Journal of the American statistical association*, 101(476):1418–1429, 2006.